DURBAN UNIVERSITY OF TECHNOLOGY
INYUVESI YASETHEKWINI YEZOBUCHWEPHESHE

Numerical and Experimental Investigations of the Impacts of the Integration of Wind Energy into Distribution Network

By

Ramesh Kumar Behara

Student No: 21649484

A thesis submitted in fulfillment of the requirements for the Master of Engineering Degree in the Department of Electrical Power Engineering, Faculty of Engineering and the Built Environment

Durban University of Technology

Supervisor: Dr. Evans E. Ojo
Co-Supervisor: Mr. Timothy K. Akindeji

June 2021

DECLARATION

I hereby declare that this dissertation is my work, and each text has been correctly referenced or cited. Moreover, this work has not been previously published in portion or whole for another degree at any other University.

This research was duly supervised by Dr Evans E. Ojo and Mr. Timothy K. Akindeji at the Durban University of Technology.

Submitted by:

26.07.2021

Date

Ramesh K. Behara

Student Number: 21649484

Approved for Final Submission by:

26/07/2021

Date

Supervisor: Dr Evans E. Ojo

26/07/2021

Date

Co-Supervisor: Mr. K.T Akindeji

Abstract

The growing needs for electric power around the world has resulted in fossil fuel reserves to be consumed at a much faster rate. The use of these fossil fuels such as coal, petroleum and natural gas have led to huge consequences on the environment, prompting the need for sustainable energy that meets the ever increasing demands for electrical power. To achieve this, there has been a huge attempt into the utilisation of renewable energy sources for power generation. In this context, wind energy has been identified as a promising, and environmentally friendly renewable energy option. Wind turbine technologies have undergone tremendous improvements in recent years for the generation of electrical power. Wind turbines based on doubly fed induction generators have attracted particular attention because of their advantages such as variable speed, constant frequency operation, reduced flicker, and independent control capabilities for maximum power point tracking, active and reactive powers. For modern power systems, wind farms are now preferably connected directly to the distribution systems because of cost benefits associated with installing wind power in the lower voltage networks.

The integration of wind power into the distribution network creates potential technical challenges that need to be investigated and have mitigation measures outlined. Detailed in this study are both numerical and experimental models to investigate these potential challenges. The focus of this research is the analytical and experimental investigations in the integration of electrical power from wind energy into the distribution grid. Firstly, the study undertaken in this project was to carry out an analytical investigation into the integration of wind energy in the distribution network. Firstly, the numerical simulation was implemented in the MATLAB/Simulink software. Secondly, the experimental work, was conducted at the High Voltage Direct Centre at the University of KwaZulu-Natal.

The goal of this project was to simulate and conduct experiments to evaluate the level of penetration of wind energy, predict the impact on the network, and propose how these impacts can be mitigated. From the models analysis, the effects of these challenges intensify with the increased integration of wind energy into the distribution network.

The control strategies concept of the doubly fed induction generator connected wind turbine was addressed to ascertain the required control over the level of wind power penetration in the distribution network. Based on the investigation outcomes we establish that the impact on the voltage and power from the wind power integration in the power distribution system has a goal to maintain quality and balance between supply and demand.

Acknowledgment

I wish to thank the almighty God for giving me life and enabling me to reach the heights that I have reached.

I would like to sincerely thank and express my appreciation to my Supervisor Dr. Evans. E. Ojo for introducing the field of Wind Renewable Energy to me, his great supervision, and for his consistent assistance and help during the course of my project. Also, my gratitude goes to my co-supervisor Mr. Timothy K. Akindeji for his invaluable support and guidance throughout this study.

I am indebted to Mr. Pravesh Moodley for assisting with the experimentation at Smart Grid laboratory of the Westville campus of the University of KwaZulu-Natal

Also, my appreciation goes to Mr. Anuoluwapo Aluko for providing some meaningful reviews and discussions which helped me in my research work.

I wish to thank my parents and my siblings, for their tireless and relentless love, continuous support, and the countless sacrifices they have made on my behalf. To my wife Mrs. Behara Kavita, you deserve special mention, for being a great wife and believing in me even when I had stopped believing in myself. This would not have been possible without your help.

Finally, I wish to everyone not mentioned above but directly or indirectly contributed to my work, your input is much acknowledged.

Dedication

I dedicate this work to my parents Mr. Behara Venkata Krishna Rao and Mrs. Jyoti Behara, my wife Mrs. Behara Kavita, and kids Miss Shriya Behara and Master Shreyansh Behara.

Table of Contents

List of Figures

List of Tables

List of Acronyms

ABL	Atmospheric boundary layer
AC	Alternating Current
AEP	Annual Energy Production
AMI	Amplitude Modulation Index
BB	Back to Back
BEM	Blade Element Method
Ce	Centrifugal Forces
CO	Coriolis forces
DC	Direct Current
DEA	Department of Environmental Affairs
DFIG	Doubly fed Induction Generator
DNV	Det Norske Veritas
DoE	Department of Energy
DPC	Direct Power Control
DS	Distribution System
DSC	Direct Speed Controller
DSM	Demand Side management
DSO	Distribution System Operator
DSR	Demand Side Response
DTC	Direct Torque Control
FACTS	Flexible Alternating Current Transmission System
FMI	Frequency Modulation Index
Fr	Friction Force
FSWT	Fixed Speed Wind Turbine
FZCD	Filtered Zero Cross Detection
GHG	Green House Gas
GL	Germanischer Lloyd
GLLR	Generation Load Level Ratio
GSC	Grid Side Controller
HAWT	Horizontal Axis Wind Turbine
HCS	Hill Climbing Searching

HVDC	High Voltage Direct Current
IEA	International Energy Agency
IEC	International Electro-technical Commission
IEEE	The Institute of Electrical & Electronics Engineers
IG	Induction Generator
IGBT	Insulated Gate Bipolar Transistor
IPP	Independent Power Producer
IRP	Integrated Resource Plan
ISC	Indirect Speed Controller
MOE	Ministry of Energy
MPPT	Maximum Power Point Tracking
MV	Medium Voltage
NERSA	National Energy Regulator of South Africa
NSP	National Strategic Plan
OSIG	OptiSlip Induction Generator
PBL	Planetry Boundary Layer
PCC	Point of Control of Coupling
PCF	Plant Capacity Factor
PDF	Probability Distribution Function
PEC	Power Electronic Converter
PGF	Pressure Gradient Force
PLL	Phased Locked Loop
PMSG	Permanent Magnet Generator
PSB	Power System Block Set
PSF	Power Signal Feedback
PWM	Pulse Width Modulation
RE	Renewable Energy
REIPPPP	Renewable Energy Independent Power Production Procurement Programme
RL	Roughness Layer
RMD	Ring Main Distribution
RMSE	Root Mean Square Error

RPP	Renewable Power Plant
RSC	Rotor Side Converter
SAREGC	South Africa renewable energy grid code
SCIG	Squirrel Cage Induction Generator
SEIG	Self-Excited Induction Generator
SG	Synchronous Generator
SL	Surface Layer
SO	Service Operator
SPS	Sim Power Systems
SPSB	Sim Power Systems Blocks
SVC	Static VAr Compensator
THD	Total Harmonic Distortion
TS	Transmission System
TSO	Transmission System Operator
TSR	Tip Speed Ratio
VAWT	Vertical Axis Wind Turbine
VSC	Voltage Source Converter
VSCs	Voltage Source Controllers
VSI	Voltage Source Inverter
VSWT	Variable Speed Wind Turbine
WASA	Wind Atlas for South Africa
WECEG	World Energy Consumption and Economic Growth
WECS	Wind Energy Conversion System
WECS	World Energy Conservation System
WPP	Wind Power Plant
WRIG	Wound Rotor Induction Generator
WRSG	Wound Rotor Synchronous Generator
WSSD	World Summit on Sustainable Development
WT	Wind Turbine
WTG	Wind Turbine Generator
WTGCS	Wind Turbine Generator Control System

List of Symbols

A	Area swept by turbine blades (m^2)
C_L	Lift coefficient
C_D	Drag coefficient
C_p	Performance coefficient
C	DC-link capacitor of PWM converter (μF)
$e_a(t), e_b(t), e_c(t)$	Three phase voltage of AC side of PWM converter (volts)
f_s	Stator frequency (Hz)
f_r	Rotor frequency (Hz)
F	Aerodynamic Force (Newton)
F_D	Drag Force (Newton)
F_L	Lift Force (Newton)
i_L	Load current on AC side of PWM converter (amps)
i_{dc}	DC-link current of PWM converter (amps)
i_d, i_q	Rotor currents in dq0 synchronously rotating frame of reference (amps)
i_{ds}, i_{qs}	Direct axis and quadrature axis of stator current in reduced order model in synchronously rotating frame of reference (amps)
i_{dr}, i_{qr}	Direct axis and quadrature axis of rotor current in reduced order model in synchronously rotating frame of reference (amps)
i_D, i_Q	Stator currents in DQ0 synchronously rotating frame of reference (amps)
i_{ag}, i_{bg}, i_{cg}	Three phase current of AC side of PWM converter (amps)
i_a, i_b, i_c	Phase current of rotor (amps)
i_A, i_B, i_C	Phase current of stator (amps)
$\underline{I}_{ABC}, \underline{I}_{abc}$	Stator and rotor current vectors respectively (amps)

$\underline{I}_{DQ0}, \underline{I}_{dq0}$	Current of stator and rotor in DQ0 frame of reference (amps)
J	Inertia constant of machine
L_{ss}	Self-inductance of stator winding (Henry)
L_{rr}	Self-inductance of rotor winding (Henry)
L_{ms}	Mutual inductance between two stator windings (Henry)
L_{mr}	Mutual inductance between two rotor windings (Henry)
L_m	Maximum mutual inductance between phase winding of stator and rotor (Henry)
$\underline{L}_{rs}$	Stator and rotor mutual inductance matrix (Henry)
L_S	Leakage inductance in stator (Henry)
L_R	Leakage inductance in rotor (Henry)
L_M	Magnetizing inductance (Henry)
L_g	Inductance of AC side of PWM converter (Henry)
$\underline{M}_s, \underline{M}_r$	Transformation matrix on the stator and rotor side respectively
$\underline{M}_{STO}, \underline{M}_{rro}$	Stator and rotor transformation matrices in DQO-dq0 frame of reference stationary of the rotor
$\underline{M}_{sst}, \underline{M}_{rst}$	Stator and rotor transformation matrices in DQO-dq0 frame of reference stationary of the stator
N_r	Rotor Speed (rpm)
p	Number of pole pairs
P_m	Mechanical power (watts)
P_s	Stator active power (watts)
P_r	Rotor active power (watts)
Q_s	Stator reactive power (watts)
R	Radius of turbine blade (m)
R_g	Resistance of AC side of PWM converter (ohms)

R_L	Load resistance of AC side of PWM converter (ohms)
$\underline{R}_{ss}, \underline{R}_{rr}$	Stator and rotor resistance matrices respectively (ohms)
$r_A, \mathrm{r}_B, \mathrm{r}_C$	Resistance in each phase of stator (ohms)
$r_a, \mathrm{r}_b, \mathrm{r}_c$	Resistance in each phase of rotor (ohms)
s	Slip
S_a, S_b, S_c	Switch in the three-phase PWM converter
T_m	Mechanical torque (N-m)
T_{em}	Electromechanical torque (N-m)
v_{dc}	DC-link voltage of PWM converter (volts)
v_d , v_q	Rotor voltages in dq0 synchronously rotating frame of reference (volts)
v_{ds} , v_{qs}	Direct axis and quadrature axis of stator voltage in reduced order model in synchronously rotating frame of reference (volts)
v_{dr} , v_{qr}	Direct axis and quadrature axis of rotor voltage in reduced order model in synchronously rotating frame of reference (volts)
$v_{(a,0)}, v_{(b,0)}, v_{(c,0)}$	Phase-to-neutral voltage of PWM converter (volts)
v_D , v_Q	Stator voltages in DQ0 synchronously rotating frame of reference (volts)
V_W	Wind speed (m/s)
V_A, V_B, V_C	Phase voltages of stator (volts)
V_a, V_b, V_c	Phase voltages of rotor (volts)
$\underline{V}_{ABC}, \underline{V}_{abc}$	Stator and rotor voltage vectors respectively (volts)
$\underline{V}_{DQ0}, \underline{V}_{dq0}$,	Voltage of stator and rotor in DQ0 frame of reference (volts)
ρ	Density of air (Kg/m^3)
λ	Tip speed ratio
β	Pitch angle (degrees)

ω_s	Angular frequency in stator winding (rad/sec)
ω_r	Angular frequency in rotor winding (rad/sec)
ω_m	Electrical angular frequency in rotor winding (rad/sec)
Ω_m	Mechanical speed of rotor (rpm)
φ_D , φ_Q	Stator flux linkages in DQ0 synchronously rotating frame of reference (Wb)
φ_d , φ_q	Rotor flux linkages in dq0 synchronously rotating frame of reference (Wb)
φ_{ds} , φ_{qs}	Direct axis and quadrature axis of stator flux linkage in reduced order model in synchronously rotating frame of reference (Wb)
φ_{dr} , φ_{qr}	Direct axis and quadrature axis of rotor flux linkage in reduced order model in synchronously rotating reference (Wb)
$\underline{\varphi}_{ABC}$, $\underline{\varphi}_{abc}$	Stator and rotor flux linkage vectors respectively (Wb)
$\underline{\varphi}_{DQ0}$, $\underline{\varphi}_{dq0}$	Flux linkage of stator and rotor in DQ0 frame of reference (Wb)
φ_A,φ_B,φ_C	Flux linkage in stator windings (Wb)
φ_a,φ_b,φ_c	Flux linkage in rotor windings (Wb)

Chapter 1

Introduction

1.1 General Background

The increasing demand for electrical power has prompted the need to explore alternative sources of energy for generating electricity. This trend has encouraged the energy policy planners around the world to explore these forms of alternative energy sources. These alternative sources such as renewable energy are in the form of solar, wind or geothermal energy that can be harnessed to meet the increasing electricity demand. The International Energy Agency (IEA) estimated that, based on the current consumption of electricity, global energy demand would double in the year 2030 [1]. Figure 1.1 shows how energy consumption has increased as the world economies are constantly growing [2]. Currently, the major sources of energy for power generation are amongst others are coal, oil, and natural gas. These energy sources are being depleted at a faster rate and they are non-renewable energy sources.

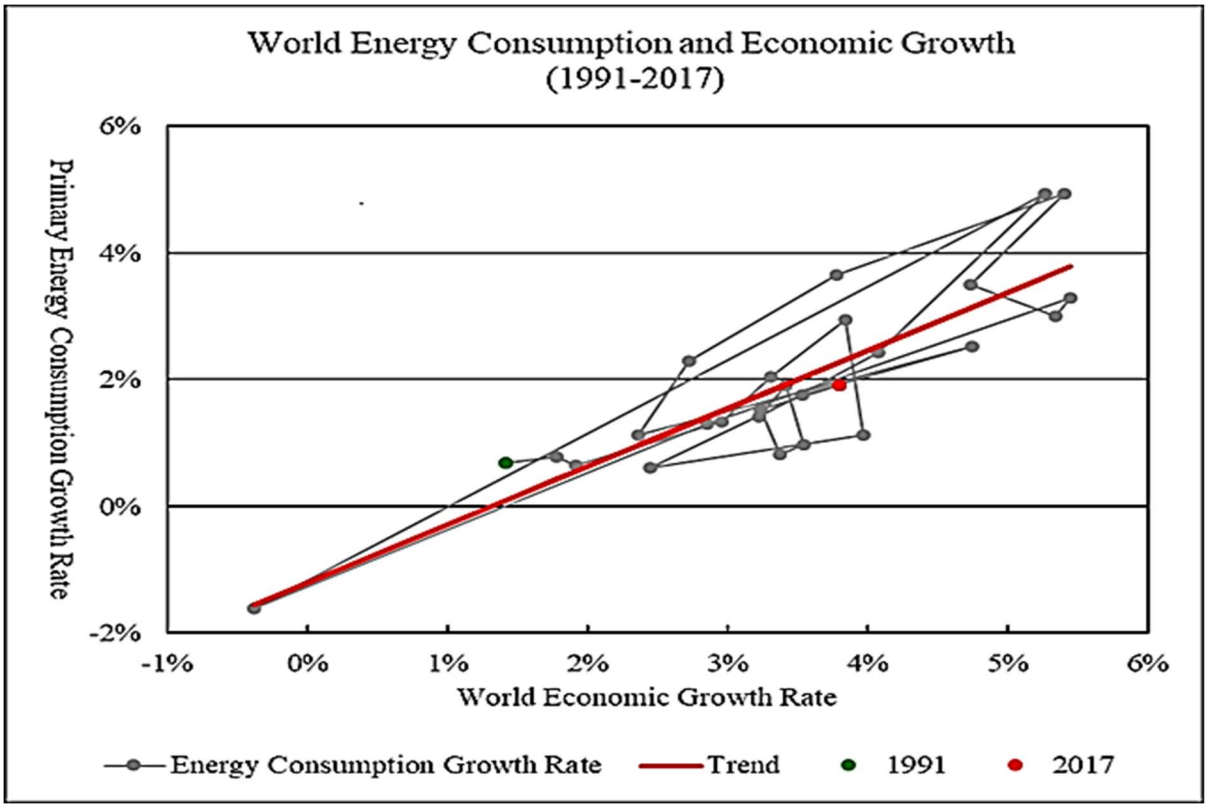

Figure 1.1: World Energy Consumption and Economic Growth (1991-2017) [2]

In addition, the world electricity generation capacity has been increasing in line with energy consumption, and the generation growth versus economic growth is shown in Figure 1.2. It can be observed, when comparing Figure 1.1 with Figure 1.2 that the world electricity generation

capacity has gradually been increasing at a slightly higher rate than the energy consumption growth rate. This trend shows the importance of electricity generation towards the growth of an economy. As such, there is a need to ensure the continued growth in the electricity generation capacity without destroying the environment. It is a known fact based on research that non-renewable sources contribute towards climate change and global warming and, as such, there is a general shift towards using more renewable energy resources to generate electricity. Renewable energy resources include wind, solar, geothermal, and tidal/wave energy, amongst others.

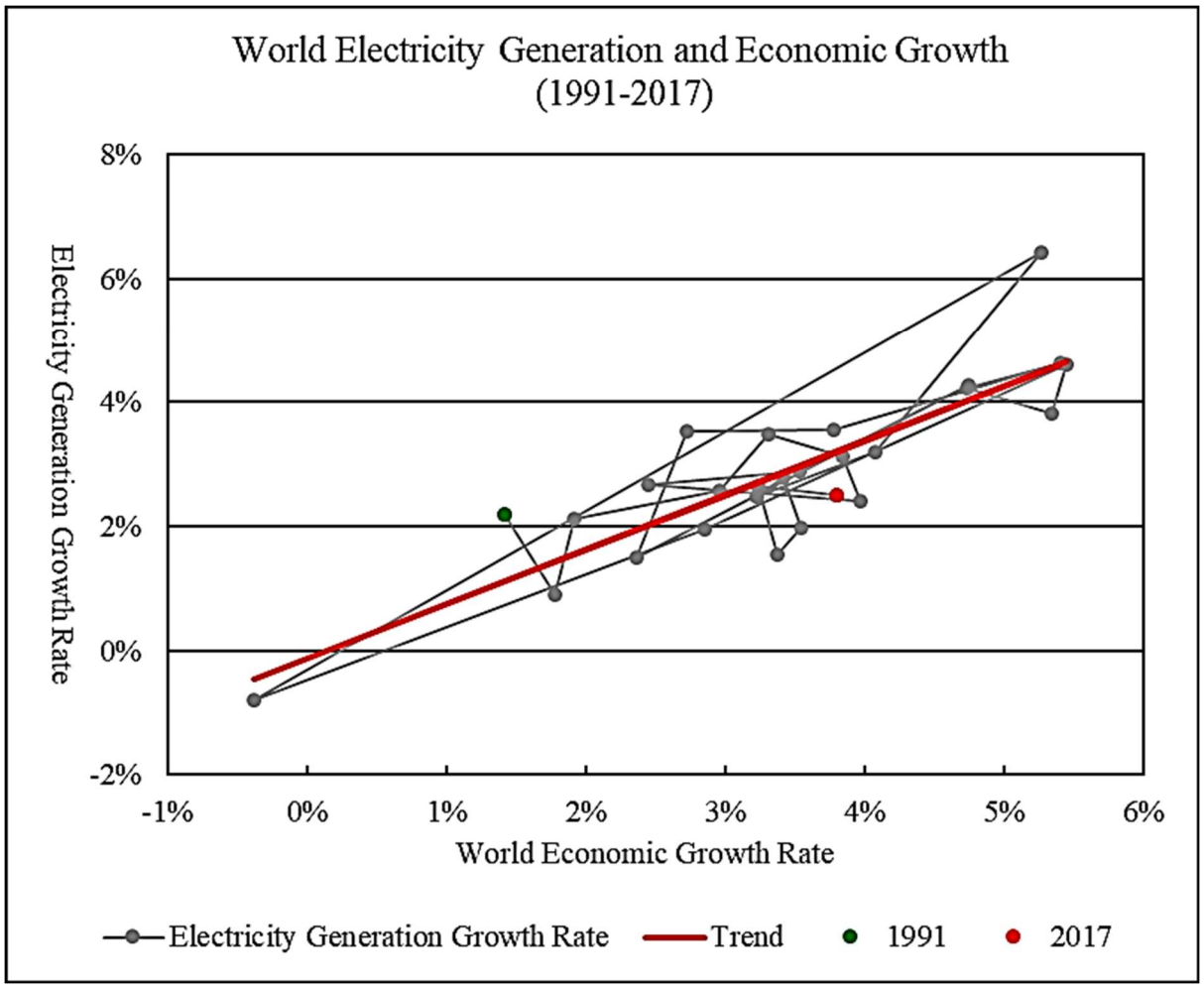

Figure 1.2: World Electricity Generation and Economic Growth (1991-2017) [2]

The global trends of economic growth coupled with the energy needed to sustain this demand are generally mirrored in South Africa. The economic growth combined with increasing population, industrialization, and bulk rural electrification, have resulted in a high demand for energy in the country. South Africa's energy supply presently, is a combination of renewable and non-renewable energy sources, of which the proportion of energy supply is about 59 % is

from coal which is in abundance and economical, and the remainder is from crude oil 16%, natural gas 3%, nuclear 2%, renewable and wastes 20% [3] as shown in Figure 1.3.

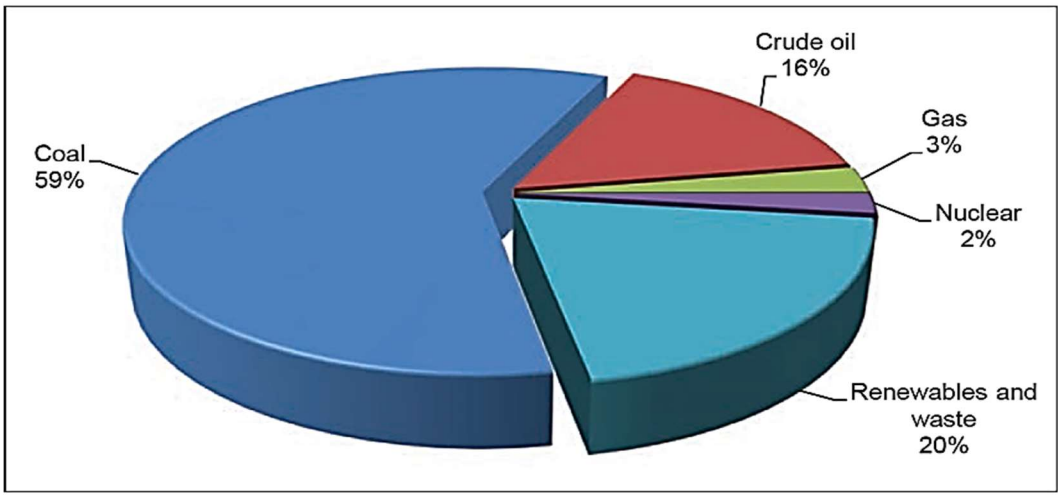

Figure 1.3: South Africa's Total Primary Energy Supply (2015) [3]

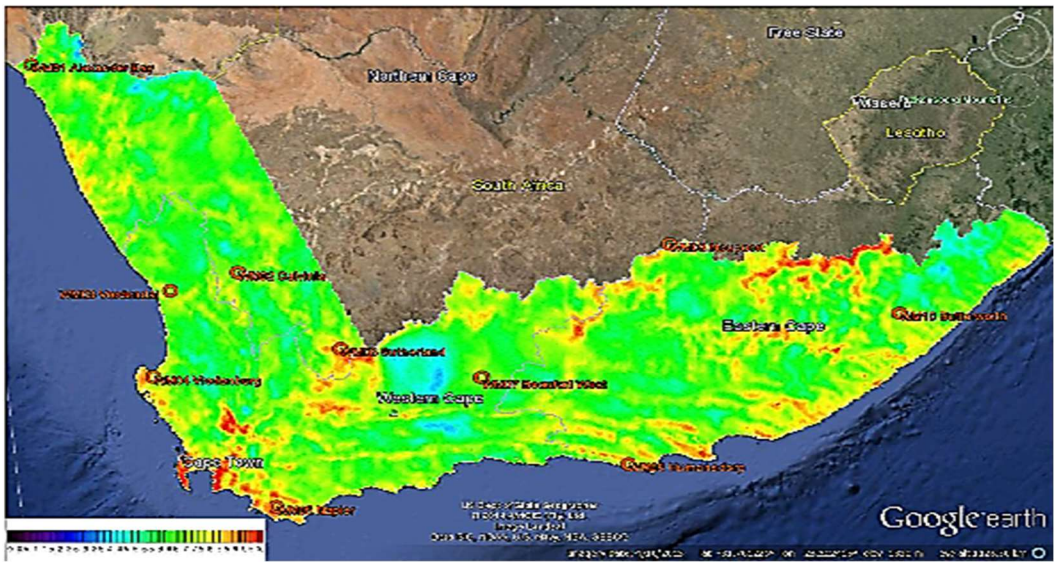

Figure 1.4: WASA Wind Source Map [3]

In line with the global trend, South Africa is gradually shifting from the use of non-renewable energy sources to renewable energy sources. Among these renewable or alternate energy sources, wind energy has gained much prominence. The mesoscale modelling dataset by Wind Atlas for South Africa (WASA), shown in Figure 1.4, revealed a huge potential for wind energy which can be harness for electrical power generation [3].

1.2 Distribution Systems: Role of South African Municipalities

The South Africa government has committed to the international community effort of reducing environmental pollution due to the high emission of Green House Gases (GHG). Part of the

plan to honour this commitment is contained in the "Integrated Resource Plan (IRP)" which stipulated that 56% of wind power will be required in the first phase of its renewable energy feed-in-tariff programme. As a result, significant research has been initiated into wind energy to determine the optimum approach for South Africa to harness of wind energy for electricity [1]. One of the approaches is the generation and integration of wind power directly into the distribution network.

In the South African power systems, generation and transmission of power are undertake by South Africa's power utility, Eskom [5]. The role of the design, operation, and maintenance of the distribution network is that of the local governments or Municipalities. Thus, this section of the grid is normally controlled and/or administered by municipalities. As such, it is important that one highlight the plight or plans of municipalities emanating from the electricity sector transformations. In recent times, municipalities have been tasked to reconsider their place in the electricity supply value chain, resulting in a business model as documented in Table 1.1. Three different "roles" were developed, one of which is the building electrical generation capacity [5].

Table 1.1: 'The South African municipalities' business model [5]

Roles	**The realm of business models**
Building generating capacity	Building embedded power systems (e.g. installing rooftop solar PV systems on municipal buildings with or without feeding into the municipal grid)
	Building stand-alone power plants (e.g. building a large farm or solar park on municipal land used for municipal grid with possibility of on-selling to Eskom)
Procuring energy	Procuring electricity from embedded generators (e.g. procuring electricity from rooftop PV systems installed by residential customers)
	Procuring electricity from an independent power producer (e.g. procuring electricity from an independent solar park / wind farm in the vicinity of the municipality)
Playing facilitation role	Playing a trading/aggregating role (e.g. buying electricity from local producers for on-selling to willing customers at a premium)
	Operating a storage facility (e.g. store electricity in time of excess and sell it in time of high demand)
	Providing electricity services (e.g. installing power systems, providing maintenance)

To comply with constitutional and statutory duties, the South African municipalities have to supply basic services including "the best possible energy solution and service" to its inhabitants. The municipalities consideration in building the generation and supply of electricity can be achieved by purchasing renewable energy (RE) from independent power producers (IPPs), and by building their generation capabilities. This will enable municipalities to reduce their over-dependence on Eskom while widening the domain of the activities the municipalities can deliver on. The model whereby municipalities purchase or generate renewable energies and then feed this into their networks comes with huge technical challenges. These challenges are in the form of power quality problems such as voltage sag/dip, voltage swell/rise, reactive power control, synchronization, harmonics, cost, and reliability of the control system [5].

1.3 Motivation

Introducing REs into the distribution systems has the advantage of proving massive electrification in South Africa. This will enhance the liberalization of the energy sector including the transformation of the electricity distribution sector into a regional electricity distribution. This comes with huge benefits as renewable energy sources can then be used for the electrification of rural communities and commercial applications far from the national electricity grid. Large-scale utilization of renewable energy will also reduce the emissions of carbon dioxide, thus contributing to an improved environment both locally and worldwide.

As mentioned in the last section, the generation and integration of renewable energies (REs) into the distribution networks come with huge challenges as the distribution networks are being managed by municipalities in South Africa. Because of its intermittent nature, the supply of wind-generated electricity into the distribution network, wind power will not be able to adequately cater for the loads. Thus, for variable conditions or where no power is available, the grid will supply the deficit in synchronization. The block diagram of this process is shown in Figure 1.5.

The focus of this research is the analytical and experimental investigation into the integration of electrical power from wind energy into the distribution grid. Therefore, the focus of this project will be to carry out an analytical and experimental investigation into the integration of wind energy in the distribution network. This will include both numerical simulation and experimental work that will be conducted at the High Voltage Direct Centre (HVDC) at the University of KwaZulu-Natal. The goal of this project was to simulate the introduction of wind power, to evaluate the penetration of wind energy introduced, to predict the impact on the network, and then to propose how these impacts can be mitigated. The research investigated the

power integration impacts on voltage and power quality in a distribution system and how to use the control strategies to maintain the balance between supply and demand.

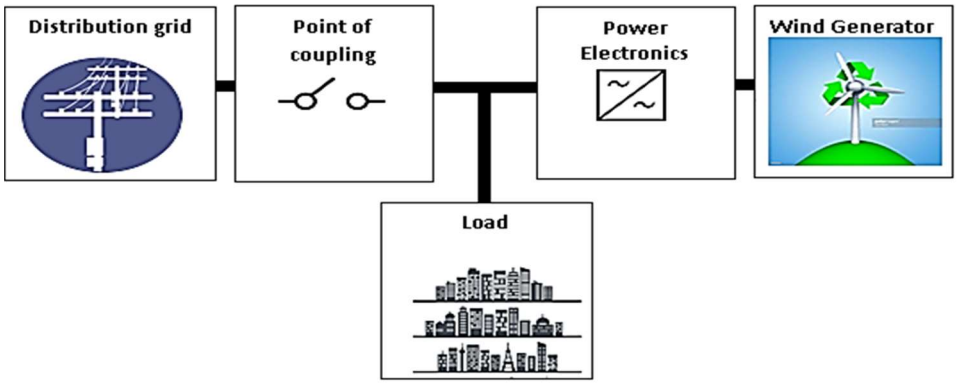

Figure 1.5: Block diagram used to illustrate the integration of wind power into the distribution network

1.4 Problem Statement

Recently, the use of small wind turbines has gained popularity and they are being installed in rural areas and urban centres to generate electricity. This has the advantage of eliminating power line losses in the grid. Due to the intermittent nature of wind, the integration of wind power into the grid presents technical challenges such as reactive power control for voltage provision, starting and synchronising of wind farms onto the grid, short-circuit protection, and the efficiency of the grid. These are also power quality problems such as voltage sag/dip, voltage swell/rise, flicker, harmonics, short interruptions, design and optimization of power electronics, and cost and reliability of the control system. Of all these challenges, power quality has gained attention in research because it is directly linked to other challenges such as load dispatch, sub-synchronous resonance as a result of the electric network and wind turbine interaction and system fault levels.

This research project was formulated to investigate how to curtail the impacts associated with the integration of wind power into the distribution network, as the wind power producers prefer to disconnect the wind turbines from the grid during faults which lead directly to low voltage conditions and an imbalance of inactive power at the point of common coupling. This is normally done to prevent damages to the wind turbine control system components, which can consequently cause a partial or total blackout. Hence, this work will investigate how this problem can be mitigated as outlined in the next section.

1.5 Research Aims and Objectives

The project was carried out to analytically and experimentally analyse the wind energy integration into the distribution network. To achieve this, the following were done:

- Carried out an analysis of energy conversion processes in wind farms.
- Carried out the power flow analysis from wind input to its integration into the distribution network.
- Carried out an analysis on the problems associated with power quality associated with the direct integration of wind power into the distribution network.
- Carry out analytical simulations in a MATLAB environment to analyse the performance of the network when wind power is integrated.
- Carried out experimental work at the HVDC laboratory to validate the analytical simulations.

The objective of this research will be

- To investigate an efficient framework to optimize the distribution network operation with the introduction of wind power and to address the issues to be addressed before wind turbines can be connected.
- To investigate the voltage change, power quality and undesirable voltage increase in periods with high wind speed and the possible solutions to maintain a stable network, under various wind conditions.
- To develop a model to evaluate the performance of the distribution network when injecting a significant level of wind power, into the distribution network.

1.6 Research Questions

The following investigative questions would be answered when this research study is completed:

- How will the existing distribution network parameters (voltage, current, losses, plant loading, fault levels, etc.) be affected by the possible ways of integration of wind energy supply and the possible solutions to maintain a stable network?

    - Wind turbine connected Doubly Fed Induction Generator (DFIG) and its control strategies are generally based on detailed voltage source back to back (BB) converters. Therefore, such a model has been developed and implemented using a *PI* algorithm controller as demonstrated via simulation results in the design of the controller of the

machine side converter to enhance the operation of the system by mitigating the effect of wind speed disturbances and satisfying maximum power extraction from the wind.

- Development and demonstration of the control scheme using a *PI* logic controller for both the machine side and grid side converters reduces the overshooting of the generator rotor speed, and maintains the output voltage and frequency within the rated values in cases of wind speed disturbances.

1.7 Brief Chapter Overview

This document consists of six chapters. These are summarized as follows:

- Chapter One – This chapter, introduces the study, outlining the background of wind as a form of renewable energy. The motivation for the study is discussed, highlighted the problems of wind turbine integration into the distribution networks. Also included in this chapter are the aims and objectives of this study followed by the investigation questions to be answered after the research study.
- Chapter Two – This chapter outlines the technical literature review carried out to determine scholarly concepts of this research. It provides an overview of wind characteristics, wind turbine aerodynamics, its impact on power, as well as the wind turbine generator coupled with electronic controllers, and distribution network. The integration with wind generator challenges, control strategy, standard, and policies are discussed.
- Chapter Three - This chapter details the analytical modelling of wind turbine with respect to both the mechanical and electrical models of subsystems of a wind turbine. These include the analysis of analytical models for the aerodynamic phenomenon at the wind rotor interface and the mechanical model for the gearbox. An overview of the DFIG based wind turbine and its dynamic modelling in stationary and rotating reference frames for the development of machine control and control system aspects are presented. The power converters, distribution grid, and control system models are discussed.
- Chapter Four - This chapter details the work of simulation tools to analyse the steady-state and dynamic impact of the interconnection of wind turbine generators (WTG) to the distribution grid. The explanation of the various MATLAB simulation model was presented as well as the simulation results.
- Chapter Five - This chapter describes the laboratory work and the operation procedure of the DFIG based wind energy conversion system simulator. The description of the experimental set-up that was provided outlines how the test set-up was used to simulate and

evaluate the amount of wind energy introduced and the impact of integration on the network was discussed.

- Chapter Six –This chapter outlines the conclusions of the investigation, the achieved goals and the recommendations of the prospects of possible areas of future study were discussed.

Chapter 2

Literature Review

2.1 Introduction

This chapter introduces a comprehensive assessment done on published and unpublished research works, journal articles, thesis works, electronic and internet documents, e-books and government publications related to the numerical and experimental investigations of the impacts of the integration of wind energy in to the distribution network that will serve as the basis of accomplishing the research goal. Electrical power generation from renewable energy sources has been increasing in the past few years. Wind power is one of the renewable energy sources currently being explored. Consequently, there is an increase in the quantity and size of wind farms installed globally, creating a rapid expansion of the wind energy industry.

The source of wind can be explained as the horizontal movement of air in response to the change in atmospheric pressure [6]. This aerodynamic phenomenon can be converted into electrical power using the wind turbine. The wind turbine aerodynamics are based on the basic principles of fluid-solid interaction with regards to lift and drag, and angle of attack, resulting from the pressure variations. Thus, the resultant thrust on the wind turbine blades causes the rotation of the blades due to differential pressure resulting in lift and drag forces. For blade rotation to occur, the component of the lift force must be greater than the component of the drag force F_D. Wind is erratic and uncertain, and to compensate for the wind's intermittent behaviour on wind turbine operation and control, a wind turbine generator's output forecast planning should be put in place. This valuable tool operates by calculating the standard deviation of the wind turbine generator load compared to the standard deviation of the combined load and wind signal, thereby determining the expected power from the wind turbine. This will help network management schedulers and distributors curb any imbalance in the active power which can consequently cause a partial or total blackout [7]. The natural characteristics of wind have significant challenges with regards to power system stability, economics and load dispatch on the wind turbine power integration into the distribution network. Due to the continuous growth of grid-connected wind farms, it has become necessary to study the behaviour of the wind farms in relation to other power plants and the network in general [8].

Integrating wind power into the distribution network comes with its challenges. To introduce wind power, the grid-connected wind energy system needs to meet certain standards or requirements before being integrated into the grid, these standards are presented later in this

chapter. Wind turbine manufacturers and grid operators have developed Wind Turbine Generators Control System (WTGCS) for connecting Wind turbine generators, through the frequency converters, into the grid while simultaneously disconnecting the wind turbines from the grid during faults which can result in low voltage conditions at the point of common coupling. This is done to prevent damage to the WTGCS components, especially the power electronic converters. The function of this power electronic converter is to regulate the generator speed, consequently adjusting the generator frequency, the voltage at the grid connection, as well as active and reactive power flow. The challenges associated with the penetration level of wind power into the grid were reviewed, and a mitigation plan as documented in literature was studied.

To achieve the goal of this chapter, the following section outlines the characteristic of wind, this was followed by the explanation of wind power and wind turbine. This was followed by the description of the wind energy conversion theory and power impacted on the wind turbine. The chapter concludes with a discussion on the impact of the integration of wind power into the distribution network and the analysis of the control strategies to curb the impact.

2.2 Characteristics of Air Flow

This section describes the characteristic of airflow as a function of altitude. It is well known that air pressure decreases with elevation, and air molecules become more widely spaced with an increase in altitude. As shown in Figure 2.1, the increased intermolecular space results in lower air density and lower air pressure. Changes in air pressure are not solely related to altitude but to the intensity of insolation, the general movement of global circulation, local humidity, and precipitation [6]. The causes of the horizontal variation in air pressure are grouped into two categories: the thermal (caused by temperature change) and the dynamic (related to the rotation of the earth and the broad patterns of air circulation). In an area with cold air such as the poles, the air is denser with a resultant decrease in volume. This causes the air to sink and pressure increases, this indicates the poles are areas where high pressures occur. Conversely, the opposite occurs in the equatorial region.

Thus, the constant low pressure in the equatorial zone and the high pressure at the poles is thermally induced due to uneven heating of the atmosphere by the sun and the irregularities of the earth's surface [6]. The hot air rises from the equator and expands, and the cold air from the poles moves towards the equator resulting in wind. The wind blowing towards the equator from the north and south poles gets deflected due to the earth's self-rotation, known as the Coriolis Effect [6], which is an important factor that affects the wind direction and speed.

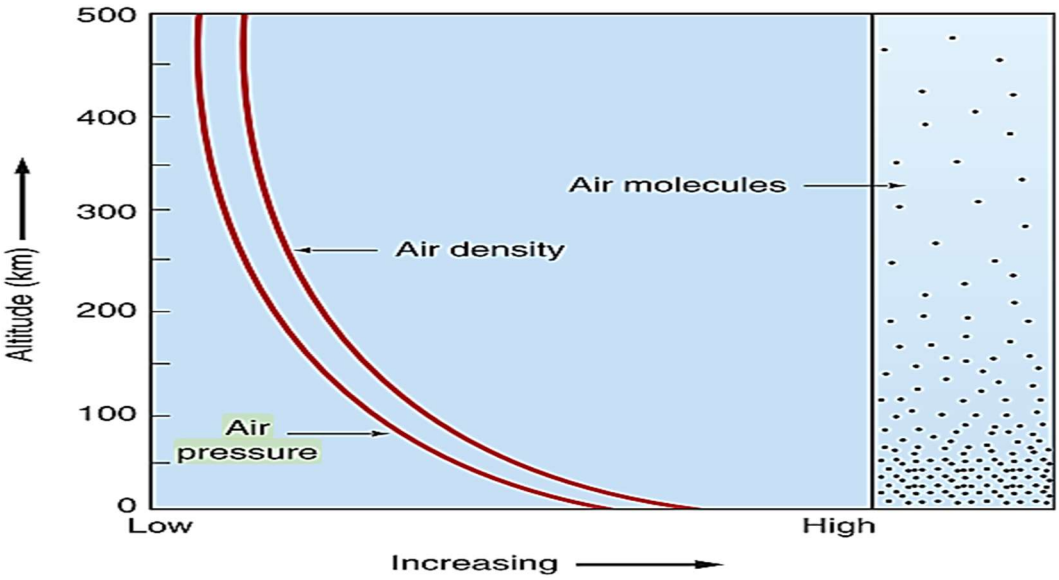

Figure 2.1: The plot of altitude against air pressure and air density [6]

Frictional drag and obstructions near the earth's surface generally retard wind speed and induce a phenomenon known as wind shear. The rate at which wind speed increases with height varies based on local conditions of the topography, terrain, and climate with the greatest rates of increase observed over the roughest terrain. In [6], wind characteristics such as velocity, duration, and direction are defined as varying in nature. Much of their strength depends on the size or strength of the rate of change of atmospheric pressure between two points. The greater this change, the steeper the pressure gradient, hence the faster and stronger will be the wind's speed as shown in Figure 2.2.

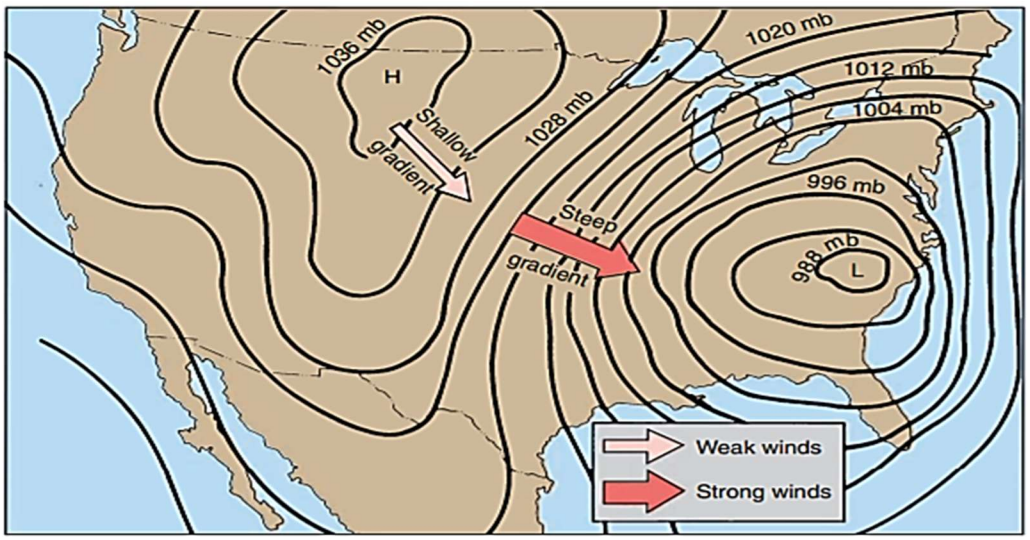

Figure 2.2: The illustration of wind due to the pressure gradient [6]

2.2.1 Erratic nature of Wind Energy

The fluid movement over a plane surface exerts a horizontal force on the surface in the direction of the fluid motion known as the drag force, and this force exerts shearing stress on the surface. The vertical shearing stress parameter is important in analysing wind energy as it flows across a region. As wind flow in the lowest part of the atmosphere, turbulence in the wind is caused by the dissipation of the wind's kinetic energy into thermal energy through the creation of progressive small eddies [9]. This turbulent fluctuation always has a three-dimensional spatial distribution, and visualization of turbulent flow reveals a rotational flow pattern. The problem with the turbulent flow is that small changes can lead to large differences in flow patterns within a short amount of time, hence the turbulence is chaotic and hard to predict. The instantaneous wind speed in three dimensions, u, v, and w can be defined as [9]:

$$u = U + u' \tag{2.1}$$

$$v = V + v' \tag{2.2}$$

$$w = W + w' \tag{2.3}$$

Where, U , V, and W are the short term wind mean speed for the longitudinal, lateral, and vertical directions respectively and u',v', w' are the respective superimposed fluctuating wind [9].

2.2.2 Determination of Wind Speed Probability

The wind conditions close to the ground area, known as the boundary layer, are influenced by the energy transferred from the undisturbed high-energy stream of the geostrophic wind to the layers below as well as by regional conditions. Owing to the roughness of the ground, the local wind stream near the ground is turbulent. The wind speed varies continuously as a function of time and height. The daytime peak depends on daily wind speed variations and the synoptic peak depends on changing weather patterns, which typically vary daily, weekly and also includes the seasonal cycles. Statistically, the wind speed distribution determines the wind density which directly determines the amount of wind power impacted on structures like the rotor blades. Using the Weibull probability function, the wind speed distribution can be determined as [10]:

$$f(V) = \left(\frac{k}{c}\right)\left(\frac{v}{c}\right)^{k1} \exp\left[-\frac{v^k}{c}\right] \tag{2.4}$$

Where, $f(V)$ is the probability of observing wind speed (meter/sec), k is dimensionless constant, and c (meter/sec) as a function of Weibull shape and scale parameters [10]. The most

probable wind speed V_{mp} in (meter/sec) using the k and c parameters, the maximum wind energy can be evaluated by:

$$V_{mp} = c\left(\left(\frac{k-1}{k}\right)\right)^{\frac{1}{k}} \tag{2.5}$$

Hence, the wind turbine operating range can be estimated as $V_{max} \le V_{\infty} \le (2...to...4)V_{max}$ and probable assessment of power density can be obtained using [10]:

$$P = \frac{1}{2}\rho A\int_{0}^{\infty} V^3 f(V)dV \tag{2.6}$$

Where A is the swept area in m^2, ρ is the air density in Kg/m^3 and P is the power in watts [10].

2.3 Concept of Wind Power

When the wind flows over an object of various shapes and sizes, it generates forces. Considering a rectangular-shaped plate, placed at an angle to the path of wind flow, as shown in Figure 2.3, the wind creates a differential pressure across the plate, causing the plate to rotate due to the resultant force, and hence torque is produced [11].

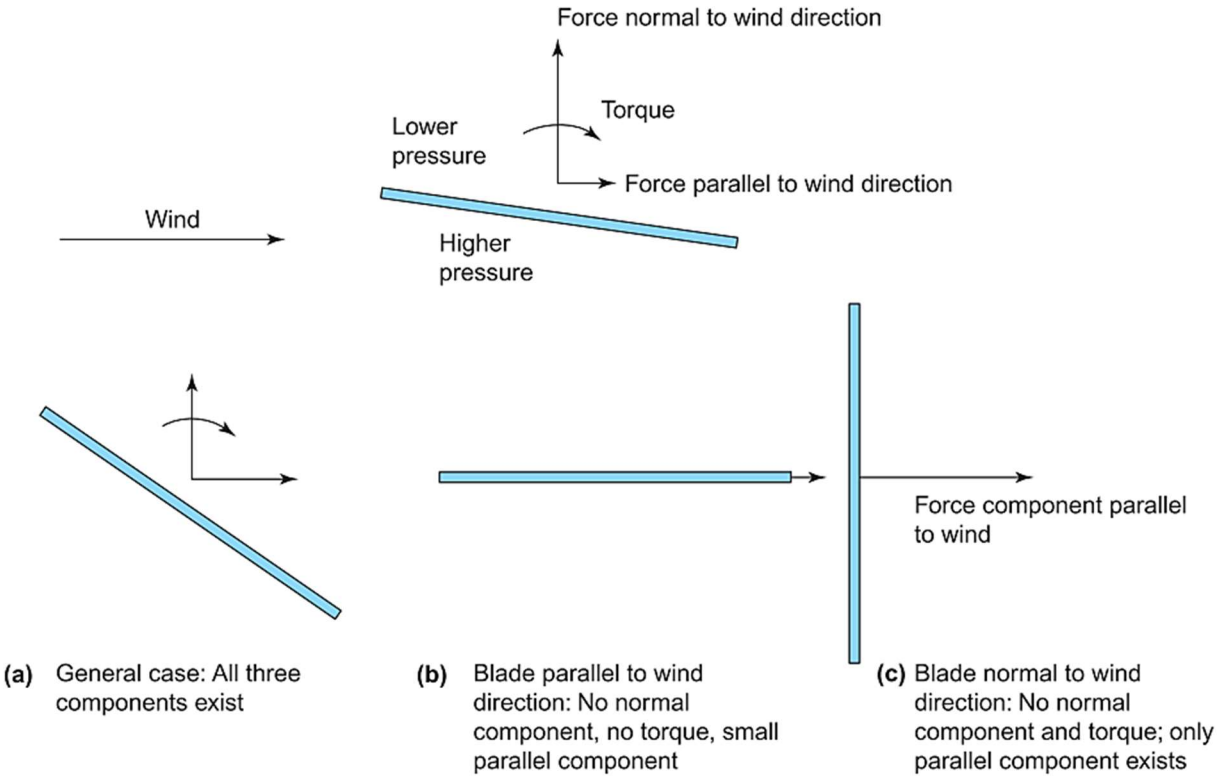

Figure 2.3: Aerodynamic phenomenon of wind on a plate [11]

The angle of inclination of the plate concerning wind direction is called the angle of attack. The force component which is parallel to the wind direction is referred to as aerodynamic F_D which opposes the motion of the blade and this must be minimized. The force component perpendicular to the wind direction is referred to as aerodynamic lift and must be maximized because it is responsible for the rotation of the plate as shown in Figure 2.4. The drag and lift forces are always perpendicular to each other and have an inverse relationship. The magnitudes of lift F_L and drag F_D forces are dependent on the angle of attack and also on the shape of the blade design. When the angle of attack is small, the lift force is larger than the drag force, so as the angle increases the lift decreases, and drag increases. When the angle of attack is at 90 degrees, the lift is zero and the F_D is maximum [11].

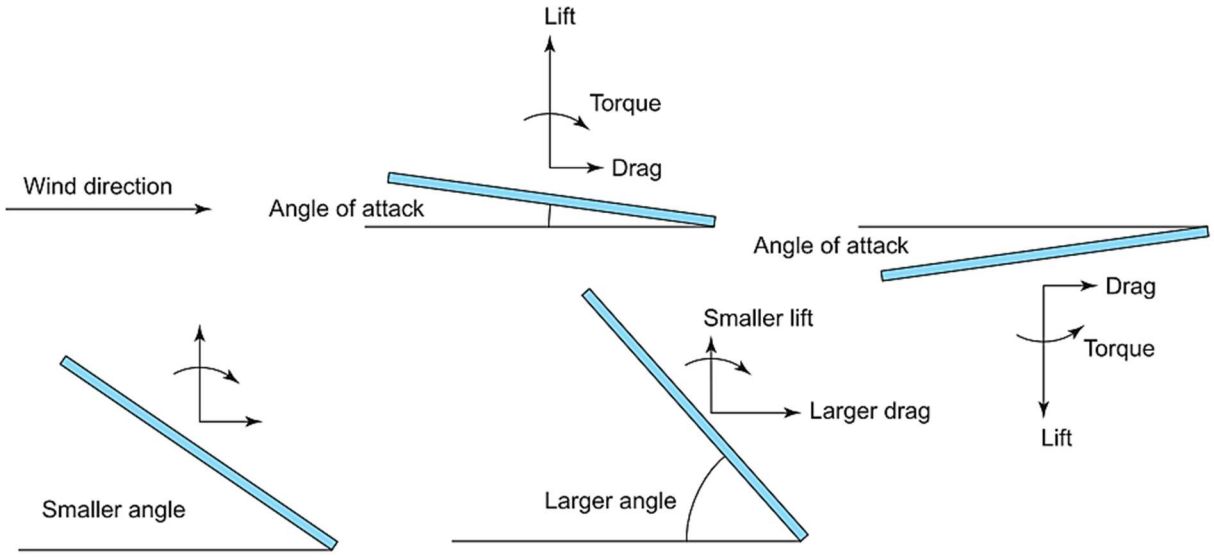

Figure 2.4: Lift and drag forces at a various angle of attack [11]

A better blade design such as the aerofoil can reduce this drag force by bending or twisting the blade and also tapering it along its length which can be used to produce an efficient wind turbine blade. Based on the analysis of the plate, the aerodynamic force F, in Newton, exerted on the plate can be calculated as [10]:

$$F = P \times A = \frac{1}{2} \times \rho \times \left(V_w\right)^2 \times A \tag{2.7}$$

Where A is the surface area in m^2, P is the wind pressure in N/m^2, ρ is the air density in Kg/m^3, and V_w is the wind speed in m/s. Hence, an aerofoil section with a high lift to drag ratio must be chosen for the design of the rotor blade and this is discussed in the next section.

2.3.1 Aerodynamics of Aerofoil

Aerodynamic performance is very important for determining the efficient rotor blade design. The aerofoil profile is formed with a rear side that is much more curved than the front side facing the wind. As shown in Figure 2.5, the two portions of air molecules move side by side in the airflow moving towards the aerofoil profile. At point A the air molecules separate and pass around the profile, once again combine side by side at point B after passing the profile's trailing edge. Air molecules flowing over the rear side have to travel a longer distance from point A to B than the air flowing over the front side [12].

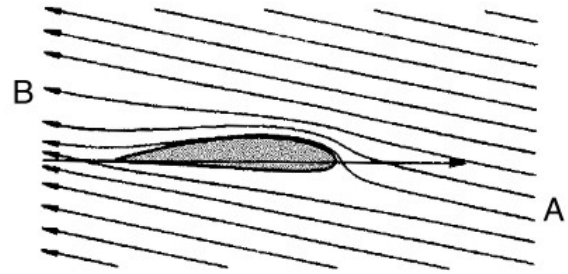

Figure 2.5: Air Flow over the curved aerofoil blade [12]

The air moving over the curved top of the profile travels faster than under the flat side of the profile. This makes a lower pressure area on top and a high-pressure area below the aerofoil, and as a result, the aerofoil blade is subjected to aerodynamic lifting force. Hence, it is essential to maximize this force using an appropriate design of the aerofoil blade which is dependent on the lift and drag coefficients.

Normally, the lift C_L and drag C_D coefficients are the same for similarly shaped objects. However, for unsymmetrical objects with an angle of attack $\emptyset$ the values of C_L and drag C_D are different. The aerodynamic forces F as defined using equation (2.7), as a function of the lift and drag coefficients components are givens as [10]:

$$\mathrm{F}_L = C_L(\phi) \times F \tag{2.8}$$

$$\mathrm{F}_D = C_D(\phi) \times F \tag{2.9}$$

$$\text{Lift to drag ratio} = C_L / C_D \tag{2.10}$$

As shown in Figure 2.6, assuming a symmetrical blade profile and a wind velocity V_{ref} in (m/sec) with an angle of attack $\emptyset$. The F_L and F_D developed by an airflow [10]**:**

$$F_L = \frac{1}{2} \times \rho \times C_L(\phi) \times V_{ref}^2 (c \times b) \tag{2.11}$$

$$F_D = \frac{1}{2} \times \rho \times C_D(\phi) \times V_{ref}^2 (c \times b) \tag{2.12}$$

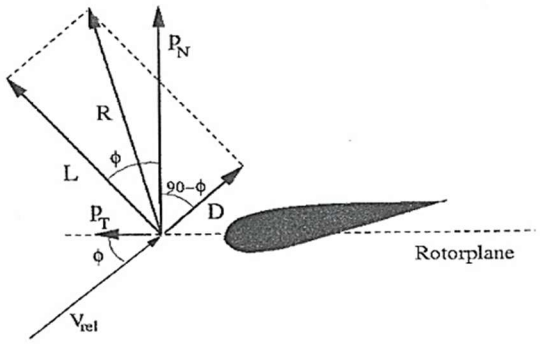

Figure 2.6: A symmetrical blade profile with a wind velocity [13]

The lift coefficient increases linearly with the angle of attack (range $0 < \emptyset < 100$), reduces in the range of ($\emptyset > 150$), and the drag coefficient increases rapidly with the angle of attack $\emptyset$. The resultant of the lift and drag forces constitute the thrust force which effectively rotates the turbine rotor blade.

2.3.2 Wind Turbine Blade: Rotor

A wind turbine rotor blade can be analysed using the fundamental theories of conservation of mass, momentum, energy, and phenomenon of aerodynamics. Hence, the wind turbine rotor blade is a key element in a wind turbine system in converting wind energy into mechanical energy. Modern wind turbines catch the wind by turning into or away from airflows. The wind moves the propellers mounted on a rotor and the movement turns a high-speed shaft via a mechanical gearbox, coupled to an electric or induction generator [13].

As shown in Figure 2.7, at the root, the blade sections have a large width (thick profile) and minimum thickness which is essential for the intensive loads carried by the blade.

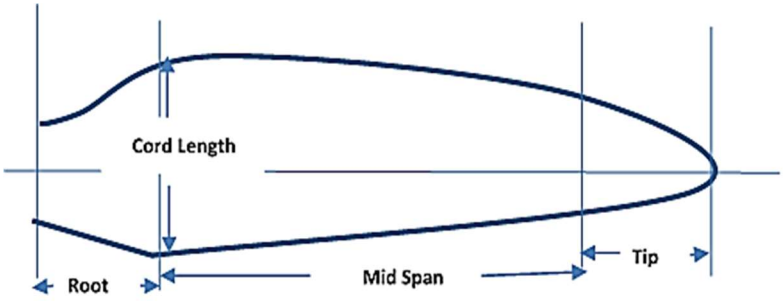

Figure 2.7: Rotor blade design [13]

Rotor blade design parameters such as chord, twist angle, and length are carefully selected to achieve optimum aerodynamic performance. On dividing the rotor blade into small elements, each element acts independently of surrounding elements and operate aerodynamically as two-dimensional aerofoils. The high efficiency of the turbine blades can be achieved by using twisted, tapered propeller-type rotor blades along its length to improve the angle of attack, increasing speed and efficiency while reducing drag. Tapered blades are also stronger and lighter than straight blades as the bending stress is reduced. At times, the stall phenomenon is used to restrict the wind turbine power output by actively varying the stalled process by having a fixed triangular stall strip as shown in Figure 2.8.

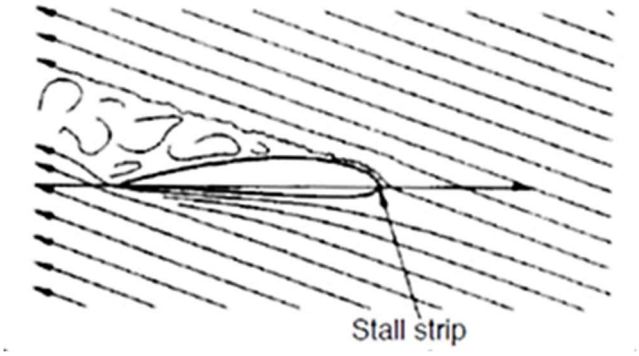

Figure 2.8: Interference in the stalled process (stall strip) [12]

2.4 Wind Turbine

A wind turbine converts the kinetic energy of the wind into mechanical power that drives an alternating current (AC) induction generator to produce electricity [14]. A typical horizontal axis wind turbine and its components are shown in Figure 2.9.

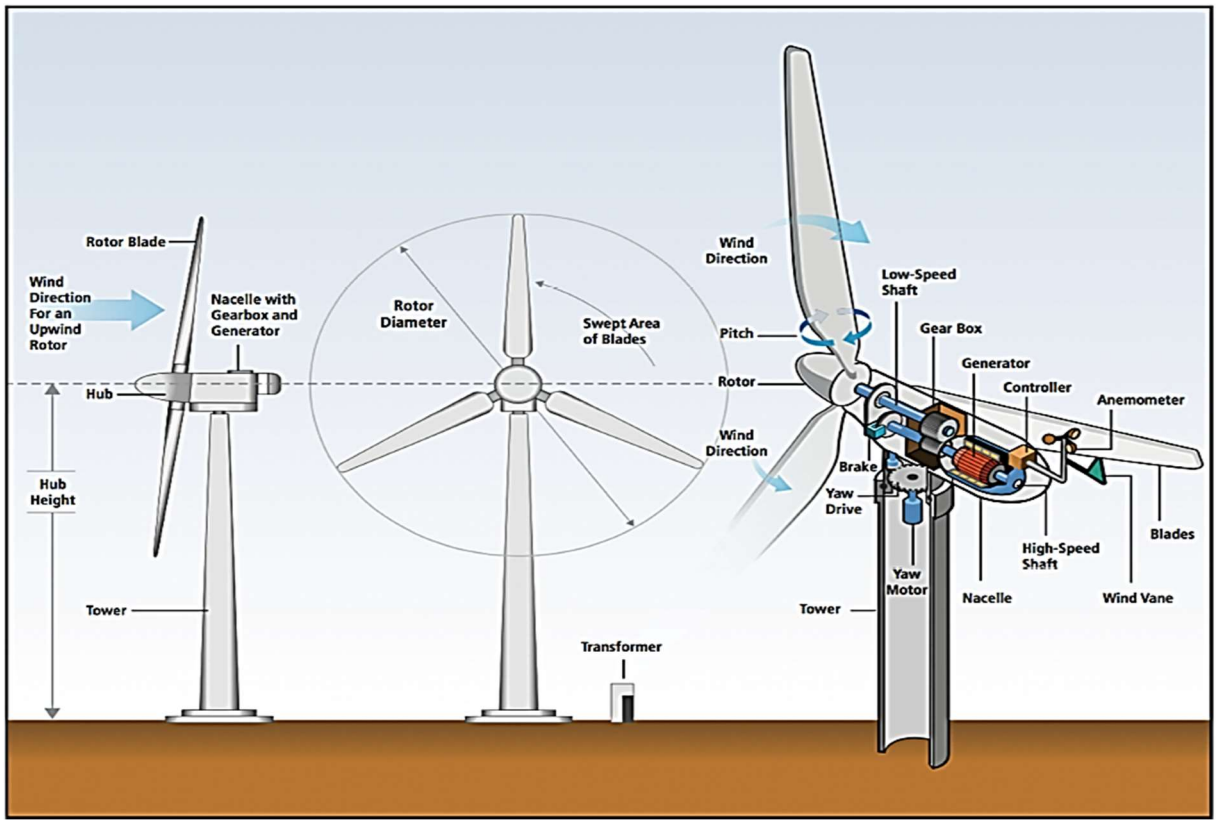

Figure 2.9: Components of a horizontal axis wind turbine [14]

The major components of a wind turbine include a low-speed rotor consisting of three (or two in some cases) light-weight blades with optimum aerofoil shapes operating, a high-speed shaft mechanically coupled to a low-speed shaft via a gearbox assembly, a pitch motor drive assembly, a yaw motor drive assembly, a nacelle, a wind vane indicator, an AC induction generator operating at high speed, a speed controller unit, a tower structure, an anemometer, and other accessories necessary to provide mechanical integrity under heavy wind gusts [14].

The wind turbine blade operation is entirely dependent on the blade design tip speed ratio and the number of blades [13]. The tip speed ratioλ, is defined as the relationship between rotor blade velocity Ω (rad/sec), radius r (meters), and relative wind velocity V_w in (meter/sec), as [10]:

$$\lambda = \frac{\Omega\, r}{V_w} \tag{2.13}$$

$$C_{opt} = \frac{2\pi r}{n} \times \frac{8}{9C_L} \times \frac{U_{wd}}{\lambda V_r} = \frac{2\pi r}{n} \times \frac{8}{9C_L} \times \frac{U_{wd}}{\lambda^2 \sqrt{V_w^2 + U^2}} \tag{2.14}$$

Where, C_{opt} is the optimum cord length of the rotor blade in (meters), n is the quantity, C_L is Lift coefficient, V_r is local resultant air velocity (meter/sec), U is the wind speed in (meter/sec), and U_{wd} is designed wind speed in (meter/sec).

Turbine blade efficiency, torque, mechanical stress, aerodynamics, and noise are considered, which is why a slender aerofoil is preferred and specially designed tip geometries used when selecting the appropriate tip speed. The efficiency of a turbine can be increased with higher tip speeds, which is limited by increased noise (approximately proportional to the sixth power), aerodynamic, and centrifugal stresses [13]. As tabulated in Table 2.1, a higher tip speed requires a reduced chord width which leads to a narrow blade profile. At the same time, an increase in centrifugal and aerodynamic forces is associated with higher tip speeds. This indicates the difficulties that exist with maintaining structural integrity, self-starting, and preventing blade failure.

Table 2.1: Tip speed ratio design consideration table [13]

Tip-Speed Ratio	**Low** ⟵	**High** ⟶
Value	Tip Speed one to two is considered low	Tip Speed higher than 10 is considered high
Utilization	Traditional windmills and water pumps	Mainly single or two blade prototypes
Torque	Increases	Decreases
Efficiency	Decrease significantly below five due to rotational wake created by high torque	Insignificant increase after eight
Centrifugal Stress	Decrease	Increases as a square of rotational velocity
Aerodynamic Stress	Decrease	Increases proportionally with the rotational velocity
Area of Solidity	Increases, multiple 20+ blades required	Decrease significantly
Blade Profile	Large	Significantly narrow
Aerodynamics	Simple	Critical
Noise	Increase to the sixth power approximately	

2.4.1 Wind Turbine Classification

Wind turbines are generally classified as:

- **Lift type turbines:** This form of wind turbines is turned by aerodynamic lift force. As shown in Figure 2.10, the lift propelled wind turbines have blades that resemble wings similar to that of airplanes. These blades move at right angles to the wind direction, at a higher speed than the actual wind speed. They work with the wind, like a sail, instead of against the wind. This is why these kinds of turbines are fundamentally more suitable for harvesting wind energy. Moreover, the blades cover only a fraction of the rotor surface. This means much less material is needed for the rotor. Aside from these advantages, the most important feature of the lift propelled turbine is its high efficiency. The maximum efficiency is 59%, also called the Betz limit, this is the maximum power that can be extracted from the wind in the open flow [15].

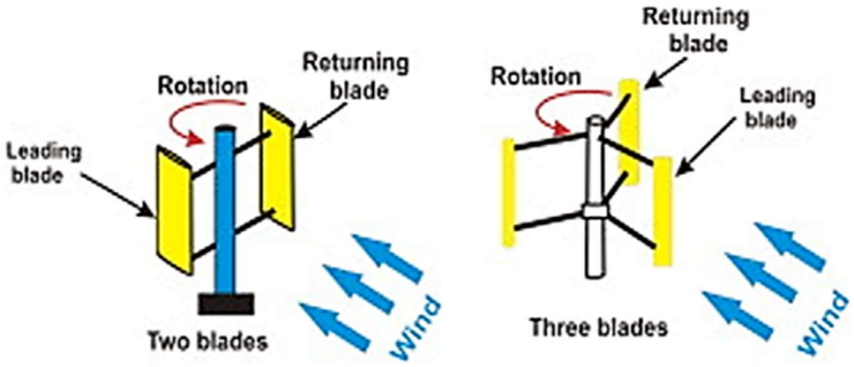

Figure 2.10: Lift type wind turbine VAWT [11]

- **Drag type turbines:** In drag-based wind turbines, the force of the wind pushes against a surface, like an open sail. Figure 2.11 shows a drag-type device, consisting of two scoops. Looking down on the rotor from above, a two-scoop machine would look like an "S" shape in cross-section. Because of the curvature, the scoops experience less drag when moving against the wind than when moving with the wind. The differential drag causes the turbine to spin. Because they are drag-type turbines, they extract much less of the wind's power than other similarly-sized lift-type turbines. Much of the swept area of a drag type turbine rotor may be near the ground, it has a small mount without an extended post, making the overall energy extraction less effective due to the lower wind speed found at lower heights [15].

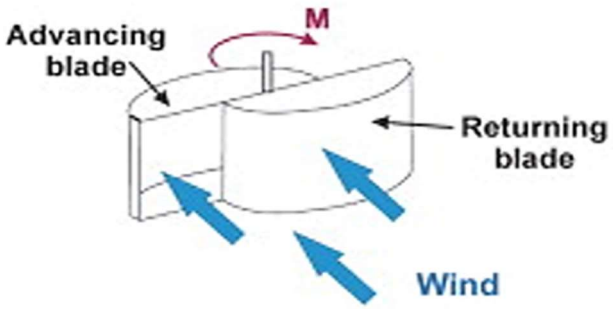

Figure 2.11: Drag type two-scoop turbine [11]

- **Axis type turbines:** These are based on their axis, whether it is horizontal or vertical. The axis here refers to the turbine's main shaft about which the rotating parts revolve. Certain turbine types can work only with a horizontal axis, while others can work with a horizontal or a vertical axis, and can be installed with their axis at an angle. In this sense, a wind turbine can be classified as a horizontal-axis wind turbine (HAWT) or a vertical-axis wind turbine (VAWT) [11]**.** Since in most cases wind blows horizontally, a horizontal-axis wind turbine is sensitive to the wind direction and changes. However, this is not factual for a vertical axis wind turbine, because, such a turbine can catch the wind in any direction. Another advantage of a vertical-axis turbine is the fact that not all the accessories such as the generator and gearbox need to be on the top of the tower, as is usually the case for a horizontal axis wind turbine. Therefore, they are easier to access when necessary.
- **Propeller Wind turbine:** A propeller wind turbine is the most popular wind turbine in use with a configuration for the three rotor blades installed on top of a tower. A propeller wind turbine works based on lift force as the wind flows perpendicular to the blade. The propeller wind turbines can be installed either downwind or upwind direction as shown in Figure 2.12.

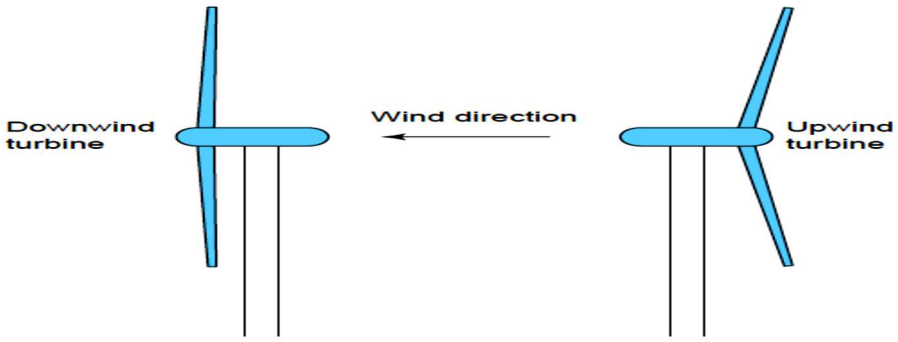

Figure 2.12: Two differently installed propeller horizontal axis Wind Turbines [11]

- **Vertical axis H rotor wind turbine:** As shown in Figure 2.13, a vertical axis turbine has an active vertical blade segment in an "H" shape connected to the moving turbine shaft. The two lift forces on the blades of an H-rotor generate a torque around the turbine shaft which rotates the turbine. During operation, one blade is upwind and the other blade is downwind. The aerodynamic angle of attack varies constantly for each blade during rotation. The downwind blade moves 180 degrees to 360 degrees wake of the upwind blade, and thus, captures less energy than the other blade due to the reduced wind speed caused by the upwind blade energy extraction. It's recommended to have three or more blades for an H-rotor as compared to two blades of this kind of wind turbine, to avoid pulsation.

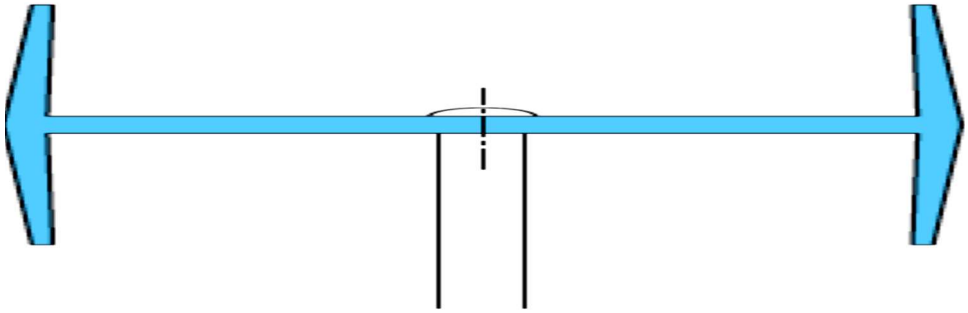

Figure 2.13: Schematic of H rotor vertical axis turbine [11]

2.5 Wind Energy Conversion Theory

The wind energy conversion system (WECS) includes wind turbine rotor blades, gearbox, generators, control systems, and interconnection apparatus in different sizes and types, depending on the power generating capacity and the rotor design deployed. Wind power is captured by the blades of the turbine and converted to mechanical power. The mechanical power is transferred through the gearbox to the generator where it is converted to electrical power. The gearbox synchronizes the low speed of the turbine rotor into a high speed that is coupled with the generator. The generators used for the wind energy conversion system are generally either the DFIG or permanent magnet synchronous generator (PMSG) types. The wind turbine electrical and mechanical parts are mostly linear, however, the blade aerodynamics of the wind turbine are nonlinear, and hence the overall system model becomes nonlinear.

2.5.1 Maximum Power Conversion

Albert Betz [16] developed the theory of wind machines at the Gottingen Institute in Germany. In the late 1920s. A. Betz was able to evaluate the maximum power extractable by an ideal turbine rotor from wind. The Betz equation deals with the wind turbine's limitations in term of efficiency and this can instigated by decelerating the upstream wind speed V_1 to its downstream

wind speed V_2 due to the viscous and pressure drag on the rotor blades. The ideal wind rotor is taken at rest and is placed in a moving fluid atmosphere, as shown in Figure 2.14.

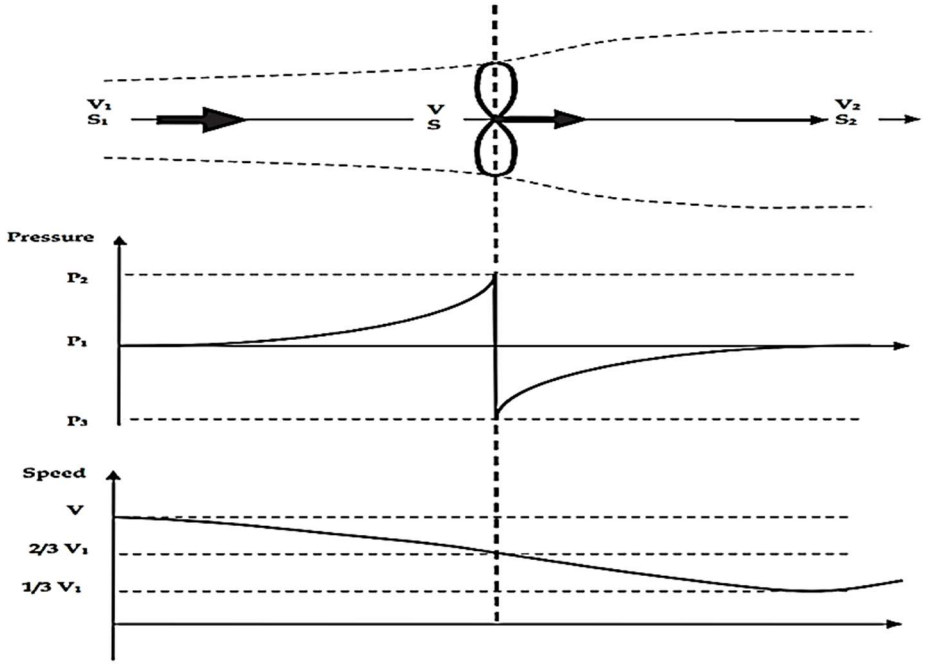

Figure 2.14: Pressure and speed variation in an ideal model of a wind machine [17]

As per the ideal model shown in Figure 2.14, the cross-sectional area swept by the turbine blade is designated as S with the air cross-section upwind from the rotor designated as S_1, and downwind as S_2. The wind speed passing through the turbine rotor is considered uniform as V, with its value as V_1 upwind, and as V_2 downwind at a distance from the rotor. Extraction of mechanical energy by the rotor occurs by reducing the kinetic energy of the air stream from upwind to downwind, or simply applying a braking action on the wind [16]. Using the proper units for measuring mass, M of the air that flows in one second, at a speed V (m/s), the relationship to determine the energy, E in (joules/s), of a moving object [10]:

$$E = \frac{1}{2} \times M \times (V)^2 \tag{2.15}$$

$$M = \rho \times S \times V \tag{2.16}$$

Hence, the amount of energy P (watts) in one sec for the area is given by a pipe cross-section of the size of an object in the stream of an open flow with no boundary [10].

$$P = \frac{1}{2} \times \rho \times S \times V^3 \tag{2.17}$$

Betz Limit and Power Coefficient C_p is the ratio of power extracted by the turbine kinetic power P_t to the total contained in the wind resource P_w [10].

$$C_p = \frac{P_t}{P_w} = \frac{16}{27} = 0.59259 = 59\% \quad (2.18)$$

The 59 % efficiency is the best a conventional wind turbine can do in extracting power from the wind power [17].

2.5.2 Power Impacted on Wind Turbine

The wind speed passing through the turbine rotor is considered uniform as V (m/s), where the downwind velocity V_2 < its upwind value V_1, and downwind air cross-sectional area S_2 > its upwind air cross-sectional area S_1 [16]. The air pressure in front of the turbine increases and perceives a sudden drop at the fluid-turbine interface, which can be interpreted as responsible for the creation of suction on the other side. The suction effect in turn creates a vortex of the train, which in turn enhances the energy extraction process by further reducing the pressure behind the turbine.

Hence, the conservation of mass can be written as [16]:

$$m = \rho \times S_1 \times V_1 = \rho \times S \times V = \rho \times S_2 \times V_2 = K, \text{ where } K \text{ is a constant} \quad (2.19)$$

As per the Euler's theorem, the force exerted by the wind on the rotor [16]:

$$F = m \times a = m \times \frac{dV}{dt} = \rho \times S \times V \left(V_1 - V_2\right) \quad (2.20)$$

Hence, the incremental work is done by air stream [16]:

$$dE = Fdx \quad (2.21)$$

Power content of the wind stream in watts [16]:

$$P = \frac{dE}{dt} = F \frac{dx}{dt} = F \times V = \rho S V^2 \left(V_1 - V_2\right) \quad (2.22)$$

Power extraction of the ideal turbine requirement, considering $V_2 = 1/3\, V_1$ [16]**:**

$$P_m = P_{upwind} - P_{downwind} \quad (2.23)$$

As suggested by Betz equation that a wind turbine can extract at most 59.25% of the energy in an undistributed wind stream. Including this into equation (2.23) will result to [16]:

$$P_m = \frac{1}{2}\rho S_1 V_1^3 - \frac{1}{2}\rho S_2 V_2^3 = \frac{16}{27} \times \frac{1}{2} \times \rho S V_1^3 = 0.59 \times \frac{1}{2} \times \rho S V_1^3 \quad (2.24)$$

By considering the additional losses such as friction, blade surface roughness, and mechanical imperfections, the wind power extraction is further lowered to 35-40%. Power in watts for the rotor diameter [16]:

$$P_{\text{ideal max}} = \frac{16}{27} \times \frac{\rho}{2} \times V_1^3 \times \frac{\pi \times D^2}{4} \tag{2.25}$$

Hence, $P_{ideal\ max}$ increases as the square of the rotor diameter and more significantly as the cube of the wind speed [16].

The air density is a function of air pressure and air temperature, above sea level [18]:

$$\rho(z) = \frac{\rho_0}{RT} \exp\left(\frac{-gz}{RT}\right) \tag{2.26}$$

Where $\rho(z)$ is air density as a function of altitude in kg/m^3, ρ_0 is standard sea-level atmospheric density in Kg/m^3, R is the specific gas constant for air $287.05 J/Kg - K$, g is the gravity constant 9.81 m/s^2, T is temperature Kelvin, z is the altitude above sea level in meters [18].

The coefficient of performance is the fraction of the wind power extracted by a wind turbine [18]:

$$C_p = \frac{P_m}{\frac{1}{2}\rho S V^3} \tag{2.27}$$

2.5.3 Wind Turbine Power Output

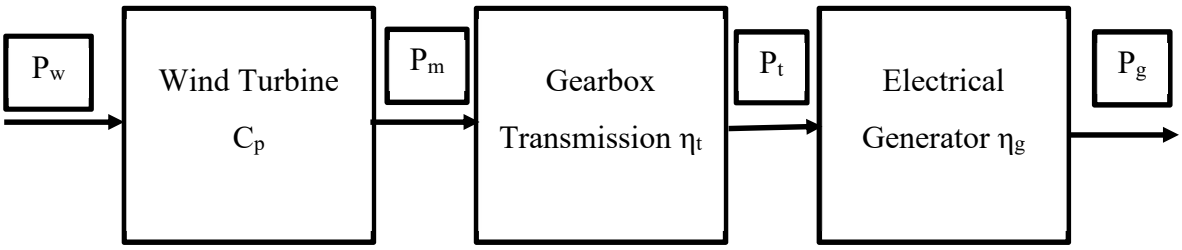

Figure 2.15: Wind Turbine efficiencies block [18]

The wind turbine efficiency block diagram as shown in Figure 2.15 is used to illustrate the power flow from the rotor blades to the power out from the generator.

Thus, the actual mechanical power in the rotation of the rotor blades in watts is [18]:

$$P_m = C_p \times \frac{1}{2}\rho S V^3 = C_p \times P_w \tag{2.28}$$

The mechanical power in the rotor blade rotation is coupled to the gearbox introducing a transmission or gearbox efficiency, so the gearbox transmission power in watts is given by [18]:

$$P_t = C_p \times \eta_t \times \frac{1}{2}\rho S V_1^3 = C_p \times \eta_t \times P_W \tag{2.29}$$

The power from the electrical generator can be evaluated as [18]:

$$P_g = C_p \times \eta_t \times \eta_g \times \frac{1}{2}\rho S V_1^3 = C_p \times \eta_t \times \eta_g \times P_W \tag{2.30}$$

The actual electrical production will be further affected by the plant capacity factor (PCF), so the actual electrical power generation of the wind turbine in watts at its rated speed [18]:

$$P_e = CF \times C_p \times \eta_t \times \eta_g \times \frac{1}{2}\rho S V_1^3 = CF \times C_p \times \eta_t \times \eta_g \times P_W \tag{2.31}$$

The power production of a wind power plant is related to the wind speed. The available energy in the wind varies with the cube of the wind speed. Hence, a 10 % increase in wind speed will result in a 30 % increase in available energy from the generator. The power curve of a wind turbine as shown in figure 2.16, illustrate the relationship between cut-in wind speed (the speed at which the wind turbine starts to operate) and the rated capacity. The wind turbine usually reaches rated capacity at a wind speed of between 12 m/s -16 m/s, depending on the design of the individual wind turbine [18].

If the wind speed exceeds the cut-out wind speed (i.e. 25 meters/sec for the wind turbine as in Figure 2.16) the turbine shuts down and stops producing energy. When the wind drops below cut-out wind speed, the turbines will not immediately start operating again. There may be a substantial delay, depending on the individual wind turbine technology (pitch, stall, and variable speed) and the wind regime in which the turbine operates.

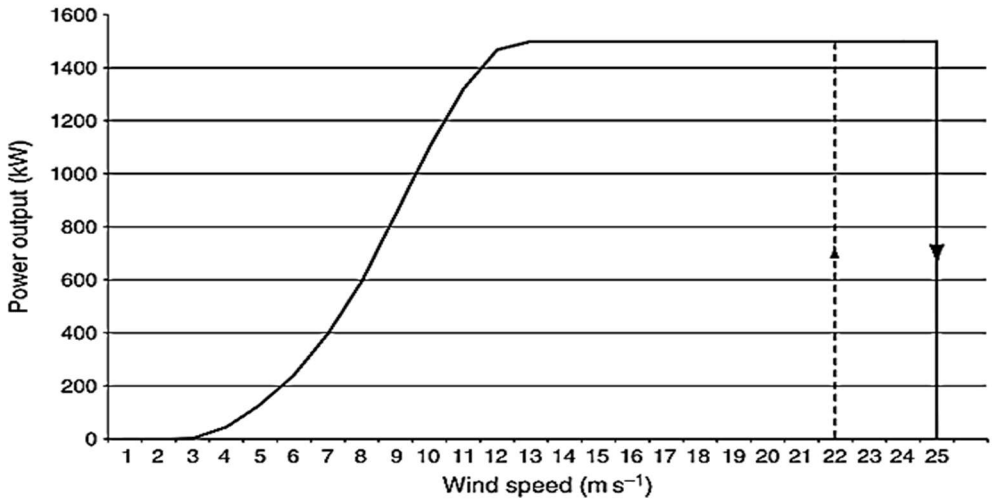

Figure 2.16: Power output of wind turbine vs wind speed [18]

The restart of a wind turbine also referred to as the hysteresis loop (shown as the broken line in Figure 2.16), usually requires a drop in wind speed of 3 to 4 (meter/sec).

2.6 Type of Wind Turbine-Generator Systems

Various types of wind turbine–generator systems can be employed to generate electrical power and they can be broadly classified as either fixed-speed (Type-1 and Type-2) or variable-speed systems (Type-3 and Type-4). Figure 2.17, shows a simplified schematic of a Type-1 wind power system. It is composed of a wind turbine coupled with an asynchronous generator via a gearbox to interface the slowly rotating turbine shaft and generator with higher rotor speed N_r [14]. In this type, the asynchronous generator is a squirrel cage induction machine that produces power when operated above the synchronous speed. In this type of wind power system, the machine is directly connected to the grid without any power electronic interface. Since the asynchronous machine consumes reactive power, it is equipped with shunt capacitors, as seen in Figure 2.17. For a constant wind speed under steady-state, the turbine speed is almost linearly related to the torque. With a sudden change of wind speed, the inertia of the rotating mass including the turbine, drive train, and generator rotor results in a slow change in rotor speed and power output.

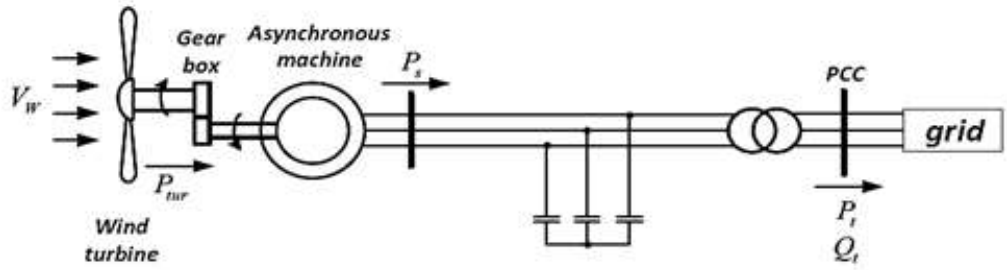

Figure 2.17: Schematic of a constant speed wind power system [14]

Figure 2.18, shows the schematic of a Type-2 wind turbine. It is very similar to the Type-1 system as it also uses an asynchronous machine, in this case, a variable resistor wound-rotor induction generator, directly connected to the grid and requires shunt capacitors for supplying reactive power. The variable resistors can be introduced by using the power electronic switches. These switches and their controller module can be separately connected to the rotor winding using slip rings or they can be mounted on the rotor, eliminating the slip ring. These variable resistors can control the rotor currents very fast and help maintain constant power output in the presence of wind gusts. They can also improve the dynamic response of the machine during system disturbances. Similar to Type-1 turbines, the asynchronous machines provide power output when operated above the synchronous speed [14].

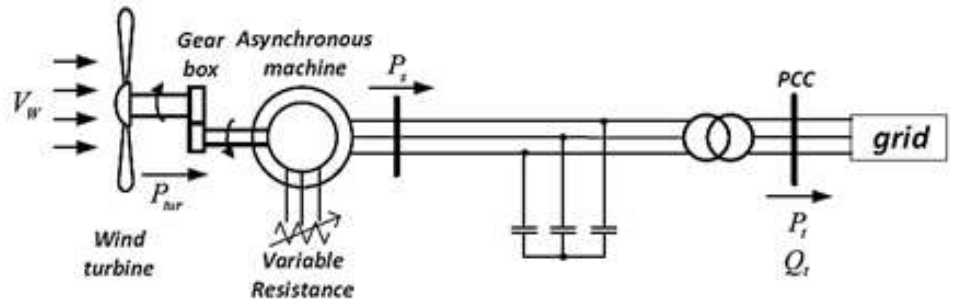

Figure 2.18: Schematic of variable speed wind power system based on a synchronous generator and converter [14]

Figure 2.19, shows a Type-3 wind generator, which is based on the (DFIG) topology. In this case, the asynchronous machine is a wound-rotor induction generator. A power electronic converter system consisting of two AC–DC and DC–AC, voltage source converters (VSCs) in the back-to-back configuration is used, which allows bidirectional power exchange between the generator rotor and the grid. The VSCs connected to the rotor is called the rotor-side converter (RSC), and the VSC connected to the stator terminals is called the grid-side converter (GSC). Each of RSC and GSC typically has a rating of 25%–30% of the rating of the generator. As can be seen from Figure 2.19, the stator of DFIG is directly connected to the grid and hence the stator frequency is determined by the grid frequency [14].

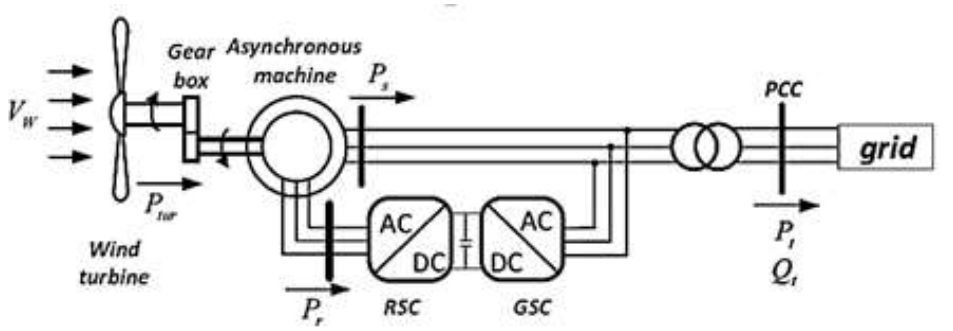

Figure 2.19: Schematic of variable speed wind power system based on DFIG [14]

Both the RSC and GSC can provide the reactive power demanded by the asynchronous machine. When the wind speed changes, the RSC can regulate the speed of the rotor to extract maximum power from the turbine, as seen in the turbine characteristics in Figure 2.20, which leads to a variable rotor frequency. This operation is known as maximum power point tracking (MPPT).

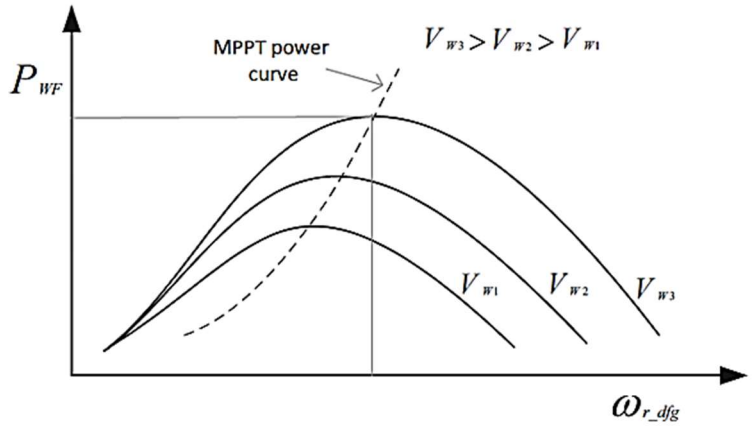

Figure 2.20: Torque – Speed characteristics of wind turbine across different speeds [14]

Type-3 wind turbines can generate power at sub-synchronous and super synchronous speeds of the generator, and are therefore called “variable-speed” turbines.

A Type-4 wind energy system is illustrated in Figure 2.21, based on a full converter (FC) topology. Here, the stator is connected to the grid via two (BB) AC–DC and DC–AC VSCs. Each of these has the same rating as the generator. The generator can be an asynchronous generator (squirrel-cage induction machine) or an asynchronous generator (with rotor exciter or with permanent magnet rotor). The turbine–generator mechanical interface may or may not include a gearbox. The latter option is known as the “direct drive” option, which becomes realistic when a synchronous machine with a high number of poles is used because such a generator can operate at a low speed. The converter system adjusts the frequency of stator circuit excitation to allow a variable rotor speed demanded by the MPPT operation. Most modern wind farms are based on Type 3 and Type 4 wind turbines [14].

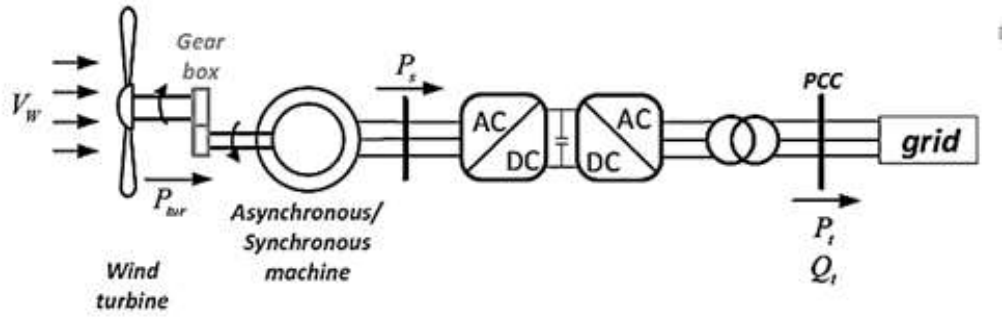

Figure 2.21: Schematic of variable speed wind power system based on PMSG and converter [14]

2.7 Type of Wind Turbine Generators

The rotating electrical machines are commonly used in wind energy systems and most of these electrical machines can function as either a motor or a generator, depending upon their particular application. The growing popularity in the use of an induction machine operating as a generator for low-cost electric power generation from renewable energy sources such as wind. Figure 2.22 shows the variable speed wind energy converter topologies [5].

For economy and reliability, many wind power turbines use induction motors as generators which are driven by a mechanical gearbox, designed to increase their speed of rotation. WTGs can be divided into the following categories either the synchronous or asynchronous generator, the fixed-speed wind turbines, or the variable-speed wind turbine generator.

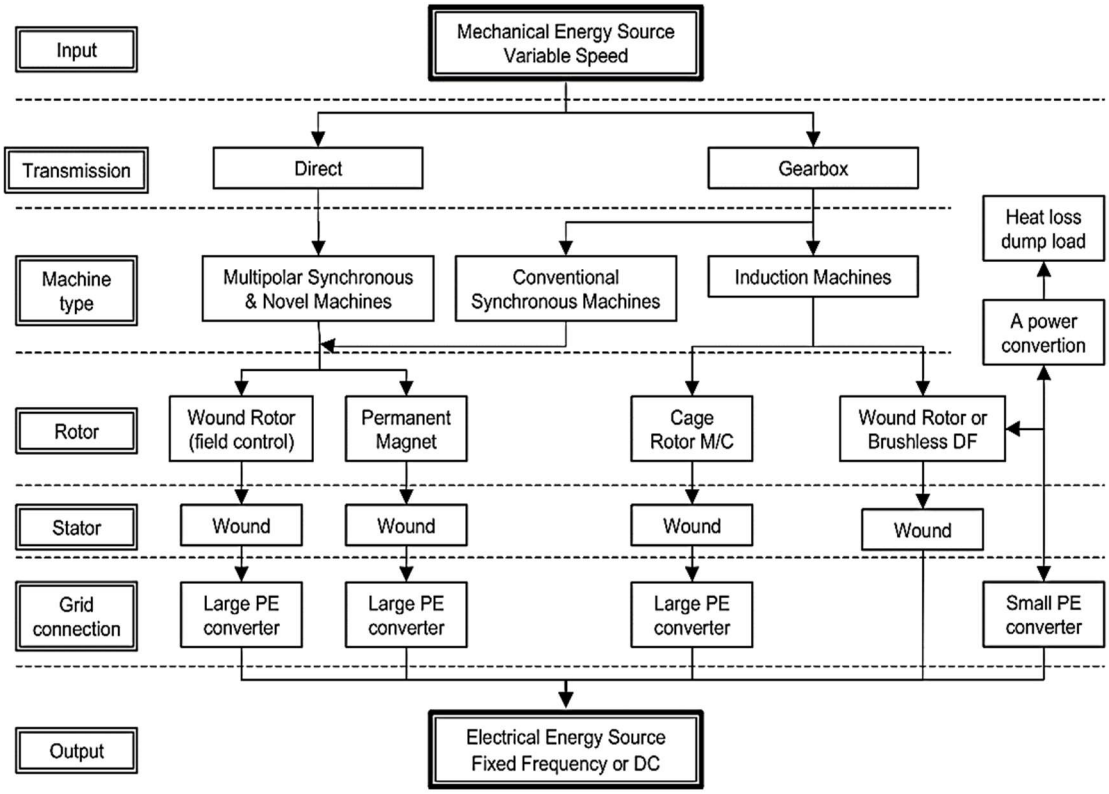

Figure 2.22: Variable speed wind energy converter topologies [19]

2.7.1 Synchronous Generators

The synchronous generator does not require a reactive magnetizing current; the magnetic field of the synchronous generator can be generated using a permanent magnet or field windings. It is suitable for total power control because it uses the power electronic converter to transfer power to the grid but its cost implication and mechanical complexity make induction generators preferable [20]. The synchronous generator used in a wind turbine can be a wound-rotor

synchronous generator (WRSG) or PMSG, as shown in Figure 2.23. The WRSG consists of a stator directly connected to the grid and a rotor excited by direct current from slip rings and brushes. In the rotor winding, the flow of direct current generates an excitation field that rotates at synchronous speed [5].

The synchronous speed is determined by the frequency of the rotating field and the number of poles [19]. The PMSG employs full power conversion from the converters to modify the voltage and frequency generated to match the voltage and frequency of the grid or load. The stator of the PMSG is wound and the rotor has a permanent magnet pole system. The excitation needed is provided without energy dissipation as compared to induction generators.

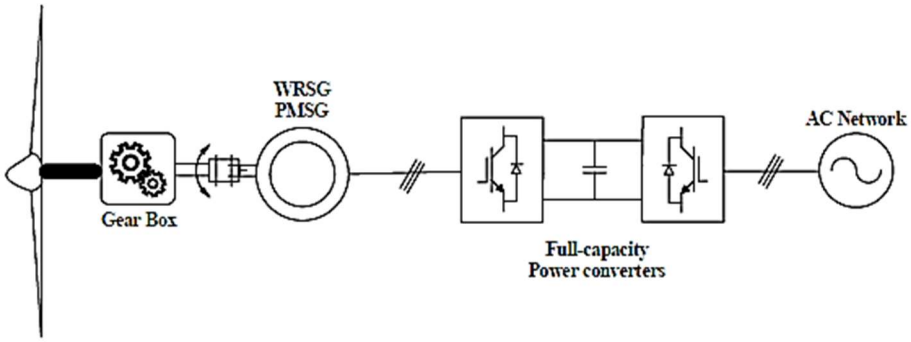

Figure 2.23: Wound Rotor or Permanent Magnet Synchronous Generator [21]

2.7.2 Induction Generators

Induction machines are sometimes used as a generator, which is known as induction generators or asynchronous generators. An induction machine will behave as an induction generator when:

- Slip becomes negative due to this the rotor current and rotor electromagnetic force attains a negative value.
- The prime mover torque becomes the opposite of electric torque.

It is the most widely used generator in wind turbines because it is mechanically simple, cheap, low maintenance, longer life span (over 50 years), and reduced power to weight ratio than conventional synchronous generators. The induction generator produces power by mechanically rotating the rotor above the synchronous speed. It does not use a permanent magnet and therefore needs excitation from an external source thereby consuming reactive power [22].

The induction generator is not a self-excited machine. Therefore, when running as a generator, the machine takes reactive power from the AC power line and supplies active power back into

the line. Reactive power is needed for producing a rotating magnetic field. The active power supplied back in the line is proportional to slip above the synchronous speed. Self-excited induction generators produce useful power even at varying rotor speeds. Hence, they are suitable for wind turbines.

An example of a generator rotating due to a prime mover is observed in Figure 2.24. Advantages of induction or asynchronous generators are being more rugged, relatively cheaper, small size per kW output power, no synchronization with the supply line is required, and no commutator and brush arrangement like a synchronous generator. The major disadvantages of induction generators are that they take a large amount of reactive power [22].

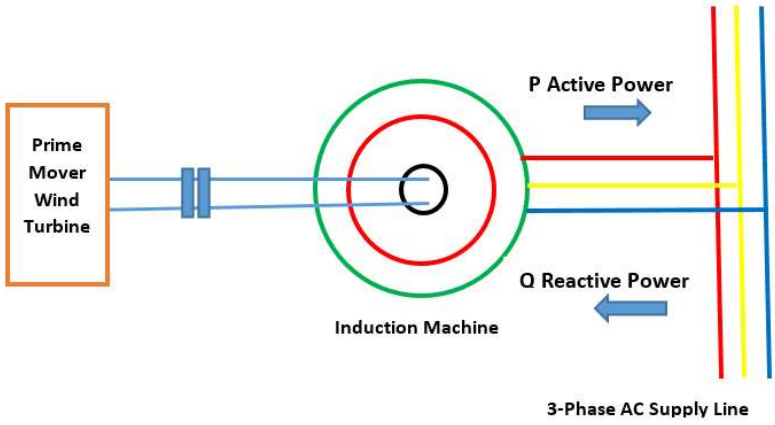

Figure 2.24: Induction Generator with Wind Turbine as Prime Mover [23]

2.7.3 Squirrel Cage Induction Generator (SCIG)

The SCIG which found its application in the early technology in wind turbine system, is coupled to the turbine by a gearbox. The stator is connected directly to the grid with a transformer in between as shown in Figure 2.25. The rotor of the SCIG rotates at a speed directly proportional to the grid frequency and generates a real power (P) when the turbine shaft rotates faster than the electrical grid frequency, creating a negative slip. Normal operating slips for this induction generator is between 0 % and -1 %.

At high wind speed, active power generation increases leading to uncontrolled and increased reactive power absorption from the grid, this could cause grid instability. This generator has a very low full load power factor due to the absorption of magnetizing current from the grid during start-up. The pitch angle is controlled using active-stall control to permit soft-starting without power electronic converters [24]. SCIG application in FSWT implies that the fluctuations in wind speed will result in varying output power transferred to the grid.

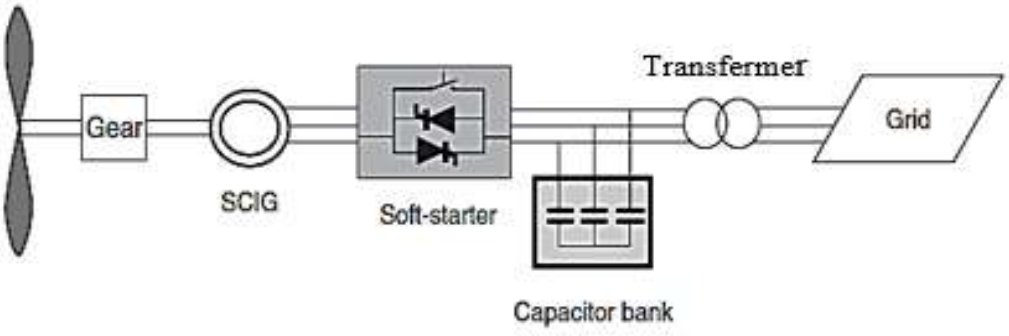

Figure 2.25: Grid-connected SCIG [18]

2.7.4 Wound Rotor Induction Generator (WRIG)

As shown in Figure 2.26, the configuration of the WRIG finds application in variable-speed wind turbines. The WRIG differs from the SCIG because the rotor and the stator can be excited independently but it is expensive compared to the SCIG. The rotor can be excited from an external source using the power electronic converter [20][19].

The WRIG can be a variable resistance induction generator also known as OptiSlip induction generator (OSIG) or DFIG [19]. For these generator, the slip is varied by adjusting the resistance of the rotor and the stator is directly connected to the grid. The OSIG is simple, has less mechanical stress, reduced power fluctuations when compared with the SCIG. Its drawbacks are that the speed range is proportional to the size of the variable rotor resistance making it less cost-ineffective, with ineffective control of reactive power, and power losses as a result of slip power in the variable resistor.

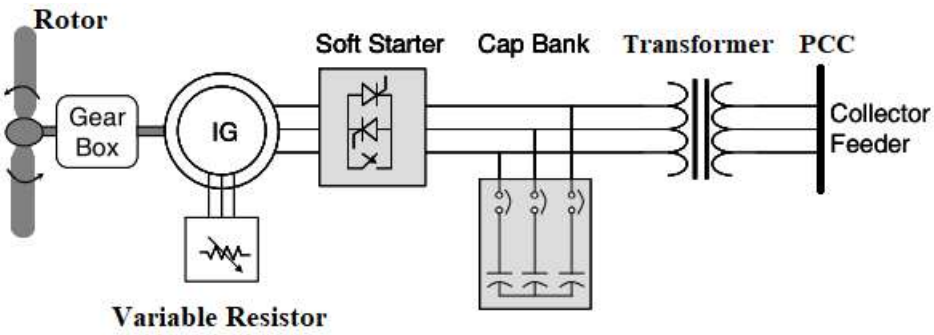

Figure 2.26: Wound Rotor Induction Generator [20]

2.7.5 Doubly Fed Induction Generator (DFIG)

In the DFIG, the stator is connected directly to the grid and the rotor is connected via power electronic converters to the grid as shown in Figure 2.27. The power electronic converter is

mostly a voltage-source converter (VSC) that uses an insulated gate bipolar transistor (IGBT) scheme. The grid supplies the stator voltage and the converter supplies the rotor voltage. The converter supplies the rotor with the current of variable frequency to compensate for the difference in the frequency of the turbine and frequency of the grid. Because of this, double-fed induction generators can be directly connected to the AC power network and remain synchronized at all times with the AC power network. The DFIG can control active and reactive power by controlling the excitation current in the rotor independently, generate reactive power to be transmitted to the stator by the GSC [25].

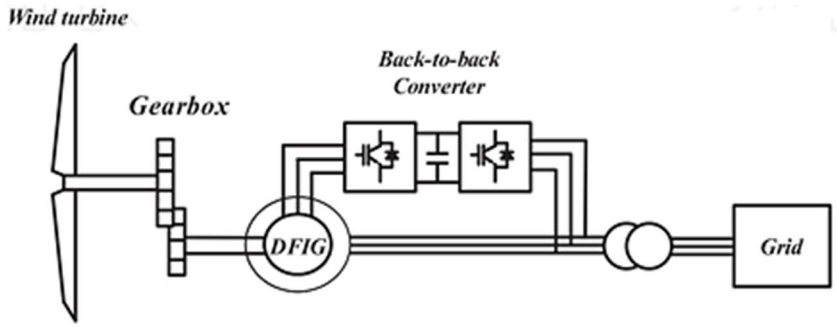

Figure 2.27: Grid-connected DFIG [25]

Theoretically, there is the absence of reactive power flow at the stator because the GSC operates at unity power factor. A major benefit of the DFIG which has made it widely used is the fact that power electronic converters in the rotor circuit handle about one-quarter of the rated power. This implies reduced losses and cost in comparison to wind turbines that uses full-power converters.

2.7.6 Variable-Speed Generators

During the last few years, the variable speed wind turbines with a self-excited Induction generator (SEIG) has dominated the WECS. There are several reasons for using variable-speed SEIG based wind turbines [26]; including:

(i) Possibilities to reduce stresses on the mechanical structure,

(ii) Acoustic noise reduction

(iii) The possibility to control active and reactive power.

The fixed-speed generator has a low efficiency of wind power conversion and cannot provide reactive power support. The most widely used variable speed generator DFIG in the wind turbine system is shown in Figure 2.28.

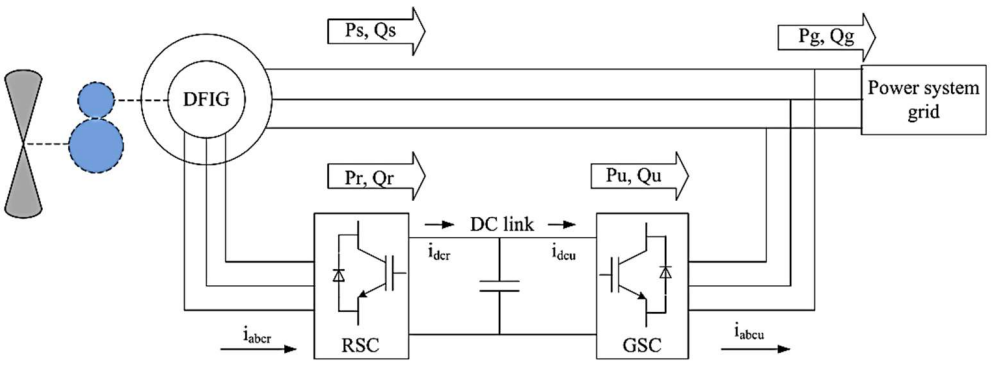

Figure 2.28: DFIG Configuration [26]

The stator is connected, either directly or through a transformer depending on the level of its output voltage concerning the grid voltage, to the grid bus. It also has a wound rotor which is brought out through slip rings and carbon brushes connect to a power electronic converter (PEC) and then either directly or through a transformer, to the stator terminals [26].

As indicated in Figure 2.28, is the DC link. The prime purpose of the dc-link is to maintain the constant voltage.

Advantage of variable speed generators are:

1. Complete control of the reactive power using the RSC and the GSC.
2. Rotor speed can vary ±33% from the synchronous speed of the machine.
3. The converters for this topology needs to be rated, at most, around 25% to 30% for supplying slip power to the machine. This reduces the size of power electronic switches as well as the losses in the converter; and
4. Four quadrant active and reactive power flow capabilities with constant frequency [26].

2.8 Control Strategy

Power electronics have found a very useful application in the wind power system because they are used to synchronise the characteristics of the wind turbine with the grid connection requirements such as voltage, frequency, harmonics, as well as active and reactive power to achieve high efficiency [32]. A basic power electronic converter consists of a rectifier, a capacitor, and an inverter. The rectifier is a diode and the inverter is majorly an IGBT. The difference in power output characteristics of the fixed speed wind turbine (FSWT) generating system and variable speed wind turbine (VSWT) generating system is due to the power electronic converters present in the latter.

This section presents the prevailing situation of generators and power electronics in wind turbine generation systems in terms of the control strategies of the output power from the wind turbine.

2.8.1 Power Electronics for Wind Turbine

The wind turbines can operate either with a fixed or variable speed. In the early 1990s, the wind turbines were operated at a fixed speed, determined by the frequency of the supply grid. In recent years, the variable-speed wind turbine has become the dominant type used in wind turbines. These turbines are designed to achieve maximum aerodynamic efficiency, equipped with a synchronous generator, and connected to the grid through a power converter [27]. The power fluctuations caused by a wide range of wind speed V_w variations are absorbed mainly by changes in the rotor generator speed and consequently accelerate or decelerate the rotational speed over a wide range of wind, keeping the generator torque constant. In this way, the tip speed ratio is kept constant at a predefined value that corresponds to the maximum power coefficient.

The advantages of variable-speed wind turbines are an increase of the energy captured, improved power quality, and reduced mechanical stress on the wind turbine. The disadvantages are losses in power electronics, the use of more components, and the increased cost of equipment because of power electronics [27].

2.8.2 Wind Turbine Power Control Concepts

Wind turbine power control concepts classification is documented in Table 2.2. Generally, this type of control are good for active power control, assisted start-up, and emergency stop.

Table 2.2: Wind Turbine control concepts [18]

Speed Control		**Power control**		
Fixed speed	Type A	Type A0	Type A1	Type A2
Variable speed	Type B	Type B0	Type B1	Type B2
	Type C	Type C0	Type C1	Type C2
	Type D	Type D0	Type D1	Type D2

The wind turbine control concepts are explained as follows:

- **Fixed Speed-Type A:** A fixed speed type control is shown in Figure 2.29. Regardless of the power control principle in a fixed-speed wind turbine, the wind fluctuations are converted into mechanical fluctuations and consequently into electrical power fluctuations. The three versions of this control concept (Type A0, Type A1, and Type A2) are characterised as follows [18]:
  - **Type A0- Stall control:** The simplest, most robust, and cheapest control method, is the stall control (passive control) method. In this method, the blades are bolted onto the hub at a fixed angle. The design of rotor aerodynamics causes the rotor to stall (lose power) when the wind speed exceeds a certain level. The drawback of stall-controlled wind turbines is that it cannot carry out assisted start-ups, during the connection sequence.
  - **Type A1- Pitch control:** This type of control strategy is used when the blades can be turned out or into the wind as the power output becomes too high or too low, respectively. From the electrical point of view, good power control means that at high wind speeds the mean value of the power output is kept close to the rated power of the generator. Its major drawback is that, at high wind speeds, the pitch mechanism is not fast enough to prevent power fluctuations.
  - **Type A2- Active stall control:** As the name indicates, the stall of the blade is actively controlled by the pitching of the blades. At low wind speeds, the blades are pitched similar to a pitch-controlled wind turbine, to achieve maximum efficiency. At high wind speeds, the blades go into a deeper stall by being pitched slightly into the direction opposite to that of a pitch-controlled turbine. This control type has the advantage of being able to compensate for variations in air density, without high power fluctuations and carries out smoother emergency stops and start-ups of the wind turbine [18].

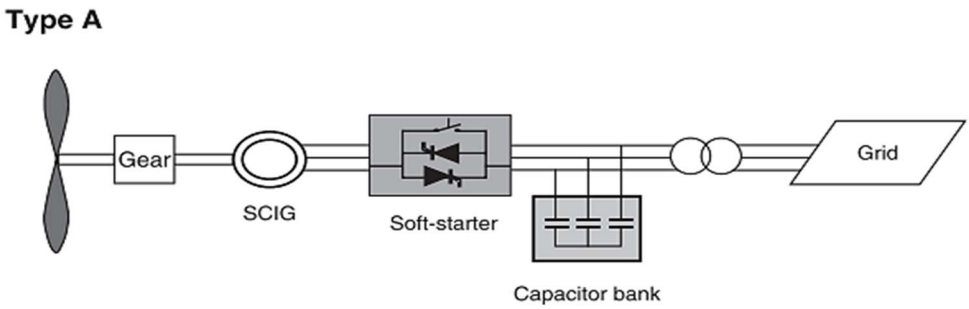

Figure 2.29: Wind turbine control concepts Type-A [18]

- **Variable Speed Type B:** This configuration as shown in Figure 2.30, corresponds to the limited variable speed wind turbine with a wound rotor induction generator's variable rotor resistance which is directly connected to the grid through a soft starter. The optically coupled rotor resistance controller controls the slip and eliminates the need for costly slip rings that need brushes and maintenance. A capacitor bank performs the reactive power compensation. Typically, the range of the dynamic speed control is 0 –10 % above synchronous speed.

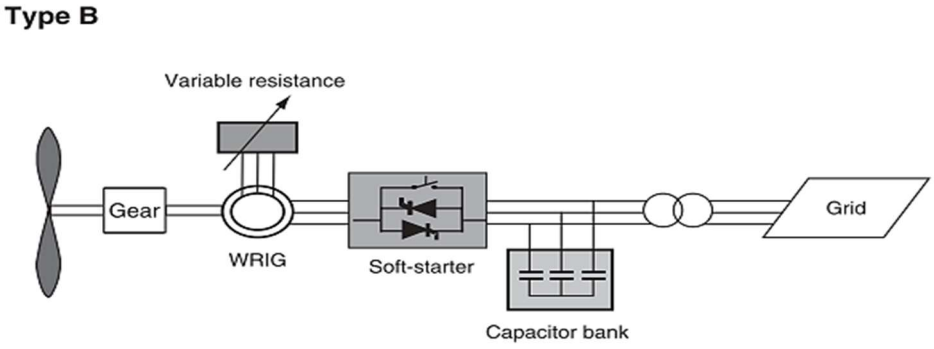

Figure 2.30: Wind turbine control concepts Type-B [18]

- **Variable speed with partial scale frequency Converter Type C:** This configuration as shown in Figure 2.31, corresponds to the limited variable speed wind turbine with a wound rotor induction generator with the stator windings directly connected to the constant-frequency three-phase grid. The rotor windings are connected to a bidirectional back-to-back IGBT voltage source converter (rated at approximately 30% of nominal generator power) to perform the reactive power compensation. Typically, the speed range comprises of a synchronous speed of between -40 % to +30 %. Its main drawbacks are the use of slip rings which require constant maintenance and grid fault protections.

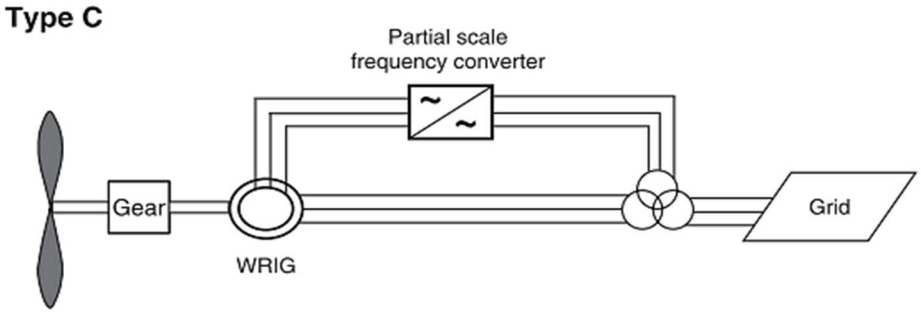

Figure 2.31: Wind turbine control concepts Type-C [18]

- **Variable speed with full-scale frequency Converter Type D:** This configuration as shown in Figure 2.32, corresponds to the full variable speed wind turbine, with the generator connected to the grid through a full-scale frequency converter. The frequency converter performs reactive power compensation and a smoother grid connection. The generator can be electrically excited using a wound rotor synchronous generator or by an induction generator. Some full variable-speed wind turbines are directly connected to large multipole generators with power converters, without using the gearbox [18].

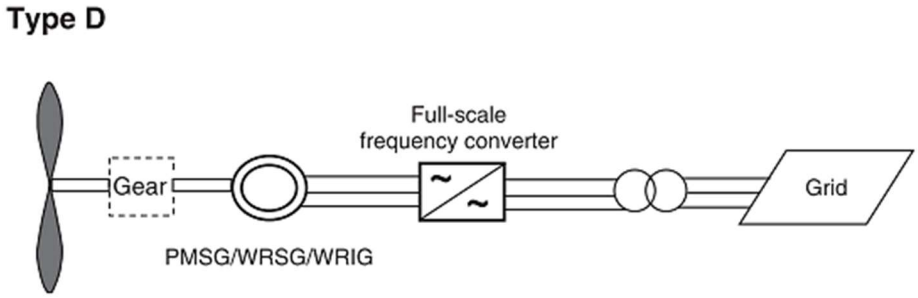

Figure 2.32: Wind turbine control concepts Type- D [18]

2.8.3 Wind Turbine Power Electronic Systems

The variable-speed wind turbine concept requires a power electronic system that is capable of adjusting the generator frequency and voltage to the grid. Power electronics have two strong features [18]:

- **Controllable frequency:** This results in the following direct benefits to the wind turbines:
  (1) Optimal energy operation
  (2) Reduced loads on the gear train, as wind speed variations are absorbed by the rotor
  (3) Load control, as life-consuming loads, can be avoided
  (4) Gearless wind turbines, as the power converter acts as an electrical gearbox; and
  (5) Reduced noise emission at low wind speeds.

- **Power plant characteristics:** The power electronics provide the possibility for wind turbine generators to become active elements in the power system, which results in several advantages, including:
  (1) The active or reactive power flow of a wind farm is controllable
  (2) The power converter can be used as a local reactive power source (e.g. in the case of weak grids);
  (3) The wind farm has a positive influence on network stability; and
  (4) Power converters improve the wind farm's power quality by reducing the flicker level as they filter out the low harmonics and limit the short-circuit power.

Power electronics include devices such as soft-starters, capacitor banks, rectifiers, inverters, and frequency converters, which have the disadvantage of generating high harmonic currents on the grid, and power losses. In recent years' different converter topologies have been developed such as back-to-back converters, multilevel converters, tandem converters, matrix converters and resonant converters amongst others. This section focuses on the most widely used three-phase, back-to-back frequency converter as shown in Figure 2.33.

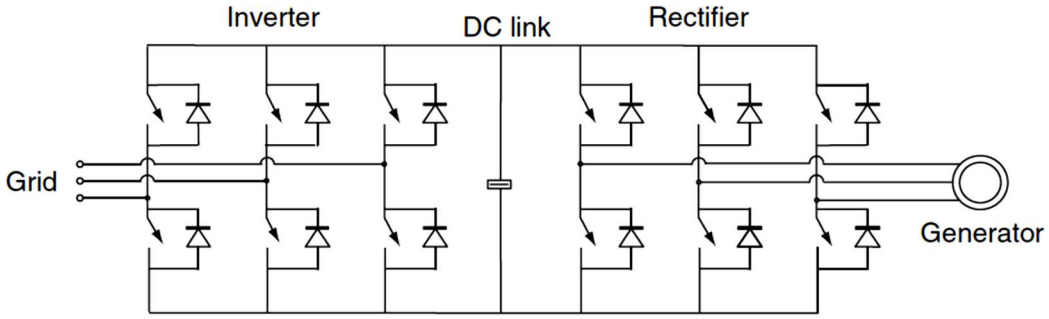

Figure 2.33: Structure of the back-to-back frequency converter [18]

The back-to-back converter is a bidirectional power converter consisting of two conventional pulse-width-modulated converters. The DC link voltage is boosted to a level higher than the amplitude of the grid line-to-line voltage to achieve full control of the grid current. The capacitor between the inverter and rectifier makes it possible to de-couple control of the two inverters and allows the compensation of asymmetry on both the generator and the grid side, without affecting the other side of the converter. The power flow at the grid-side converter is controlled to keep the DC link voltage constant, and the control of the generator-side converter is set to suit the magnetization demand and the desired rotor speed [18]. Figure 2.34 is used to illustrate how the wind turbine generator system should have the capability to work in two main modes of operation; grid-connected mode and stand-alone mode [28].

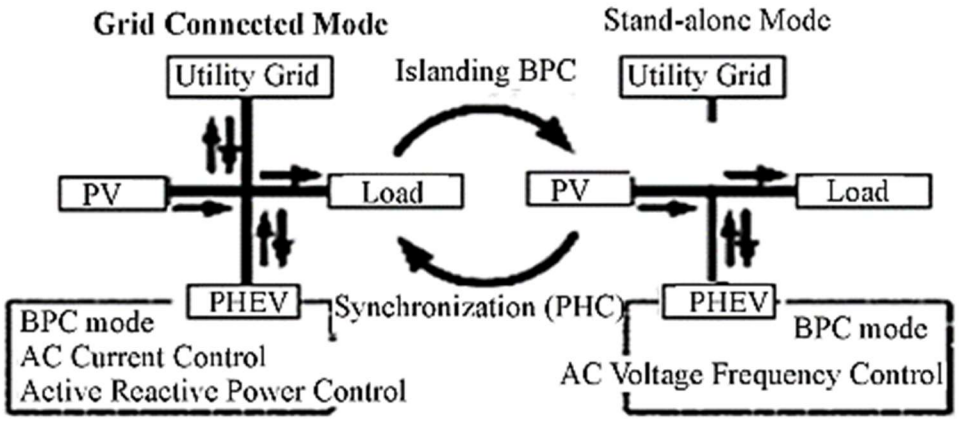

Figure 2.34: Wind turbine System Mode of operations [28]

When the power is shut off from the utility grid, the system goes into the islanding mode and when the power is available from the utility grid the system will synchronise and connect to the utility grid. Ideally, the injected wind-generated power to the grid should have a constant value. A wind power generating station has the disadvantage of unstable power output, leading to power fluctuations fed into the grid. This can be addressed by integrating the wind power generating station with a battery storage system. The power output reference tracking is achieved by coordinating the active power generated by the wind turbine and the batteries [29].

2.9 Standards and Grid Policies

The fluctuating nature of wind power poses a huge challenge when introducing a wind energy into the grid and has necessitated the formation of interconnection standards and grid codes to maintain the power quality of the grid. In the past, wind turbines were usually disconnected from the grid in the case of grid faults to prevent damage to the wind turbines.

The major challenges in the growth of wind power are grid reliability and intermittency. For good power quality to be achieved, the grid code was developed. Grid codes require wind farms to operate like conventional power generators, that is, they must provide active power and also inject and absorb reactive power to and from the grid during steady-state and fault conditions. Grid codes outlined the technical requirements that must be followed during the setup and operation of renewable energy systems that are or will be connected to the grid. The objective of the renewable energy grid code is to improve and regulate the behaviour of wind power systems, while decreasing the losses of wind power, and providing wind power operators with operational characteristics close to those of the conventional power plants.

The tripping and disconnection of wind turbine systems from the grid during faults is prohibited under the new grid codes. Grid codes are established in different countries to allow wind farm

to provide a certain level of support to the grid during faults. The common parameters for local and international renewable energy grid code are continuous operation parameters, low voltage ride-through capability, high voltage ride-through capability, active power regulation, reactive power regulation, visibility, and control of renewable power plants RPPs.

The South Africa renewable energy grid code (SAREGC) provides the minimum technical requirements that renewable power plants (RPPs) connected to or seeking connection to the South Africa electrical transmission system or distribution system must adhere to. Thus, it categorizes minimum technical requirements by the size of the RPPs (biogas, wind, photovoltaics, landfill gas, and concentrated solar power):

1) Category A: 0 – 1MVA (LV connected RPPs) – this category is subdivided into three subcategories:
    a. Category A1: 0 – 13.8kVA
    b. Category A2: 13.8kVA – 100kVA
    c. Category A3: 100kVA – 1MVA
2) Category B: 1MVA – 20MVA
3) Category C: 20MVA or higher

The current version (version 2.9) of the SAREGC was released in November 2016. It specifies the requirements for industrial standardisation, network integrity, and non-discriminatory access to the grid by RPPs. For this, the SAREGC, provides a detailed explanation, and practical methods to test the compliance of the RPPs to the grid code, as documented in [30]. The SA grid code [31] allows the RPPs to maintain a connection to the grid in areas A, B, and D, withstand voltage sag up to zero at the PCC for a period of 150 ms without disconnecting as shown in Figure 2.35.

During symmetrical faults, wind farms greater than 20MVA must provide voltage support to the grid by supplying controlled reactive current to enhance voltage stability to the grid and the active power production must be maintained during voltage drop but for voltage drop below 85 %, active power production can be reduced.

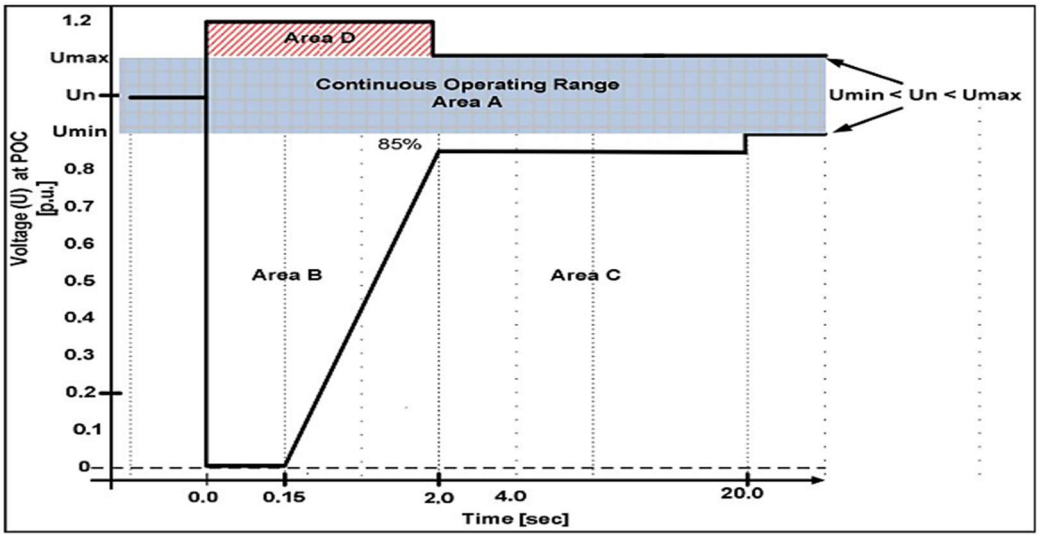

Figure 2.35: Required voltage ride-through capability of category A3, B, and C RPPs [31]

The increase in active power demand causes a reduction in grid frequency and vice versa, RPPs are required to maintain production of active power at a frequency of 50Hz and also to respond to grid frequency changes by regulating active power production within its set-points. P_{Delta} is the amount of active power reserved from the wind farm's available active power for grid frequency stability usually not less than 3 % of $P_{available}$ as seen in Figure 2.36. The frequencies $f_4, f_5, f_6, f_{min}, f_{max}$ are provided in Table 2.3 while frequencies f_1, f_2, f_3 are the agreed frequencies between the service operators (SO) and the RPP.

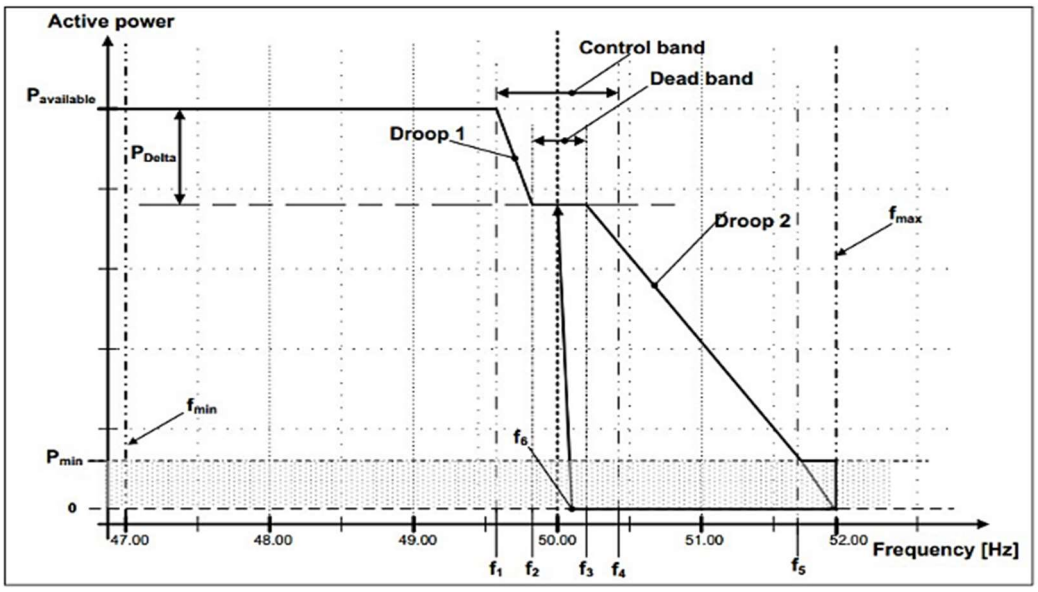

Figure 2.36: Active power and frequency response to variation in grid frequency for category C RPPs [31]

Table 2.3: Frequency settings for RPPs [32]

Frequency	Magnitude (Hz.)
f_{min}	47
f_{max}	52
f_1, f_2, f_3	Agreed with SO
f_4	50.5
f_5	51.5
f_6	50.2

The reactive power and voltage control functions are mutually exclusive, which means that only one of the three functions mentioned below can be activated at a time.

1. Voltage control
2. Power Factor control
3. Reactive Power Q control

The grid code allows the accuracy of the control performed, and that the set-point does not deviate by more than ±2% of the set-point value or by ±0.5% of maximum reactive power as shown in Figure 2.37, depending on which yields the highest tolerance [32]. The RPP should be able to receive a reactive power set point with an accuracy of at least 1kVar.

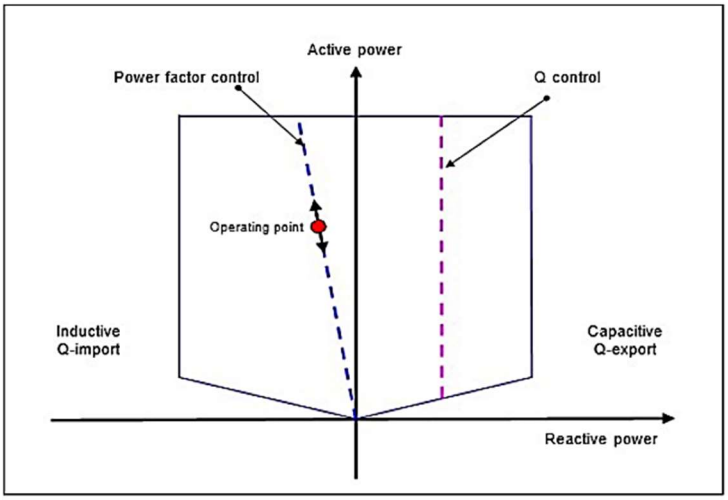

Figure 2.37: Reactive power control functions for the RPP [32]

The South African renewable energy grid code requirements are imposed at the point of connection of the wind farm. From the grid's perspective, the full wind farm will look similar to conventional synchronous generation. A wind farm will often take advantage of a variety of reactive resources to fully meet the grid code requirements. In a three-phase system, several problems such as reactive power imbalance, voltage control at varying load conditions, stability

problems, varying frequencies of different systems and short-circuit power are observed. These problems can be solved with the use of HVDC and FACTS technology, such as a STATCOM which contains power electronic components that can continuously supply both capacitive and inductive current up to its rating and are used to control system voltage or power factor [33].

2.10 Distribution Network

In a typical power system as shown in Figure 2.38, the distribution network serves as the link between the distribution substations and the customers. Distribution systems usually consist of overhead and underground circuits in a mix of branching laterals from the substation to the customers. The network begins at the 11kV, medium-voltage three-phase circuit, and step-downs at a secondary three-phase voltage and neutral, typically below 1000 V and 400V, at the customer's premise, usually at the meter. The voltage between phases is called line voltage and the voltage between phase and neutral is called phase voltage.

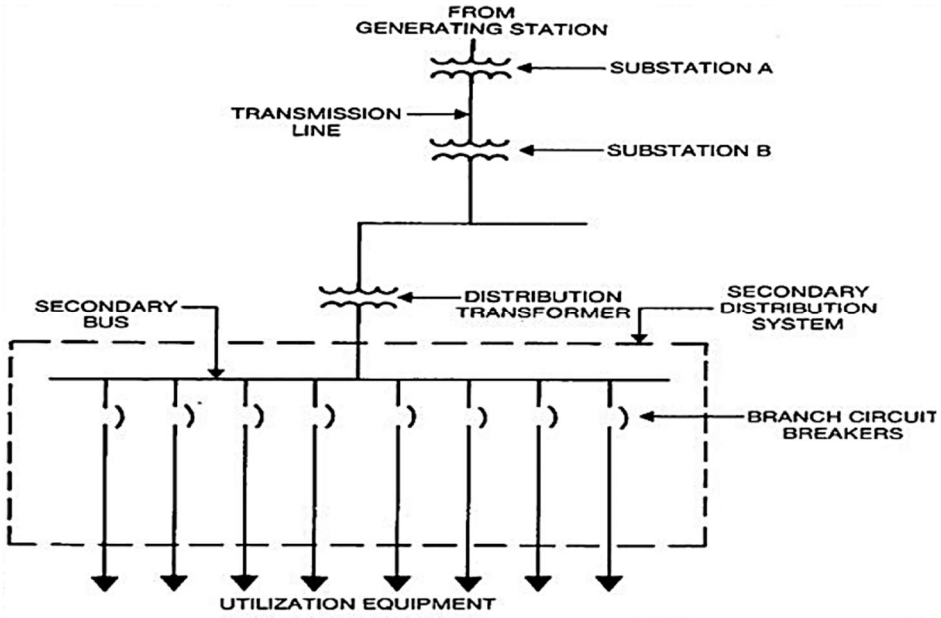

Figure 2.38: A Typical power system layout [34]

The distribution network is designed around various requirements such as peak load, voltage, and distance to customers. Other local conditions such as for active and reactive power, voltage regulations, and level of reliability/security that guarantees customer satisfaction. These various branching laterals can be operated in a radial or ring main configuration.

For a radial configuration, this arrangement is made up of two or more parts of the feeder are usually connected through a normally open distribution switch. Figure 2.39 shows a single line

diagram of an electrical power generation, transmission, and a radial form of distribution system [34].

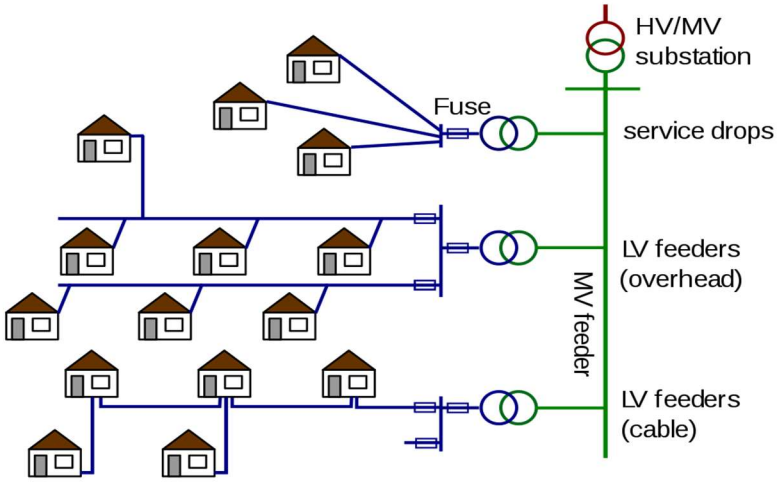

Figure 2.39: A typical radial main distribution network [34]

A ring main distribution system is one that starts at a distribution substation and runs through or around an area serving one or more distribution transformers or load centres and returns to the same substation [34]. This form of distribution network has the advantage of fewer voltage fluctuations and the continuity of power supply is maintained as each distributor is fed with two feeders. The elements of the ring main distribution system are feeders, distributors, and service main, where the feeder connects the substation (or localized generating station) to the area where power is to be distributed. Generally, no tapping is taken from the feeder so that the current remains the same. The distributor is a conductor from which tapping is taken for supply to the consumers.

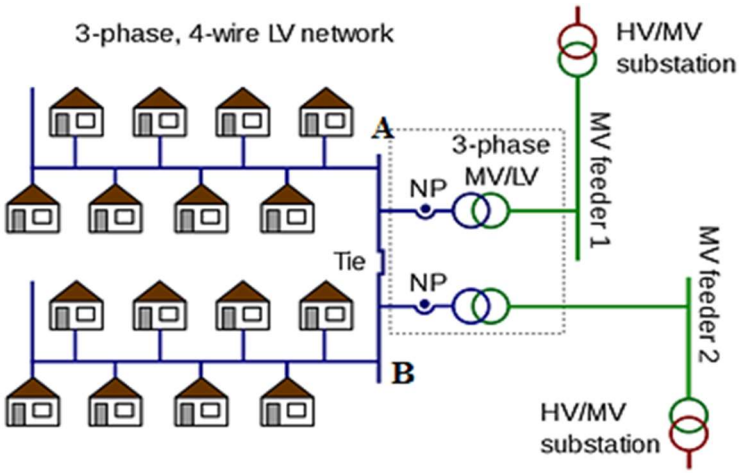

Figure 2.40: A typical ring main distribution network [34]

As shown in Figure 2.40, AB is the distributor. The current through a distributor is not constant because tapping of power is taken at various places along its length. While designing a

distributor, voltage drop along its length is the main consideration since the statutory limit of voltage variations is 10 % of the rated value at the consumer's terminals. A service mains is generally a small cable that connects the distributor to the consumer's terminals [34].

2.11 Integration of Wind Power into Distribution Network

Due to the growing penetration level of wind power into the distribution networks, it is pertinent to study the characteristics when wind power is connected to the grid as well as the interaction with other generating systems. The integration of wind power into the grid presents technical challenges due to the intermittent nature of wind. Some of the challenges include reactive power requirements for voltage support, the starting and synchronizing of wind farms into the grid, short-circuit protection, the efficiency of the grid, sub-synchronous resonance as a result of the electric network and wind turbine interaction, power quality, design and optimization of power electronics, cost and reliability, inadequate transmission lines to accommodate new power systems [35].

Production, investment, maintenance, and reliability are key factors to be considered when wind power is to be integrated into the grid. Large wind farms are expected to execute frequency, voltage, active and reactive power control and are also required to perform rapid response during transient and dynamic conditions. When the active power generated from the wind turbine changes due to fluctuations in wind speed, the reactive power and the terminal voltage of the induction generator also changes.

The integration of DFIG WECS into the grid was demonstrated in [36] using the IEEE 10-machine 39-bus system. It was observed that the DFIG provided a better transient performance and elimination of angular stability problem when compared to conventional synchronous generators while the converters of the DFIG provided a faster control and better ride-through during faults. During grid faults, most wind farms are disconnected and reconnected to the grid after the fault is cleared to avoid the destruction of the WTG. However, during and after the grid fault. DFIG can support the network by providing enough reactive power comparable to conventional generators if the proportional gain of the voltage controller is increased beyond a certain level as presented in [37]. As presented in [38], the introduction of uncontrollable sources of power into the distribution network will make the power system more complex.

The introduction of distributed energy sources into power systems with the connection at the low voltage distribution network has introduced substantial network management issues. This integration of power requires more active participation of distribution energy network operators to monitor the real-time network capacity and to manage connections of the distributed energy

sources, as part of the active network management to export power to the network at all times [39].

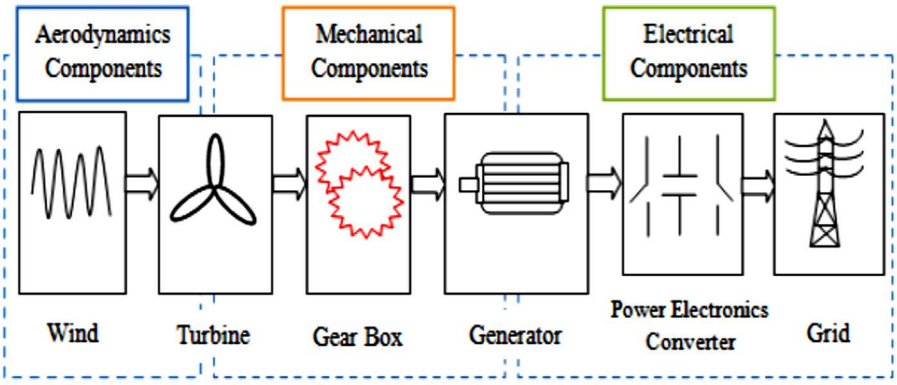

Figure 2.41: Components of the wind energy conversion system connected to the grid [8]

Wind farm integration into the distribution network as shown in Figure 2.41 includes fixed speed wind turbines composed of an aerodynamic rotor, a mechanical transmission system, either squirrel cage induction or synchronous generator, a control system, limited reactive power compensation, and a step-up transformer. The grid codes and standards set by regulating agencies for interconnection to the grid have no dynamic control in analysing the challenges in terms of power system quality, voltage regulation, reactive power compensation, optimum power flow, system stability, and the load dispatch challenges for power system operators, because of the natural characteristics of wind source [8]. The addition of the dynamic power compensation in the system provide as reimbursement for reactive power and voltage regulation and therefore, improves the power system stability.

The analysis as documented in reference [40] indicates that grid operators have developed grid codes for connecting wind turbine generators. Accordingly, the wind turbine manufacturers have developed functionality concepts in the field of wind turbine generators control design to meet requirements as stipulated by the grid codes as discussed below:

- **Frequency control:** Several grid codes require the participation of wind farms in primary and secondary frequency control, including frequency response capability and limitation of both ramp rates and active power output. Some operators also require that wind turbine generators stay connected and in operation at a wider frequency band to contribute to frequency restoration and stable power systems operation.
- **Voltage control:** The individual wind turbine generators have to control their terminal voltage to a constant value using an automatic voltage regulator. Modern wind farms can control the voltage at the point of common coupling to a pre-defined set-point of grid voltage.

- **Fault ride-through capability:** Wind turbine generators must remain connected during and after severe grid disturbances, ensuring fast restoration of active power to pre-fault levels as soon as the fault is cleared and inject reactive current to support the grid voltage during disturbances and to provide fast voltage recovery after fault clearing [40].

Power flow study for a distribution network connected to a wind farm in [41] shows, the interfaces from the wind farms to the distribution system boundaries. They are case-specific depending on several factors such as the short-circuit ratio at the point of connection, the length of the interface, the grid voltage level, the wind farm capacity, power flow, and frequency responses. As the network interfaces between the wind turbine and the power systems network the use of converters is very important. The converter is extensively used with the capability to extract maximum power in a wide range of wind conditions. It can also control both active and reactive powers independently [41].

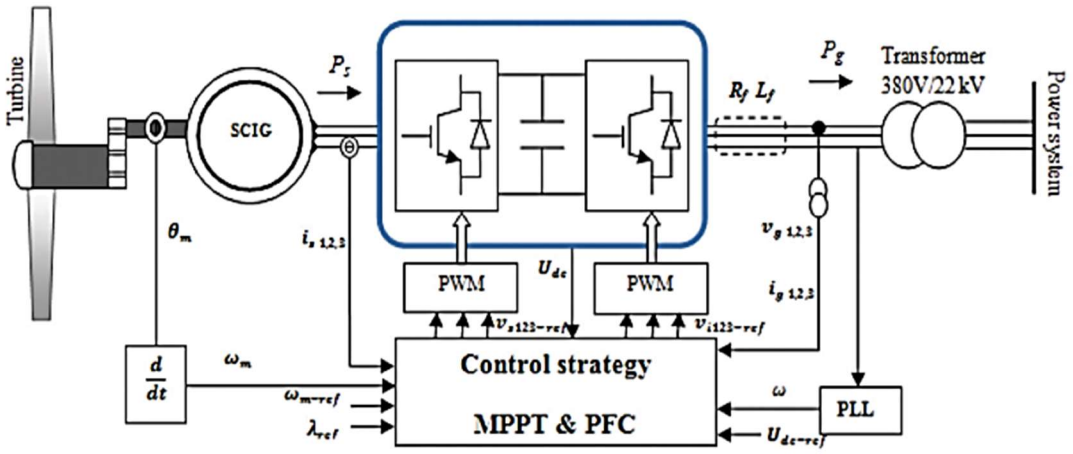

Figure 2.42: Grid-connected wind turbine [41]

Figure 2.42 shows a typical grid-connected inverter for wind energy applications through a line inductance L_f which represents the leakage inductance of the transformer. Since the power flow between the converter and grid is bidirectional, the relationship between the grid, converter voltage, and the line currents are given below [41].

$$\begin{pmatrix} v_{i1} \\ v_{i2} \\ v_{i3} \end{pmatrix} = R_f \begin{pmatrix} i_{g1} \\ i_{g2} \\ i_{g3} \end{pmatrix} + L_f \frac{d}{dt} \begin{pmatrix} i_{g1} \\ i_{g2} \\ i_{g3} \end{pmatrix} + \begin{pmatrix} v_{g1} \\ v_{g2} \\ v_{g3} \end{pmatrix} \tag{2.32}$$

The distribution network-connected operation of wind farms places demands on the wind turbine's operational behaviour and its technical equipment for distribution connection. In the situation where the penetration level of the installed wind power is small as compared to the network capacity, the effects were considered negligible. Therefore, as long as wind turbines

provided only a relatively small part of the power generation capacity, they have very little impact on the grid operation.

For large level penetration of wind power into the distribution network, the integration of wind energy has become a technical and economical challenge because of the installed capacity as shown in Figure 2.43. To integrate wind power into the distribution grid network, it has to comply with the structure and technical standards of this interconnected grid. These standards are mainly based on requirements drawn, from the structure of a distribution grid with only a few large-scale power generation plants supplying the distributed consumers.

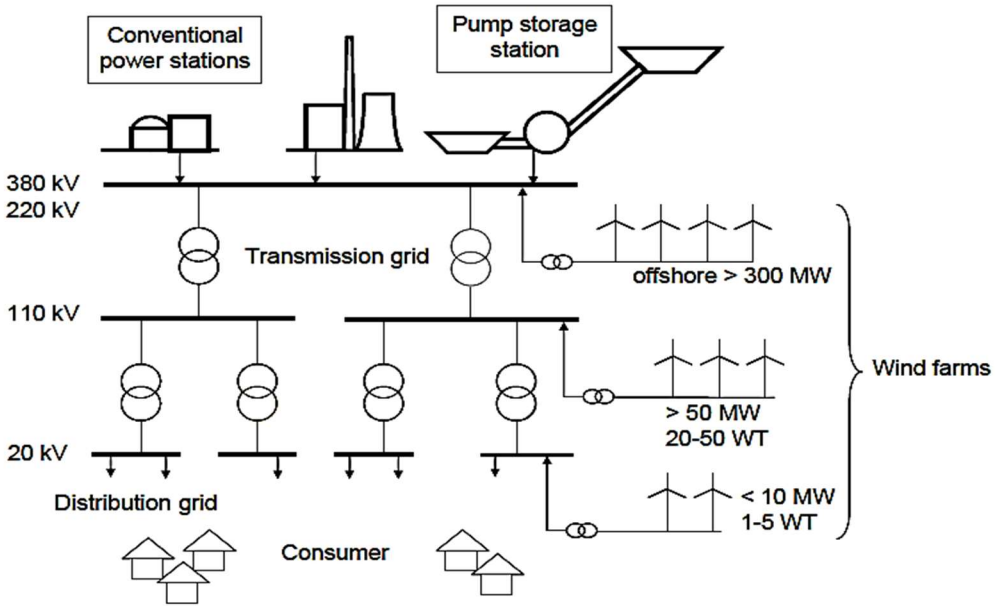

Figure 2.43: Voltage levels of the interconnected grid and the suitable wind farm sizes [14]

2.12 Impact of Wind Power on a Distribution System

There are some fundamental differences between renewable energy generations and conventional power plant generation that affect how these resources interact in an integrated system and one of the biggest differences is the intermittency of the resource, due to the dependency on weather and seasons [42]. As national energy strategies and international compacts increasingly encourage investment in renewable energy generation, the interaction between these types of generation will inherently change the way system operators plan for and manage electricity grids. In [25], the wind renewable energy generation's emerging challenges and solutions arising from the integration of renewable energy into a given interconnected electric power system were documented and the relevant impacts of wind power in the electricity system was discussed, based on the following criteria:

- Level of wind power penetration
- Grid size and demand management
- Generation mix of electricity in the system and reserves

Figure 2.44 shows the short term and long term impacts of wind power integration into the power systems. The inclusion of distributed generation is a challenge in itself with issues referring to the quality of supply, stability of the network, system balancing, voltage regulation, protection, failure (isolated mode), and reliability. The connection of distributed generation in forms of renewable energy turns the developed technology of convectional power systems in terms of the passive unilateral fed distribution network into a double-fed active network.

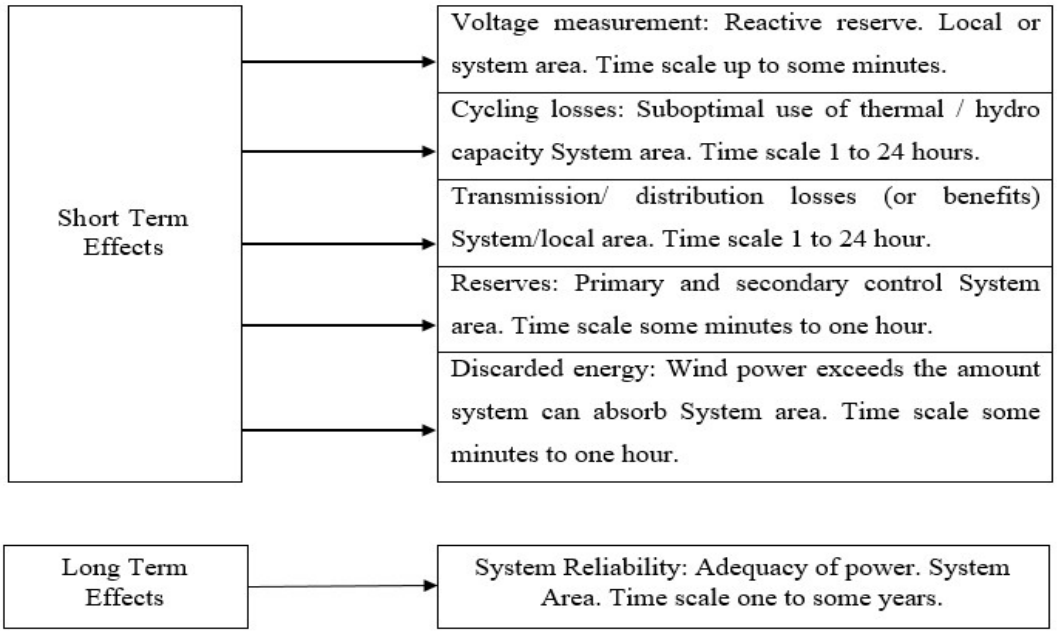

Figure 2.44: The duration effect of impacts of wind power integration [25]

The main impacts of sources of energy generation on the integrated network were studied as [25]:

- Changes in the network voltage profile, the appearance of transients when turning the sources on and off.
- An increase in short-circuit currents.
- The change of power losses depending on the production and consumption, congestion of individual lines.
- The impact on the quality and reliability of supply, and the need for coordination of the protection and efficiency.

An argument presented on the impacts of wind power on the integrated power system, considers different time scales and width of the area relevant for the studies as shown in Figure 2.45. Changes in consumption and production of renewable energy sources are synchronised with the production of conventional sources, because the production must always cover the demand plus losses, including changes in the production of variable sources.

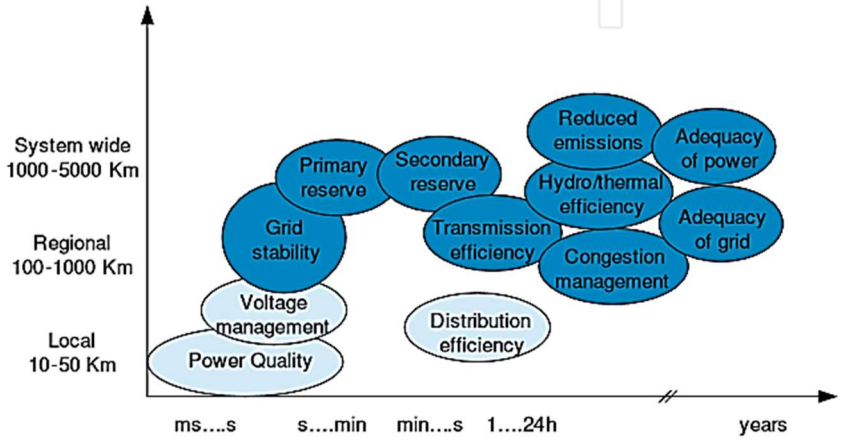

Figure 2.45: The impacts of wind power on power systems [25]

Hence, the balanced production is a “hot reserve” which ensures the stability of the system. Due to the inability of dispatch control, distributed sources are assumed as producers of energy that do not contribute to other functions of the electric power system (voltage and frequency control, network security, backup, etc.), which is why all disturbances in the system must be compensated for by conventional energy sources.

Power quality as defined in [43] is the “characteristics of electricity at a given point on an electrical system, evaluated against a set of reference parameters”. The performance of wind turbine systems in terms of power quality is determined based on the standard and measurement concerning the guidelines specified by the International Electro-technical Commission (IEC). The IEC 61400-21 defines the process for measuring the power quality of a grid-connected wind turbine system [43].

It specifies seven parameters that actively affect the power quality of a wind turbine namely: flickers, harmonics, voltage sag/dip/drop, active power, reactive power, grid protection, and reconnection time. An ideal power quality implies that the voltage is continuously sinusoidal with a steady amplitude and frequency. Amongst the parameters specified above, the voltage sag is a major parameter that affects the power quality of grid-connected wind turbines because of the characteristics of the induction generator. Voltage sag/dip is a random event in power systems majorly caused by faults in the grid, it is denoted with its amplitude and variations.

When a short-circuit fault occurs in the area connected to the wind turbine generator, the short-circuit current may cause a voltage dip at the wind turbine generator terminal as a result of torque imbalance between the generator and the turbine, when the fault is cleared and the voltage of the power system is restored, reactive power is needed from the induction generator to recover its terminal voltage. The absorption of reactive power causes a high inrush current to be drawn by the induction generator causing a voltage drop in the line connecting the wind turbine generator and the grid. The resulting voltage drop can cause slow recovery of the generator terminal voltage causing the generator to increase its acceleration which leads to increased reactive power consumption. If the generator fails to recover, it is disconnected from the system thereby leading to a significant impact on the stability of the system.

The IEC 61400-21 defines six voltage drops with the specification of magnitude and period of the voltage drop [44] as shown in Table 2.4:

Table 2.4: Specifications for voltage drops for wind turbine system [44]

Voltage drop case	The magnitude of phase-phase voltage (pu)	The magnitude of positive sequence voltage (pu)	Period (s)
$VD1^1$	0.90 ± 0.05	0.90 ± 0.05	0.5 ± 0.02
$VD2^1$	0.5 ± 0.05	0.5 ± 0.05	0.5 ± 0.02
$VD3^1$	0.2 ± 0.05	0.2 ± 0.05	0.2 ± 0.02
$VD4^2$	0.90 ± 0.05	0.95 ± 0.05	0.5 ± 0.02
$VD5^2$	0.5 ± 0.05	0.75 ± 0.05	0.5 ± 0.02
$VD6^2$	0.2 ± 0.05	0.60 ± 0.05	0.2 ± 0.02

Voltage sag is normally expressed as a relative percentage change in voltage of the wind turbine system, given by [45]:

$$d = k_u \frac{S_n}{S_k} \tag{2.33}$$

Where d is a relative change in voltage as sag, k_u is a volt, S_n *the* age reduction factor is an apparent power (rated), and S_k is an apparent power (short circuit). Voltage rise is the increase in voltage from $1.0\ pu$ to about $1.8\ pu$ in a period of 0.5 cycles to 1 minute which can be caused by switching-off large loads, the increase in voltage along unfaulty lines during a single line-ground fault, and excitement of capacitor banks [45].

Another important power quality parameter worth of mentioning is “flicker” which is caused by fluctuation. The fluctuation in voltage is a major concern when connecting the wind turbine system to the grid, and it is caused by changes in the wind speed. Voltage fluctuations have a direct effect on the active and reactive power in the system. The degree of the voltage fluctuation depends on the strength of the grid, the impedance of the network, and the characteristics of the wind turbine. Flickers are caused by fluctuations in system voltage which is visible from electric light. The magnitude of the flicker is dependent on the degree of fluctuation. It affects the voltage quality of the grid if not controlled by the generating station. Flickers mostly do not affect the VSWT system because the output of active power is relatively constant. The fluctuation in voltage and flicker emission for wind turbines connected to the grid is related to factors such as [46]:

1. Average wind speed
2. Turbulence intensity
3. Short-circuit ratio (SCR)

The reactive power of the wind turbine can be controlled to vary the active power thereby making the difference between the grid impedance angle and power factor angle tend to 90 degrees and as a result reducing the flicker level. The flicker meter as specified by the IEC 61000-4-15 is used to measure flicker emission. The IEC flicker meter operates on the principle of simulation of the “transfer function” of the set “voltage-lamp-eye-brain” and gives a corresponding output of the disturbance level known as “Instantaneous flicker sensation” (S_f). The instantaneous flicker is then analysed statistically to generate an output every 10 minutes corresponding to the flicker severity level. Another parameter that compromises the power quality of the grid-connected wind turbine system is harmonics, harmonics arise as a result of the presence of power electronic converters mostly found in VSWT coupled with DFIG. The harmonic current and voltage transferred to the grid at the PCC should be limited as specified by the IEC 614400-36 guideline, the total harmonic distortion (THD) of voltage at the PCC is given by [47].

$$V_{THD} = \sqrt{\sum_{n=2}^{40} \frac{V_n^2}{V_1} 100} \tag{2.34}$$

Where V_{THD} total harmonic distortion of voltage is, V_1 is the voltage at the fundamental frequency and V_n is the nth harmonic voltage. The THD for a connection to a 132kV grid should be less than 3%.

Although wind generation is a random nature, large penetration will increase the overall system reliability of supply. Some capacity credits are expected, depending on the three dimensional and chronological distribution of wind energy, but still difficult to quantify; probabilistic methods should be used for such estimation. Generally, the dispersion of wind farms all over a control area will lead to increased capacity credits. Nevertheless, it is doubtful if capacity credits lead to reduced thermal installed capacity.

2.13 Conclusion

Characteristics of air flow fundamentals, concept of wind energy conversion theory and wind turbine principles and control applications of WECS have been discussed in this chapter. The wind turbine system configurations, types of converters that used in the control systems and the types of controllers of these equipment were introduced and discussed in this chapter. The Grid policies and distribution network standards, integration of wind power into distribution network and its impact on a distribution system were also argued.

Chapter 3

Analytical and Numerical Modelling

3.1 Introduction

Wind power integration into the power systems has several technical challenges concerning security of supply. This include reliability, availability, and power quality. This has created the need to model the wind turbine systems in order to analyze the system response when power is integrated into the grid. This process will be of great importance for the development of control strategies. Therefore, it is essential to use appropriate models to emulate the wind turbine and power systems. The modeling should be done as a function of their parameters, some of which are intrinsic characteristics of the system, depending only on its current state .i.e. very dynamic in nature.

The models used should adequately represent the dynamic behaviour of the wind turbines with the ability to predict the critical operation conditions at which the wind integration takes place and also be able to model the dynamic performance. The dynamic model should provide information on the system during the steady-state operation, such as the dynamic oscillations, torque or current ripples, etc.

Due to the complexity of the system, it is not appropriate to fully model all the components as a whole unit, but rather as a discrete of several interconnected subsystems models, interacting with each other. The modelling processes involve both mechanical and electrical power for the WECS. The power flow in the energy conversion process from wind energy into electrical energy have been discussed in the literature review (Chapter Two). In this chapter the various subsystems for the wind turbine are modelled in which the output from one subsystems becomes the input for the next subsystem. The subsystems include a rotor aerodynamic energy conversion, a wind turbine gearbox, a DFIG for the conversion of mechanical energy to electrical, and power electronic converters which are used to transfer the electric power from AC to DC back to AC. Collectively, these subsystems operate as a unit to convert and control by harvesting the wind mechanical power and convert it into electrical power, within the rated voltage and frequency. The output from the converters can either be for local use in the form of a microgrid or fed into national grid.

Presented in this chapter, firstly, the aerodynamic model for rotor blades of the wind turbine used to analyse the conversion of the kinetic energy into the rotation motion in the rotor. Secondly, is the mechanical model for the gearbox and the drive train of a two-mass shaft model

was used. Thirdly, the electrical model for the generator configuration and the generator model used was for the DFIG. Lastly, the analysis of Type-3 back-to-back power electronic converter model coupled with the control scheme using PI controllers for connecting the generator to the grid.

3.2 Wind Turbine Aerodynamic Modelling

Wind turbine power production depends on the interaction between the wind turbine rotor and the wind. In the wind generation system, power is extracted from the kinetic energy of the wind, and can be expressed as the kinetic power available in the stream of air. Since wind speed usually varies from one location to another and also fluctuates over time in a stochastic way, J. G. Slootweg [24] proposed a mathematical model that takes into account some landscape parameters to determine the wind speed. The generated wind speed V_w in (meter/sec) for any location can be obtained by the following expression [24]:

$$V_w(t) = V_{wa}(t) + V_{wr}(t) + V_{wg}(t) + V_{wt}(t) \tag{3.1}$$

Where, $V_{wa}(t)$ is a constant component, $V_{wr}(t)$ is a common ramp component, $V_{wg}(t)$ is a gust component and $V_{wt}(t)$ is a turbulence component in (meter/sec). The kinetic energy E of the air mass m in (kg) moving at a speed V_w is given by [49]:

$$E = \frac{1}{2} \times m \times V_w^2 \tag{3.2}$$

By substituting the density and volume for mass and the volume is the speed times the area and time. Therefore, the determination of the mass in a circular interfacing area between the wind stream and the turbine blades area A can be derived as [49]:

$$m = \rho \times v = \rho \times V_w \times A \times t = \rho \times V_w \times \pi \times R^2 \times t \tag{3.3}$$

Where ρ is the air density in (Kg/m^3) with values varies from 1.1 to 1.3, t is the time, R is the radius of circular area in (meters) swiped by the wind turbine blade. Substituting equation (3.3) into equation (3.2) yields:

$$E = \frac{1}{2} \times \rho \times V_w^3 \times \pi \times R^2 \times t \tag{3.4}$$

Then the stream power of the wind P_t through a cross-sectional area normal to the wind is defined as follows [49]:

$$P_t = \frac{1}{2} \times \rho \times \pi \times R^2 \times V_w^3 \tag{3.5}$$

As discussed in chapter 2, the Betz equation was used to determine the maximum power extractable from wind by an ideal turbine rotor with countless blades under ideal conditions as 59.26 % of the available power in the wind. This limit is known as the Betz limit. In practice, wind turbines are limited to two or three blades due to structural and economic considerations. The ratio of extractable power to available power is expressed as the rotor power coefficient C_p. The power coefficient C_p can then be expressed as a function of the tip speed ratio (TSR) λ, which is defined as the ratio between the linear speed of the blades and the wind speed and the blade pitch angle β in degrees as $C_p(\lambda, \beta)$ [50], [51].

The extractable power P_t, for a wind turbine system with a non-linear aerodynamic power coefficient $C_p(\lambda, \beta)$ is defined as [52]:

$$P_t = \frac{1}{2} \times \rho \times \pi \times R^2 \times V_w^3 \times C_p(\lambda, \beta) \tag{3.6}$$

The aerodynamic torque T_t developed with rotor angular speed ω_t (in rad/sec) and $C_t = \frac{C_p}{\lambda}$ as the coefficient of torque, can be calculated as [52]:

$$T_t = \frac{P_t}{\omega_t} = \frac{1}{2} \times \rho \times \pi \times R^3 \times V_w^2 \times C_t \tag{3.7}$$

Tip speed ratio can be calculated as [49]

$$\lambda = \frac{R\omega_t}{V_w} \tag{3.8}$$

Non-linear aerodynamic power coefficient $C_p(\lambda, \beta)$ is defined as [52]:

$$C_p(\lambda, \beta) = k_1 \left(\frac{k_2}{\lambda_i} - k_3\beta - k_4\beta^{k_5} - k_6 \right) \left(e^{\frac{k_7}{\lambda_i}} \right) \tag{3.9}$$

$$\lambda_i = \frac{1}{\lambda + k_8} \tag{3.10}$$

The aerodynamic power coefficient $C_p(\lambda, \beta)$ is a nonlinear function of tip speed ratio λ and the blade pitch angle β [53]. The curve used to illustrate this non-linear relationship is plotted in Figure 3.1.

The two points on the curve can be used analyses the extractable power in the wind energy:

- When the blade pitch angle β does not change, the peak values of the power coefficient $C_p(\lambda, \beta)$ corresponds to a unique tip speed ratio λ, where the energy conversion is expected.
- As the blade pitch angle β increases, the wind energy use coefficient decreases. Thus, for tracking more wind power, β should be set into a small value.

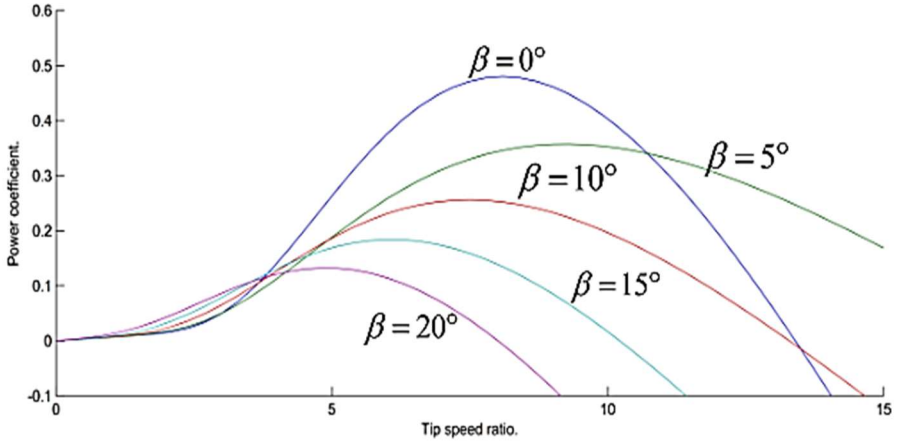

Figure 3.1: Power coefficient versus tip-speed ratio [53]

3.3 Mechanical Modelling of Wind Turbine Drive Train

Considering the mechanical aspect of the wind turbine, the mechanical representation of the train drive of the entire wind turbine is complex. For the analysis of the gear train in wind turbines, the following four types of drive train models are usually used [54].

- six-mass drive train model
- three-mass drive train model
- two-mass shaft model
- one-mass or lumped model

From the above four types of drive train model, the model that was modelled and implemented is the simplified form of the two-mass shaft model power train, shown in Figure 3.2. In this model, all masses are grouped into the low and high-speed shaft. The inertia of the low-speed shaft comes mainly from the rotating blades and the inertia of the high-speed shaft comes from the shaft connected to the generator. It is important to include all small masses of high-speed shaft since they all have an important influence on the dynamic system due to the transformation of the transmission ratio. The stiffness and damping of the shaft are combined in an equivalent stiffness K_S and damping D_S models which are placed on the low-speed side shaft.

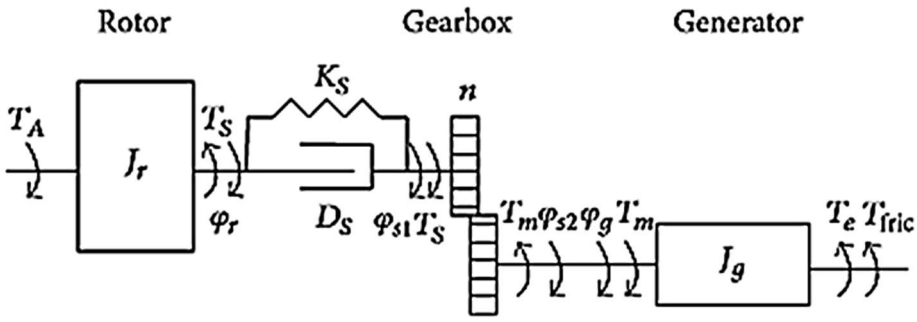

Figure 3.2: Schematic diagram for the two-mass shaft drive train model [54]

The input to the model for the two-mass system is the torque T_A, which is obtained from the aerodynamic interaction between the wind and the rotor. The output from the generator is the generator reaction torque T_e. The output is the changes in rotor speed ω_r and generator speed ω_g. The dynamic of the high-speed generator can be expressed as a machine model. The differences in the mechanical drive torque T_m, the generator torque reaction T_e, and torque losses due to friction T_{fric}, cause the change of angular velocity$\dot{\omega_g}$, which can be expressed as [54]:

$$T_m - T_e - T_{fric} = j_g \times \dot{\omega}_g \tag{3.11}$$

The change of the angular speed $\dot{\omega_r}$ is caused by the difference between the aerodynamic torque T_A and shaft torque T_s at a low speed shaft [54].

$$T_A - T_s = j_r \times \dot{\omega}_r \tag{3.12}$$

$$\dot{\omega}_g = \ddot{\varphi}_g \; and \; \dot{\omega}_r = \ddot{\varphi}_r \tag{3.13}$$

Since the mechanical driving torque T_m and T_s are connected by the gear trains of ratio n, hence mechanical drive torque T_m [54]:

$$T_m = \frac{T_s}{n} \tag{3.14}$$

Gearbox input rotor shaft torque T_s [54]:

$$T_s = K_s \cdot \Delta\varphi + D_s \dot{\varphi} = K_s \cdot \Delta\varphi + D_s \left(\varphi_r - \frac{\dot{\varphi}_g}{n} \right) = K_s \cdot \Delta\varphi + D_s \left(\omega_r - \frac{\omega_g}{n} \right) \tag{3.15}$$

The drive train angular speed can be obtained as follows [54]:

$$\dot{\omega}_r = \frac{1}{J_r}\left(T_A - D_S \cdot \omega_r + \frac{D_S}{n}\omega_g - K_S \int \left(\omega_r - \frac{\omega_g}{n} \right) dt \right) \tag{3.16}$$

$$\dot{\omega}_g = \frac{1}{J_g}\left(-T_e - \left(D_g + \frac{D_S}{n^2} \right)\omega_g + \frac{D_S}{n}\omega_r - \frac{K_s}{n} \int \left(\omega_r - \frac{\omega_g}{n} \right) dt \right) \tag{3.17}$$

Where, K_S is the stiffness constant and D_S is the damping constant of the shaft, considering a two-mass free-swinging system, the Eigen frequency is given as [54]:

$$\omega_{os} = 2\pi f_{os} = \sqrt{\frac{K_s}{J_{ges}}} \tag{3.18}$$

The total inertia of the free-swinging system on the low-speed shaft is calculated by [54]:

$$J_{ges} = \frac{J_r \cdot J_g \cdot n^2}{J_r + J_g \cdot n^2} \tag{3.19}$$

Consequently, the stiffness constant of the low speed shaft is [54]:

$$K_S = J_{ges} \cdot \left(2\pi f_{os} \right)^2 \tag{3.20}$$

And, the damping constant D_S of the low-speed shaft, with ξ_S as logarithmic decrement [54]:

$$D_S = 2\xi_s \cdot \sqrt{\frac{K_s J_{ges}}{\xi_s^2 + 4\pi^2}} \tag{3.21}$$

3.4 Mathematical Modelling of the Doubly Fed Induction Machine

The DFIG can be used to produce electrical power at a constant frequency. As shown in Figure 3.3, an induction machine works on the principle of interaction between the stator and rotor magnetomotive forces (MMF). The stator winding currents create an MMF rotating at grid frequency that induces an MMF in the rotor windings. The rotor speed does not match the stator's MMF. This induced rotor MMF will rotate at the so-called slip frequency which has the following value [55]:

$$\omega_{slip} = \omega_{mmf}^{rotor} = \omega_{mmf}^{stator} - \omega_{rotor} \tag{3.22}$$

Where, ω_{slip} is the slip frequency, corresponding to the frequency of rotor current and voltage, ω_{mmf}^{stator} is the frequency of the stator corresponding to the grid frequency in (rad/sec), ω_{rotor} is the rotor rotating frequency (rad/sec), equal to the mechanical frequency multiplied by the number of pole pairs.

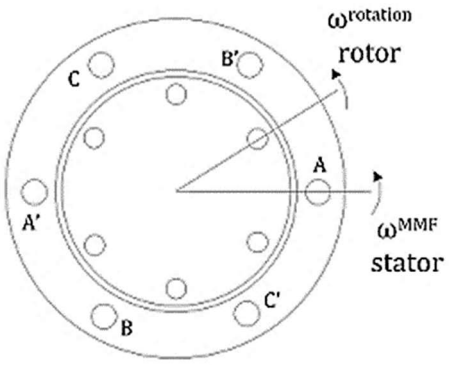

Figure 3.3: Induction machine winding layout [55]

For simulation purposes, it is assumed that both sides are connected in Y with the neutral being at zero voltage and have the same number of turns (Turn Ratio =1). Two techniques known as the Park and Clark transforms documented in [56] can be used to understand the modelling of the electrical machine. This is because the modelling allows the transformation of time dependant variables into constant values. This operation also has the great advantage of setting two independent systems of variables; the d axis and q axis that allow each converter to independently control two variables.

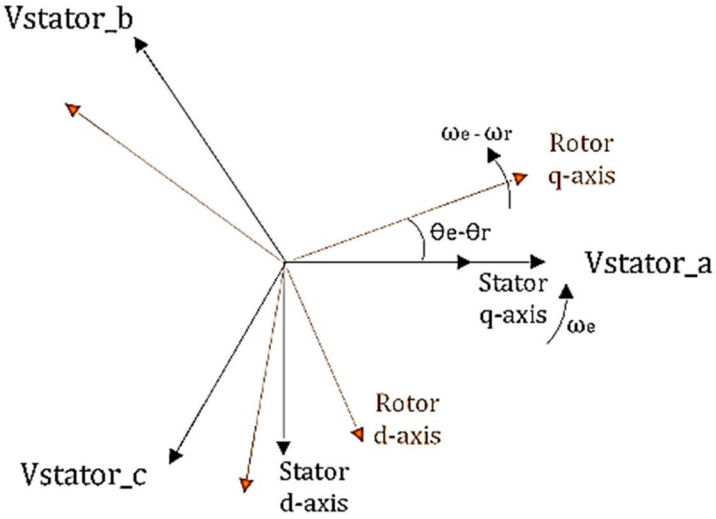

Figure 3.4: Reference frames used in Park transform [55]

The mathematical transformation depends on the selected orientation of the reference frame as shown in Figure 3.4. In this operation, the oscillating voltage and current signals are transformed into two constant signals to allow the development of two independent sets of equations relating to rotor and stator currents, voltages, and fluxes. All variables can now be expressed along two axes (d and q), facilitating the design of the control algorithm. The d-axis variables will affect the reactive power while the q-axis variables will affect the active power.

$$\begin{bmatrix} V_\alpha \\ V_\beta \\ V_0 \end{bmatrix} = T_{abc}^{\alpha\beta 0} \begin{bmatrix} V_A \\ V_B \\ V_C \end{bmatrix} \tag{3.23}$$

$$\begin{bmatrix} V_d \\ V_q \\ V_0 \end{bmatrix} = P_{abc}^{qd0} \begin{bmatrix} V_\alpha \\ V_\beta \\ V_0 \end{bmatrix} \tag{3.24}$$

The Clark transform used to change abc into $\alpha\beta$ variables is:

$$T_{abc}^{\alpha\beta 0} = \frac{2}{3} \begin{vmatrix} 1 & -\frac{1}{2} & -\frac{1}{2} \\ 0 & -\frac{\sqrt{3}}{2} & \frac{\sqrt{3}}{2} \\ \frac{1}{2} & \frac{1}{2} & \frac{1}{2} \end{vmatrix} \tag{3.25}$$

The Park transform used to change abc into $dq0$ variables is:

$$P_{abc}^{qd0} = \frac{2}{3} \begin{vmatrix} \cos(\theta) & \cos\left(\theta - \frac{2\pi}{3}\right) & \cos\left(\theta + \frac{2\pi}{3}\right) \\ \sin(\theta) & \sin\left(\theta - \frac{2\pi}{3}\right) & \sin\left(\theta + \frac{2\pi}{3}\right) \\ \frac{1}{2} & \frac{1}{2} & \frac{1}{2} \end{vmatrix} \tag{3.26}$$

The reorganized DFIG model based on a synchronously rotating reference frame has been presented in [57] by the following equations:

$$V_{ds} = R_s I_{ds} + \dot{\varphi}_{ds} - \omega_s \varphi_{qs} \tag{3.27}$$

$$V_{qs} = R_s I_{qs} + \dot{\varphi}_{qs} + \omega_s \varphi_{ds} \tag{3.28}$$

$$V_{dr} = R_r I_{dr} + \dot{\varphi}_{dr} - \omega_r \varphi_{qr} \tag{3.29}$$

$$V_{qr} = R_r I_{qr} + \dot{\varphi}_{qr} + \omega_r \varphi_{dr} \tag{3.30}$$

$$\varphi_{ds} = L_s I_{ds} + L_m I_{dr} \tag{3.31}$$

$$\varphi_{qs} = L_s I_{qs} + L_m I_{qr} \tag{3.32}$$

$$\varphi_{dr} = L_r I_{dr} + L_m I_{ds} \tag{3.33}$$

$$\varphi_{qr} = L_r I_{qr} + L_m I_{qs} \tag{3.34}$$

Where R_s and R_r are the stator and rotor resistances, L_s and L_r are the stator and rotor windings self-inductance coefficient, L_m is the mutual coupling coefficient between stator and rotor V_{ds}, V_{qs},I_{ds}, I_{qs}, V_{dr}, V_{qr}, I_{dr} and I_{qr} are the voltage and current components of the stator and rotor side in the d-q Park reference frame [58].

The per-unit electromagnetic torque equation expressed in d-q park reference is given by [57]:

$$T_e = \varphi_{ds} I_{qs} - \varphi_{qs} I_{ds} = \varphi_{qr} I_{dr} - \varphi_{dr} I_{qr} = L_m \left(I_{qs} I_{dr} - I_{ds} I_{qr} \right) \tag{3.35}$$

Neglecting the power losses associated with the stator and rotor resistances, the active and reactive stator powers for the DFIG are [57]:

$$P_s = \left(\frac{3}{2} \right) \left(V_{ds} I_{ds} + V_{qs} I_{qs} \right) \tag{3.36}$$

$$Q_s = \left(\frac{3}{2} \right) \left(V_{qs} I_{ds} - V_{ds} I_{qs} \right) \tag{3.37}$$

And the active and reactive rotor powers are given by [57]:

$$P_r = \left(\frac{3}{2} \right) \left(V_{dr} I_{dr} + V_{qr} I_{qr} \right) \tag{3.38}$$

$$Q_r = \left(\frac{3}{2} \right) \left(V_{qr} I_{dr} - V_{dr} I_{qr} \right) \tag{3.39}$$

The overall system equations can also be re-written with relation to the rotating frames [55]:

$$P_T = P_s + P_r = \frac{3}{2} \left(V_{qr}^{'} I_{qr}^{'} + V_{dr}^{'} I_{dr}^{'} + V_{ds} I_{ds} + V_{qs} I_{qs} \right) \tag{3.40}$$

$$Q_T = Q_s + Q_r = \frac{3}{2} \left(V_{qr}^{'} I_{qr}^{'} - V_{dr}^{'} I_{dr}^{'} + V_{ds} I_{ds} - V_{qs} I_{qs} \right) \tag{3.41}$$

The torque expression and the stator reactive power, which are the control objectives of the rotor-side converter control, have the following form [48]. Where, p is the number of pole pairs of the generator, I_{qs} and I_{qr} are the q component of the stator and rotor current, I_{ds} and I_{dr} are the d component of the stator and rotor current, V_{qs} and V_{ds} are the q and d components of the stator voltage. The stator and rotor flux linkages in the synchronous reference frame are expressed as [50]:

$$\psi_s = L_s I_s + L_m I_r \tag{3.42}$$

$$\psi_r = L_m I_s + L_r I_r \tag{3.43}$$

The electromagnetic torque can be expressed using the $d - q$ components as following [50].

$$T_m = \frac{3}{2} p \frac{L_m}{L_s} \left(\psi_{qs} I_{dr} - \psi_{ds} I_{qr} \right) \tag{3.44}$$

3.5 Voltage Source Converter (VSC)

In variable speed, electric machine drives, the VSC is an important device for the energy conversion process. The main task of this equipment is to convert the electrical power from AC to DC or vice versa. The VSCs have numerous advantages such as the ease of control with open-loop control, compact size, low cost and provide higher power factor as well as lower power losses [59]. This converter, used in this study, is the back-to-back converter and the models for the VSC are discussed as follows.

3.5.1 Model for Grid Side VSC System

The grid side of the wind turbine system is composed of the grid side converter, the grid side filter, and the grid voltage. Figure 3.5 illustrates a simplified model of the grid side system. The grid side converter is modelled with ideal bidirectional switches. It converts voltage and currents from DC to AC, while the exchange of power can be in both directions from AC to DC (rectifier mode) and from DC to AC (inverter mode).

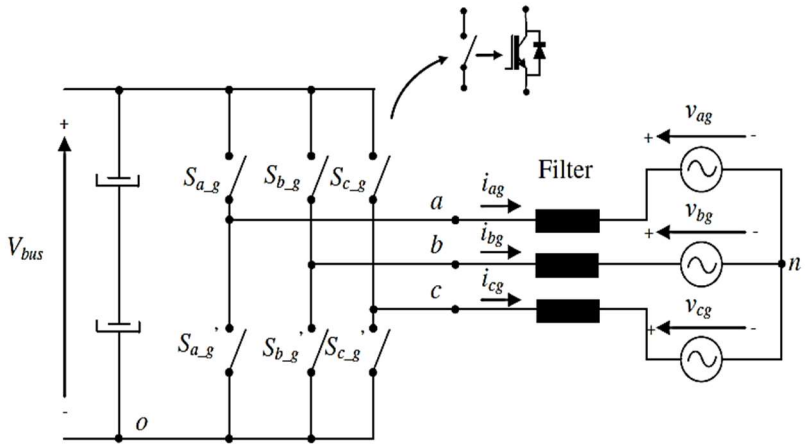

Figure 3.5: Simplified converter, filter, and grid model [52]

The ideal switch normally is created by a controlled semiconductor with a diode in antiparallel position to allow the flow of current in both directions. In this switching configuration, the controlled semiconductor used is an IGBT. The grid side filter is normally comprises of at least three inductances (L), which are the link between each output phase of the converter and the grid voltage. When there's a high filter requirement, each inductance can be accompanied by one capacitor (LC) or even by one capacitor and one more inductance (LCL). The grid voltage is normally supplied through a transformer. This AC voltage is supposed to be balanced and

sinusoidal under normal operation conditions [52].

The two-level converter is modeled with ideal switches that allow the flow of current in both directions. The command of the switches is made using S_{a_g}, S_{b_g}, and S_{c_g} signals. Under ideal conditions, the following order of commands holds, which means that in a leg of the converter, it is not possible to have conduction in both switches [52].

$$S'_{a\_g} = \overline{S_{a\_g}} \tag{3.45}$$

$$S'_{b\_g} = \overline{S_{b\_g}} \tag{3.46}$$

$$S'_{c\_g} = \overline{S_{c\_g}} \tag{3.47}$$

The voltages referenced to the zero point of the DC bus is [52]:

$$v_{jo} = V_{bus} S_{j\_g} \text{ , where } S_{j\_g} \in \{0,1\} \text{ and } j = a,b,c \tag{3.48}$$

Thus, by different combinations of, S_{a_g}, S_{b_g}, and S_{c_g} it is possible to create AC output voltages with a fundamental component of different amplitude and frequency. For modelling purposes, it is useful to know the converter output voltages referred to the neutral point of the grid three-phase system (n). As Figure 3.6 illustrates, the following voltage relationships are true [52]:

$$v_{jn} = v_{jo} - v_{no} \text{ With } j = a,b,c \tag{3.49}$$

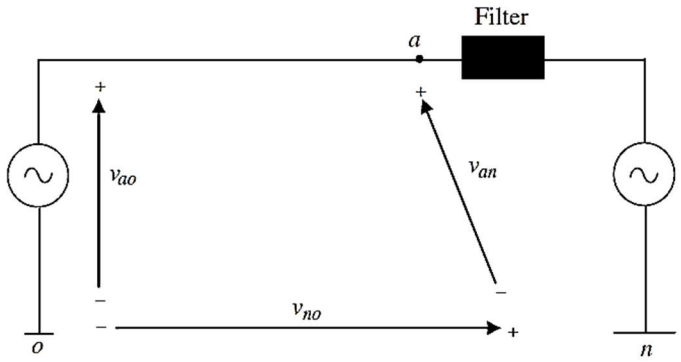

Figure 3.6: Simplified equivalent single-phase grid circuit (a phase) [52]

The voltage between the neutral point (n) and the negative point of the DC bus (0) is needed, assuming a three-phase grid system that holds, the following are obtained [52]:

$$v_{an} + v_{bn} + v_{cn} = 0 \tag{3.50}$$

$$v_{no} = \frac{1}{3}\left(v_{ao} + v_{bo} + v_{co}\right) \tag{3.51}$$

$$v_{an} = \frac{2}{3}v_{ao} - \frac{1}{3}\left(v_{bo} + v_{co}\right) \tag{3.52}$$

$$v_{bn} = \frac{2}{3}v_{bo} - \frac{1}{3}\left(v_{ao} + v_{co}\right) \tag{3.53}$$

$$v_{cn} = \frac{2}{3}v_{co} - \frac{1}{3}\left(v_{bo} + v_{ao}\right) \tag{3.54}$$

From the order command [52]:

$$v_{an} = \frac{V_{bus}}{3}\left(2s_{a\_g} + s_{b\_g} + s_{c\_g}\right) \tag{3.55}$$

$$v_{bn} = \frac{V_{bus}}{3}\left(2s_{b\_g} + s_{a\_g} + s_{c\_g}\right) \tag{3.56}$$

$$v_{cn} = \frac{V_{bus}}{3}\left(2s_{c\_g} + s_{a\_g} + s_{b\_g}\right) \tag{3.57}$$

There are eight different combinations of output voltages, according to the eight permitted switching states of, S_{a_g}, S_{b_g}, and S_{c_g} as shown in Table 3.1. As mentioned previously, the output voltages v_{ao}, v_{bo} and v_{co} take only two different voltage levels: V_{bus} and 0; that is why this converter is identified as a "two-level converter." On the other hand, output voltages v_{an}, v_{bn}, and v_{cn} take five different voltage levels:$\left(-{}^{2V_{bus}}/_{3}\right)$,$\left(-{}^{V_{bus}}/_{3}\right)$,0,$\left({}^{V_{bus}}/_{3}\right)$, and $\left({}^{2V_{bus}}/_{3}\right)$. With a simple six pulse generation scheme, the output voltage waveforms take the shape depicted in Figure 3.7.

Table 3.1: Eight different combinations of output voltages, according to switching states [52]

S_{a_g}	S_{b_g}	S_{c_g}	v_{ao}	v_{bo}	v_{co}	v_{an}	v_{bn}	v_{cn}
0	0	0	0	0	0	0	0	0
0	0	1	0	0	V_{bus}	$-\frac{V_{bus}}{3}$	$-\frac{V_{bus}}{3}$	$2\frac{V_{bus}}{3}$
0	1	0	0	V_{bus}	0	$-\frac{V_{bus}}{3}$	$2\frac{V_{bus}}{3}$	$-\frac{V_{bus}}{3}$
0	1	1	0	V_{bus}	V_{bus}	$-2\frac{V_{bus}}{3}$	$\frac{V_{bus}}{3}$	$\frac{V_{bus}}{3}$
1	0	0	V_{bus}	0	0	$2\frac{V_{bus}}{3}$	$-\frac{V_{bus}}{3}$	$-\frac{V_{bus}}{3}$
1	0	1	V_{bus}	0	V_{bus}	$\frac{V_{bus}}{3}$	$-2\frac{V_{bus}}{3}$	$\frac{V_{bus}}{3}$
1	1	0	V_{bus}	V_{bus}	0	$\frac{V_{bus}}{3}$	$\frac{V_{bus}}{3}$	$-2\frac{V_{bus}}{3}$
1	1	1	V_{bus}	V_{bus}	V_{bus}	0	0	0

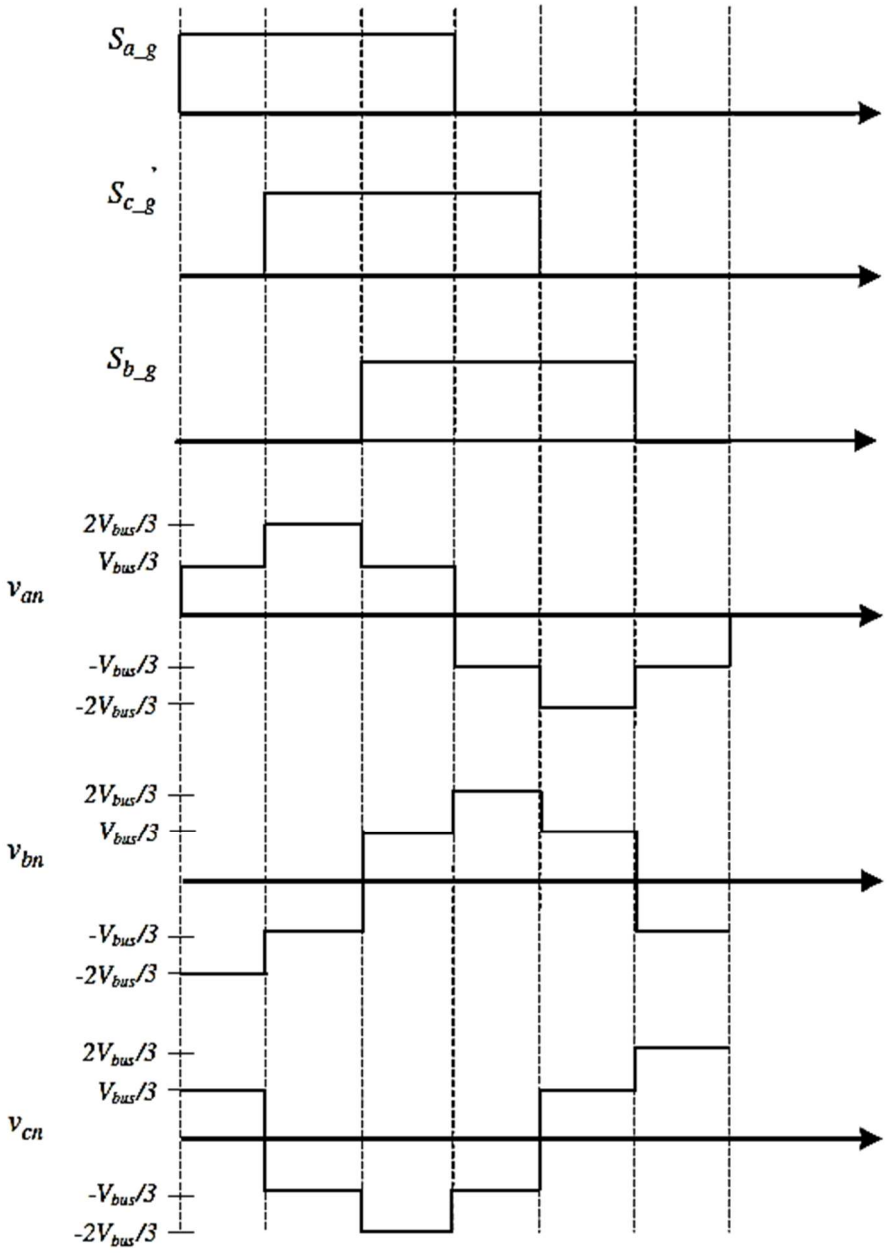

Figure 3.7: Output voltage waveforms of two-level VSC with six pulse generation [52]

By applying the Clarke transformation, it is possible to express the three-phase voltages in the $\alpha\beta$ components as [52]:

$$\begin{bmatrix} v_\alpha \\ v_\beta \end{bmatrix} = \frac{2}{3} \cdot \begin{bmatrix} 1 & -\frac{1}{2} & -\frac{1}{2} \\ 0 & \frac{\sqrt{3}}{2} & -\frac{\sqrt{3}}{2} \end{bmatrix} \cdot \begin{bmatrix} v_{an} \\ v_{bn} \\ v_{cn} \end{bmatrix} \tag{3.58}$$

Referring back to the grid side system model shown in Figure 3.6, a three-phase filter is located between the grid voltage and converters output. A simple and reliable solution adopts an inductive filter, locating an inductance in each phase.

The three-phase system can be modeled as three independent system, but the equivalent single-phase system is described in Figure 3.8. Note that the output AC voltages of the converter referred to as the neutral point are named with the sub-index $'f'$.

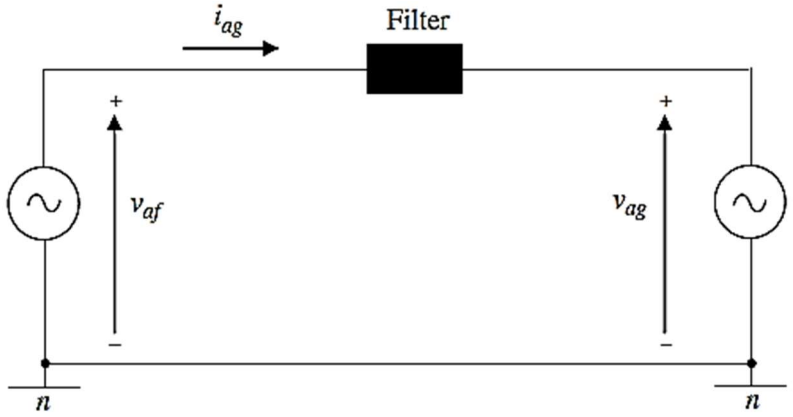

Figure 3.8: Simplified equivalent single-phase grid circuit (a phase) [52]

Thus, the electric equations of the system can be obtained as [52]:

$$v_{af} = R_f i_{ag} + L_f \frac{di_{ag}}{dt} + v_{ag} \tag{3.59}$$

$$v_{bf} = R_f i_{bg} + L_f \frac{di_{bg}}{dt} + v_{bg} \tag{3.60}$$

$$v_{cf} = R_f i_{cg} + L_f \frac{di_{cg}}{dt} + v_{cg} \tag{3.61}$$

Where L_f = inductance of the grid side filter (H), R_f = resistive part of the grid side filter (Ω) v_{ag}, v_{bg}, v_{cg} = grid voltages (V), with ω_s electric angular speed in (rad/s), i_{ag}, i_{bg}, i_{cg}= currents flowing thorough the grid side converter's output (A), v_{af}, v_{bf}, v_{cf} = output voltages of the converter referred to the neutral point of the load n (V). Consequently, for modeling purposes, it is necessary to isolate the first derivative of the currents, then the currents exchanged with the grid are calculated, taking into consideration the filter, according to expressions below [52]:

$$\frac{di_{ag}}{dt} = \frac{1}{L_f}\left(v_{af} - R_f i_{ag} - v_{ag}\right) \tag{3.62}$$

$$\frac{di_{bg}}{dt} = \frac{1}{L_f}\left(v_{bf} - R_f i_{bg} - v_{bg}\right) \tag{3.63}$$

$$\frac{di_{cg}}{dt} = \frac{1}{L_f}\left(v_{cf} - R_f i_{cg} - v_{cg}\right) \tag{3.64}$$

3.5.2 Model for Rotor Side Voltage Source Converter

The rotor side converter that supplies current to the rotor of the DFIM. Figure 3.9 illustrates the converter and the dv/dt filter used to supply the rotor of the DFIM. In this case, a two-level VSC feeds the rotor. Between the rotor and the converter, in general, a dv/dt filter is located mainly to protect the machine from the harmful effects of the voltage source converter. These include capacitive leakage currents, bearing currents, and increased stress on the motor insulation. The rotor side converter is connected to the grid side converter by the DC link.

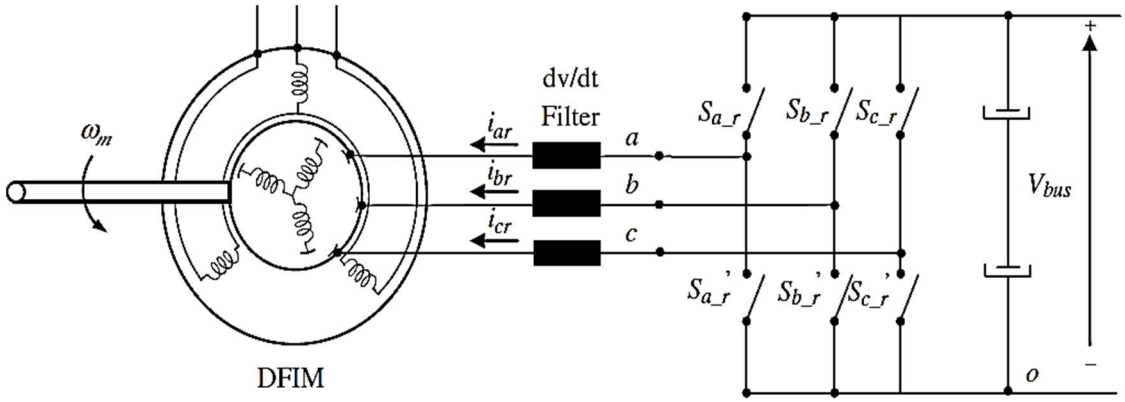

Figure 3.9: Rotor side converter and $\boldsymbol{dv/dt}$ filter supplying the rotor at the machine [52]

3.5.3 DC Link

The DC part of the back-to-back converter is typically called the DC link. The energy stored in a capacitor (or combination of several capacitors), tries to maintain a constant voltage at its terminals which is the linkage between the grid side and rotor side converters. Figure 3.10 shows a simplified model of a DC link. It is composed of a capacitor in parallel with high resistance. To derive the model for the DC link, the DC bus voltage must be calculated. This voltage is dependent on the current that passes through the capacitor [52].

$$V_{bus} = \frac{1}{C_{bus}} \int i_c dt \tag{3.65}$$

The current through the capacitor can be found as [52]:

$$i_c = i_{r\_dc} - i_{g\_dc} - i_{res} \tag{3.66}$$

Where i_{res} is current through the resistance R_{bus} (A), i_{g_dc} is the current flowing from the DC link to the grid (A) and i_{r_dc} is the current flowing from the rotor to the DC link (A). On the other hand, the DC currents can be calculated from the converter output AC currents as follows

[52]:

$$i_{g\_dc} = S_{a\_g} i_{ag} + S_{b\_g} i_{bg} + S_{c\_g} i_{cg} \tag{3.67}$$

$$i_{r\_dc} = -S_{a\_r} i_{ar} - S_{b\_r} i_{br} + S_{c\_r} i_{cr} \tag{3.68}$$

Current through the resistance is

$$i_{res} = \frac{V_{bus}}{R_{bus}} \tag{3.69}$$

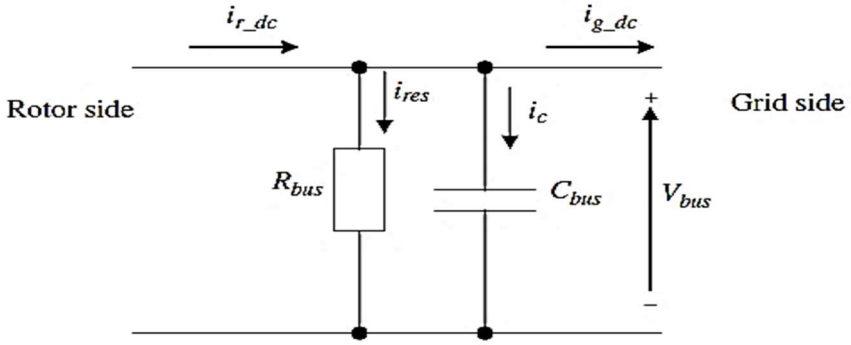

Figure 3.10: DC Link system [52]

3.6 The Control Scheme for DFIG

The control strategy used for this study is shown in Figure 3.11. A reference current calculation and current control loop presented in the diagram and both the reference reactive power Q_{sref} and Q_{gref} are usually set to zero and can be modified depending on the grid requirements. The DC link reference voltage has a fixed value while the reference torque is determined by the maximum power point tracking control system. Vector control of a grid-connected DFIM is very similar to the classical vector control of a squirrel cage machine. DFIM is controlled in a synchronously rotating dq reference frame, with the d axis oriented along with the rotor flux space vector position. The direct current is thus proportional to the rotor flux while the quadrature current is proportional to the electromagnetic torque. By controlling independently, the two current components, a decoupled control between the torque and the rotor excitation current is obtained. Similarly, in vector control of a DFIM, the components of d and q axis of the rotor current are regulated.

If a reference frame turned with the stator flux is used, the active and reactive power flows of the stator can be controlled independently using the quadrature and the direct current, respectively, as shown in Figure 3.12. The control of any electrical machine should be

performed normally in a reference frame, which rotates with one of the state space vectors of the generator to obtain steady-state control signals instead of sinusoidal signals.

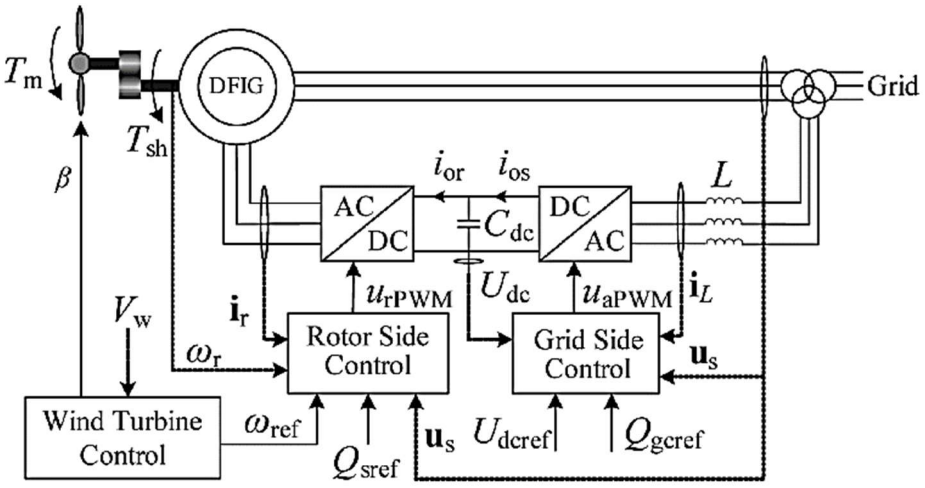

Figure 3.11: Reference values entered in DFIG back to back converter [60]

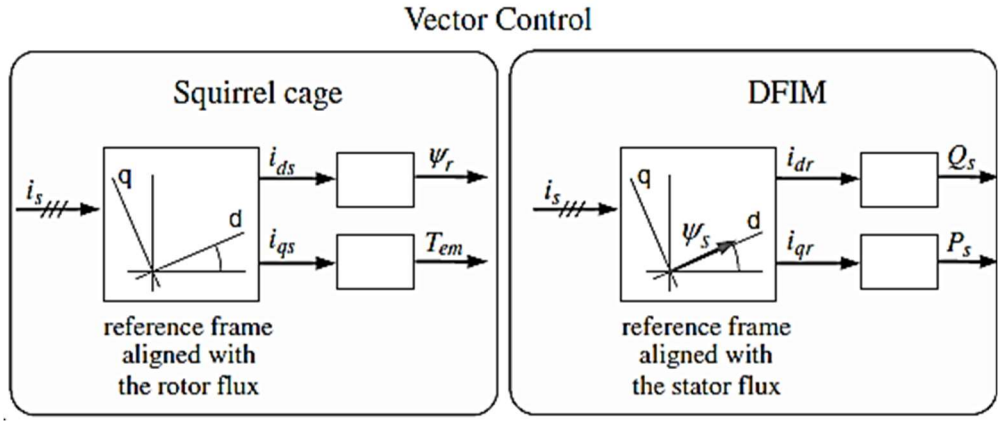

Figure 3.12: Comparison between the Vector Control of the squirrel cage machine and the DFIM [52]

Within vector-based control, field-oriented control and direct control are the most illustrative.

3.6.1 Wind Turbine Maximum Power Point Tracking

The most commonly used wind turbine control strategy is illustrated in Figure 3.13, and consists of four operation zones, this shows the wind speed as a function of the wind speed [52]:

Region-1 (Minimum speed of operation zone): The wind generator starts to run as the wind speed connection (cut-in wind speed) with a rotating speed limited to (minimum turbine speed in rad/sec) at very low wind speed. This speed can corresponds to the resonant frequency of the tower. For DFIM based turbines this limitation also serves to limit the sliding of the electrical machine and hence the rotor voltage.

Region-2: (**Maximum Power Tracking):** As wind speed increases, the rotation speed also increases until the maximum rotation speed is reached. In this operation region, the objective of the wind turbine speed control is to follow the path of maximum power extraction. Two different types of controllers have been considered; one is the indirect speed controller (ISC) where the electromagnetic torque reference related to the maximum power curve. The second is the direct speed controller (DSC), where the controller generates the optimal turbine rotational speed linked to the optimal tip speed ratio for each wind speed value. At a given wind speed, the maximum turbine energy conversion efficiency occurs at an optimal TSR [61].

Region-3 (Maximum speed limit zone at partial load operation): The wind generator operates in region-3, while the wind speed reaches its nominal value, the generator works at the rated mechanical power, and the energy captured for higher wind speeds should be regulated at this nominal value.

Region-4 (Maximum operating speed limit zone at rated power output): This corresponds to operation at full load. Here, the mechanical power can be limited either by varying the pitch or by torque control. Typically, the electromagnetic torque is maintained at a nominal value and adjusts the pitch angle to keep the turbine at maximum speed to maintain power output at higher than rated wind speed.

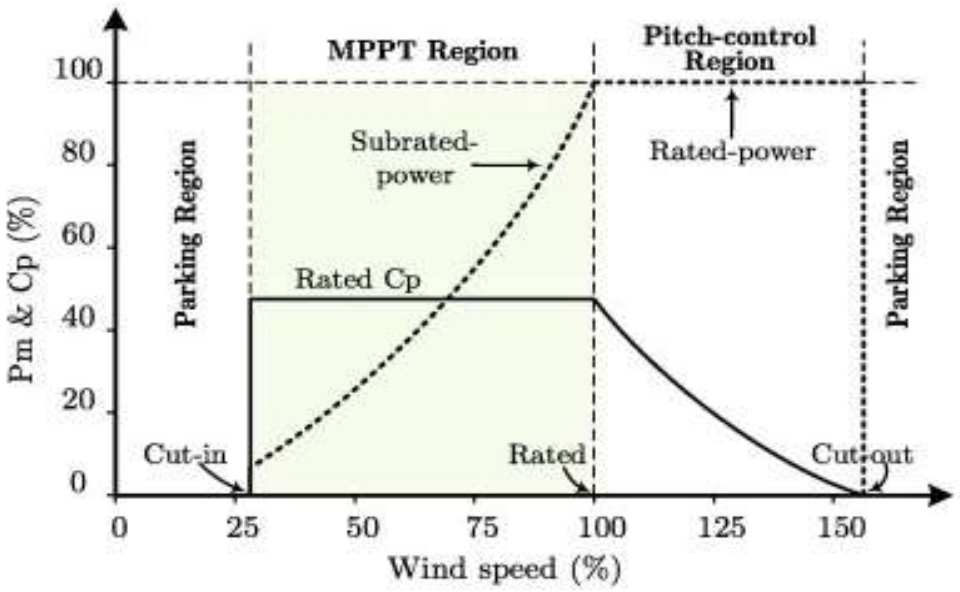

Figure 3.13: The operation zones for Power Point Tracking for wind turbine [52]

As shown in Figure 3.13, for zone 2, the wind turbine is dynamically stable around any point of the maximum power curve. This means that for any rotational speed variation around the point in the maximum power curve, the VSWT naturally goes back to its operating point. Considering that the VSWT is operating at a point of the curve in Figure 3.14, the wind speed

and the electromagnetic torque can be fixed. If the turbine rotational speed is reduced to Ω_{t_b}, the operating point passes to point b, and the corresponding turbine torque is then T_{t_b}.

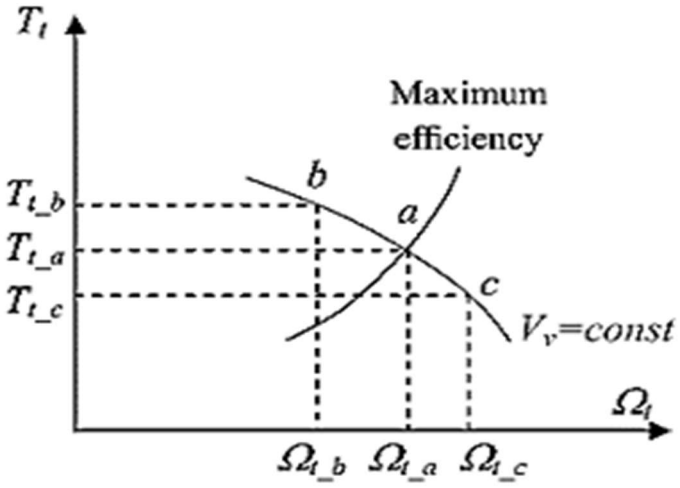

Figure 3.14: Stability curve for the point of the maximum power [52]

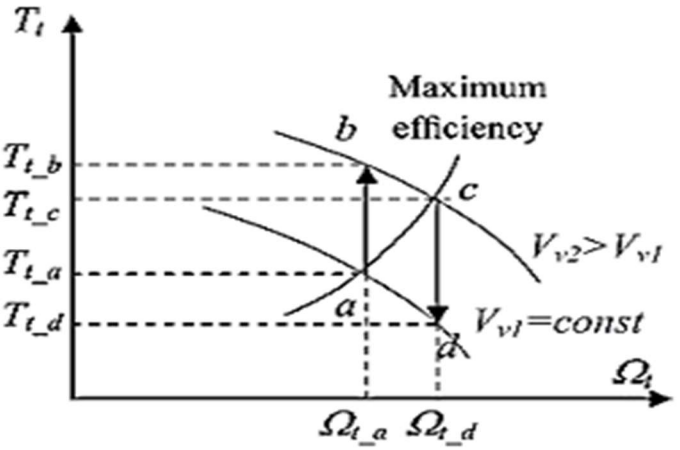

Figure 3.15: Stability curve for point of the maximum power with increased wind speed [52]

The electromagnetic torque is fixed to its preceding value which corresponding to T_{t_a}, so T_{t_b} is higher than T_{em} , and the turbine rotational speed increases until it is again stabilized around the Ω_{t_a} value. Considering this stability property, the aerodynamic torque T_t can be kept in the maximum power curve in response to wind variations. As shown in Figure 3.15, when the wind speed value increases from V_{v1} to V_{v2} , the operating point becomes (point b), and the turbine torque becomes T_{t_b}. The controller provides the electromagnetic torque corresponding to the maximum power curve (point c), which is smaller than T_{t_b}. This makes the turbine rotational to speed increase until it reaches the equilibrium point c. When the turbine is working on the maximum power point, then optimised tip speed ratio, and coefficient of performance [52]:

$$\lambda_{opt} = \frac{R\Omega_t}{V_v} \ , \ C_p = C_{\text{p\_max}} \text{ and } C_t = C_{t\_opt} \tag{3.70}$$

The aerodynamic torque extracted by the turbine is then given by [52]:

$$T_t = \frac{1}{2}\rho \times \pi \times R^3 \frac{R^2\Omega_t^2}{\lambda_{opt}^2} \times \frac{C_{p\_\max}}{\lambda_{opt}} \tag{3.71}$$

$$T_t = \frac{1}{2}\rho\pi \frac{R^5}{\lambda_{opt}^3} C_{p\_\max}\Omega_t^{\ 2} = K_{opt\_t}\Omega_t^{\ 2} \tag{3.72}$$

$$K_{opt\_t} = \frac{1}{2}\rho\pi \frac{R^5}{\lambda_{opt}^3} C_{p\_\max}\Omega_t^{\ 2} \tag{3.73}$$

Steady state of two mass mechanical model [52]:

$$J_m \frac{d\Omega_m}{dt} = T_{em} - D_m\Omega_m + T_{em} \tag{3.74}$$

$$0 = T_{em} - D_m\Omega_m - K_{tm}\left(\Omega_m - \Omega_{t\_ar}\right) \tag{3.75}$$

$$T_{em} = -\frac{T_t}{N} + \left(D_t + D_m\right)\Omega_m \tag{3.76}$$

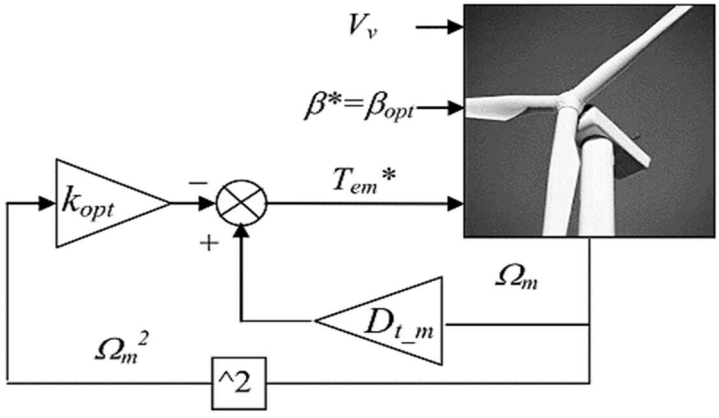

Figure 3.16: Indirect speed control [52]

Replacing T_t in Equation (3.76) by the expression $k_{opt\_t}\Omega_t^2$ in equation (3.72), the following equation is obtained [52]:

$$T_{em} = -k_{opt}\Omega_m^{\ 2} + \left(D_t + D_m\right)\Omega_m \tag{3.77}$$

Where optimisation coefficient [52]:

$$k_{opt} = \frac{1}{2}\rho \times \pi \times \frac{R^5}{\lambda_{opt}^3 N^3} C_{p\_\max} \tag{3.78}$$

k_{opt} leads to the controller as shown in Figure 3.16, this variable is defined by equation (3.78), the behaviour of the rotational speed Ω_t depends on the dynamics of the mechanical coupling and gearbox ratio N. This locus, named the MPPT-curve, can be evaluated by [52]:

$$P_{MPPT} = K_{opt}\left(\omega_r\right)^3 \tag{3.79}$$

3.6.2 Direct Speed Controller (DSC)

The (DSC) tracks the maximum power curve more closely with faster dynamics. Knowing the definition of the tip speed ratio, the optimal VSWT rotational speed Ω_{t_opt} could be found from the wind speed V_v. Unfortunately, V_v cannot be measured because it is a fictitious wind speed. The diagram of the DSC is shown in Figure 3.17.

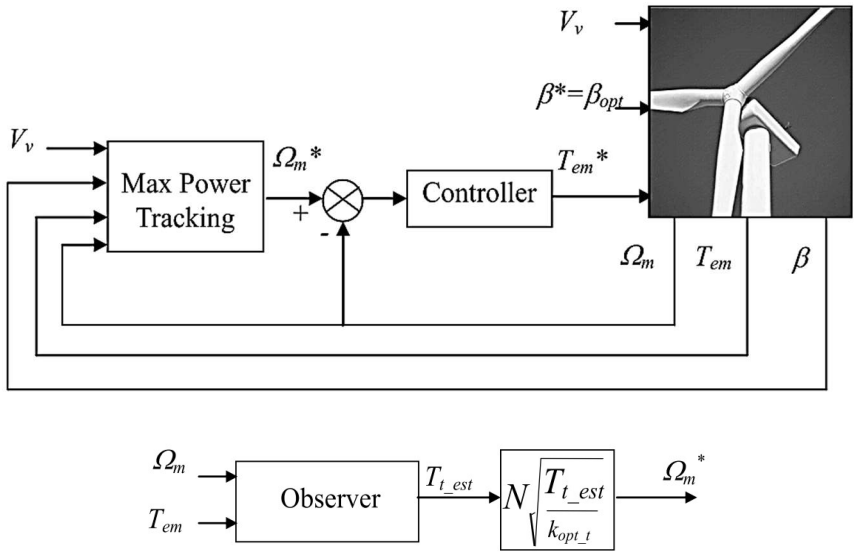

Figure 3.17: Direct speed control [52]

The rotational speed optimal value can nevertheless be obtained from the estimation of the aerodynamic torque. Based on the turbine electromagnetic torque T_{em} and rotational speed Ω_t the system can be designed to estimate the turbine aerodynamic torque T_{t_est} [62], [52]. Hence, from equation (3.71), at the optimal operating point is [52]:

$$\Omega_m^* = N\sqrt{\frac{T_{t\_est}}{k_{opt\_t}}} \tag{3.80}$$

Once the rotational speed reference is generated, the regulator controls Ω_r using the electromagnetic torque value T_{em}. Hence, the maximum power point tracking power [52]:

$$P_{\max} = \frac{1}{2}\rho\pi R^5 \frac{\left(C_{p\_\max}\right)}{\left(\lambda_{opt}^3\right)}\left(\Omega_m^*\right)^3 \tag{3.81}$$

$$P_{MPPT} = K_{opt}\left(\Omega^*{}_m\right)^3 \tag{3.82}$$

Figure 3.18 indicates that when$\beta = 0$, there exists a maximum point $C_{p\max} = C_p\left(\lambda, 0\right) = 0.48$ and $\lambda_{opt} = 8.123$ value is attained [63].

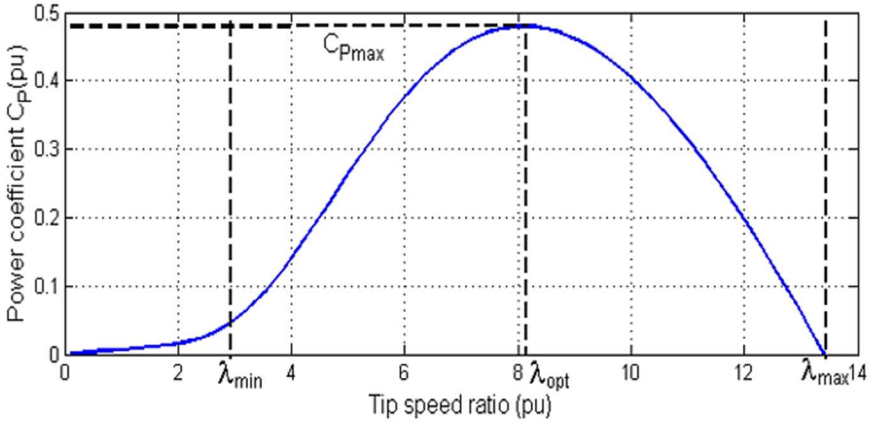

Figure 3.18: Characteristics of the wind turbine when β=0, $\boldsymbol{C_P}$ versus λ [63]

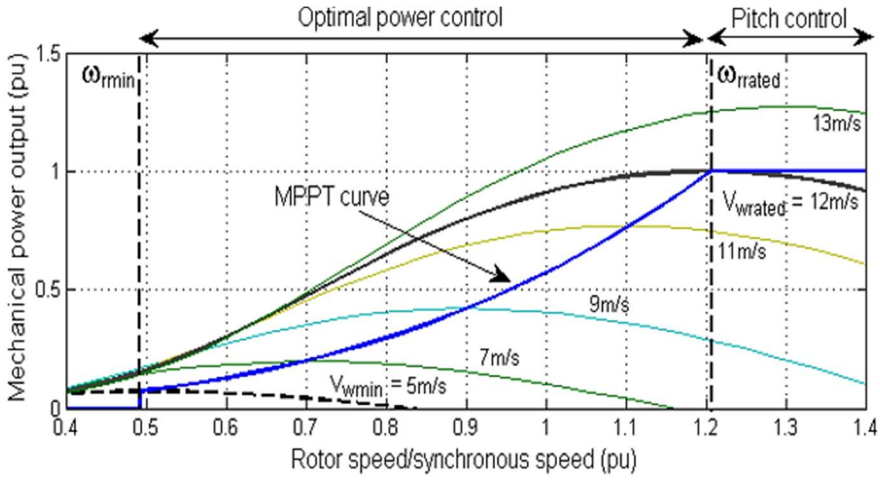

Figure 3.19: Characteristics of the wind turbine when β=0, $\boldsymbol{P_{Max}}$ versus $\boldsymbol{\omega_r}$ [63]

As can be seen in Figure 3.19, the wind turbine works in the optimal power control region when the rotor speed is between the minimum speed ω_{rmin} and the rated speed ω_{rrated} or when the wind speed is between the minimum speed V_{wmin} and the rated speed V_{wrated}. In this region, the wind turbine should operate on the locus of the maximum power-point P_{max}.

3.6.3 Pitch Angle Control

The pitch control is used for controlling the amount of generated power by the wind turbine. Its function is to maintain a constant output power from the turbine. To maintain the constant value or not exceed the rated values, is by varying the pitch angle of the rotor blades. There are two main methods of varying the pitch angle: one is from the difference between measured electrical power and power reference, and the other is to obtain the pitch angle from the difference between the measured mechanical speed and reference speed. These two signals give the error, which can be inputted in the pitch controller.

Various strategies can be used to achieve the best values of pitch angle to maintain the output power within the limit using a different controller such as P or PI controllers, and fuzzy logic control [64]. The selection of the pitch control technique using PI controller is illustrated in Figure 3.20. In this control technique, the difference between the rated power P_{rated}, which acts as the reference power, P_{ref} and the actual power P_e generates the error signal that will be sent to the PI controller to achieve an appropriate gain of output power, compared to the input mechanical power, finally changing the pitch angle of the wind turbine blade as desired.

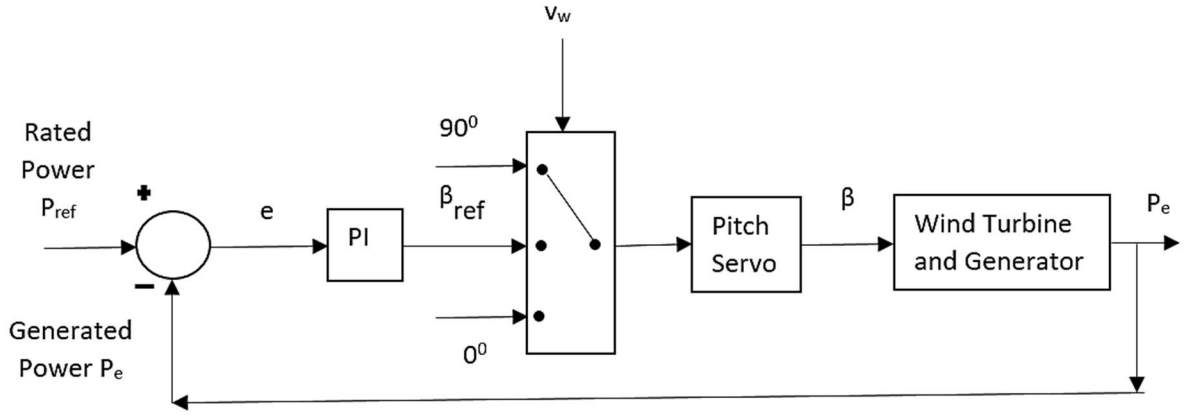

Figure 3.20: Schematic diagram of the pitch angle controller using PI controller [64]

The optimal combination of proportional and integral gain improves the speed of the response and also minimizes the steady-state error. The PI controller equation can be expressed as [64]:

$$\beta_{ref}(t) = K_p e(t) + K_i \int e(t)\,dt \tag{3.83}$$

Where K_p and K_i are proportional and integral gains respectively, that are used to control the response of the system, $e(t)$ is the error difference between output and reference powers.

For a better understanding of the pitch angle control mechanism, the following power characteristic for a typical large scale wind turbine will be explained. Four different regions are shown in the power curve as a function of the wind speed as shown in Figure 3.21.

In regions I and IV, when the wind is below cut-in wind $v_{w(cut-\ )}$ and above cut-out wind $v_{w(cut-o\ )}$, the pitch angle is kept at 90 degrees to stop the rotor from rotating. In region II, for wind speeds between $v_{r(cut-o\ )}$ and $v_{w(rated)}$ the pitch angle is fixed at 0 degrees for maximum aerodynamics of the rotor, and then maximum power captured from the wind kinetic energy.

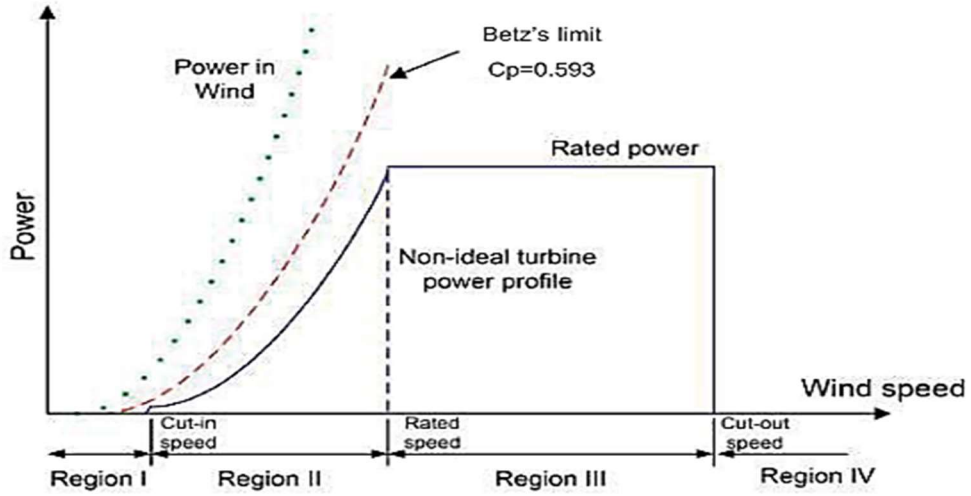

Figure 3.21: Power Output for a Wind Turbine Generator [64]

In region III for wind speeds between $v_{w(rated)}$ and $v_{r(cut-out)}$, the pitch angle β is varied (decreased with an actuator constant rate limiter of 10 degrees/sec) for keeping the power generated at its rated value.

3.7 Conclusion

In this chapter, an analytical and numerical modelling of wind turbine aerodynamics, wind turbine drive systems, DFIG and WECS. A vector control of a grid-connected DFIM has been proposed in a synchronously rotating dq reference frame, with the d axis oriented along with the rotor flux space vector position. The direct current is thus proportional to the rotor flux while the quadrature current is proportional to the electromagnetic torque. The main control system using a traditional PI controller depends up on two controllers for RSC and GSC respectively. The function of the first controller is to achieve the MPPT in RSC during variable wind speed while the second controller is working in order to keep the DC link voltage constant during simulation to keep the output voltage and frequency within acceptable limits.

Chapter 4

Computer Simulations

4.1 Steady-State Simulation of DFIG

The power system analysis for networks with WTG is complicated unlike the power system with conventional energy sources such as thermal, hydro, and nuclear plants. This is because of the following reasons:

- The power injected into the grid by WTG depends on the wind velocity, which is unpredictable because of the and intermittent nature of wind; and
- Most of the WTG use induction generators, therefore, there is the problem of slip.

The power flow in the wind turbine system was modelled using the Simulink/MATLAB model as shown in Figure 4.1. This Simulink model was executed by creating the steady-state MATLAB script functions (m-files) which were used to simulate the steady-state operation points of the simulation model. This simulation showed how the rotor speed of the induction generator with respect to the input wind speed affect the power flow in the system. In this simulation model, the MATLAB function was formulated and executed using the DFIG parameters.

In this script, a 2 MW stator power of the DFIG model parameter was implemented. The implementation was done by creating the speed and torque values as arrays which are the system inputs, stimulating these input values, the output parameter for the three-blade wind turbine was obtained. The programmed Simulink model can also calculate the moderate percentage of the variables of the magnitude of the DFIG with respect to the specified input arrays of the wind turbine speed and torque. Depending on how the reactive power of this model was controlled, two different framework of the generation strategies were used. The first strategy was to make the reactive power status Q_s zero and the second strategy was to make the rotor current I_{dr} zero. Both control strategies were simulated in a developed MATLAB script.

The simulations were carried out by running the MATLAB program for wind speeds ranging from 5 m/s (cut-in speed) to 25 m/s (cut-off speed) in progressive steps of 2 m/s, with reactive power $Q_s = 0$ and rotor current $I_{dr} = 0$ as a separate control strategy. The steady-state operation of the machine displayed the variable outputs, with respect to the rotor speed and torque input arrays, and the results for the voltage, torque, real power generated, efficiency, and reactive power consumed by the WTG in both the methods are plotted in Figure 4.2 to Figure 4.4.

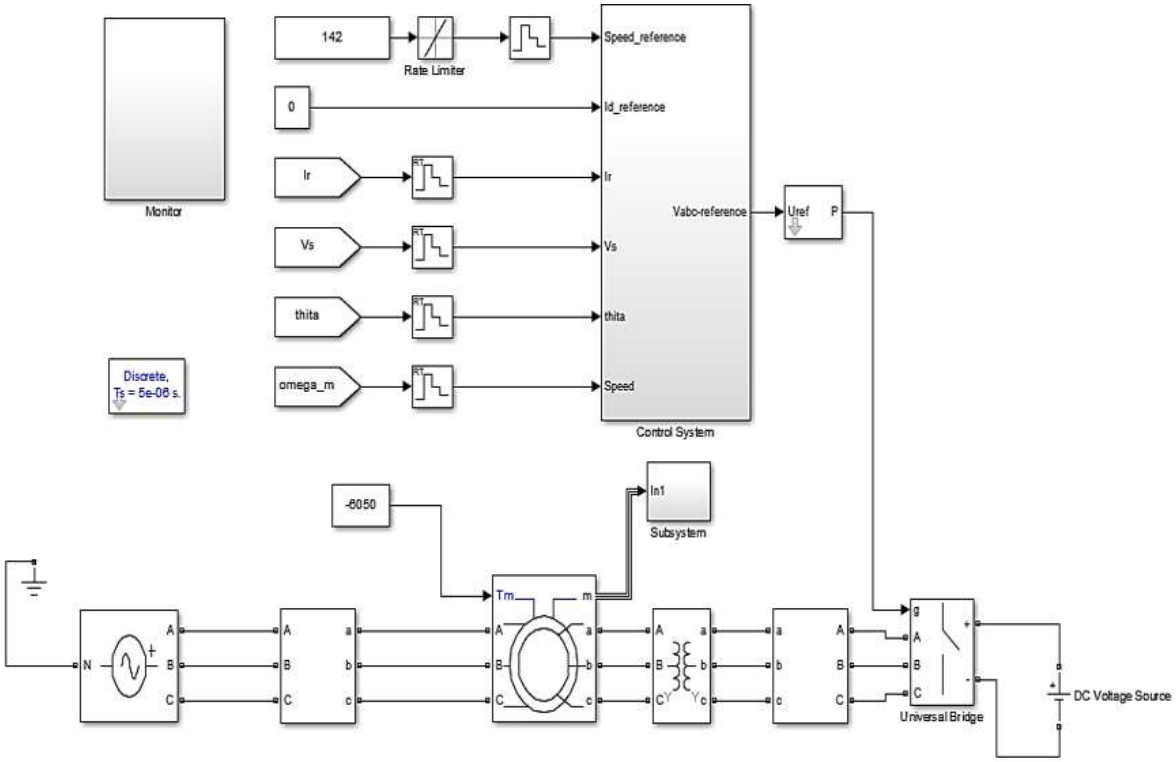

Figure 4.1: Simulink/MATLAB model for Steady-state operation of wind turbine

Figure 4.2 shows the DFIG's torque vs speed characteristics, which stimulate the three-blade wind turbine with a minimum speed of 900 rpm and a maximum speed of 1800 rpm. The DFIG can run at above and below the synchronous speed to generate power. The generating mode of the DFIG corresponding to negative torque values extends from the negative slip to the positive slip region. Hence, the turbine output power and electromagnetic torque characteristics of variable speed DFIGs are different from the traditional fixed-speed induction machine.

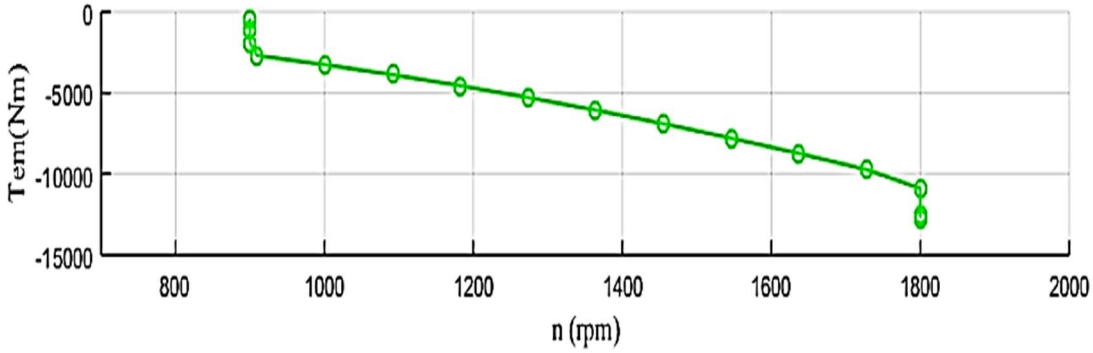

Figure 4.2: The graph of torque (T_{em}) vs rotor speed (n)

Figure 4.3 shows the total power of the turbine shaft which is a form of mechanical power. This power is the product of torque and speed. The maximum power value is -2.54 MW at 1800 rpm.

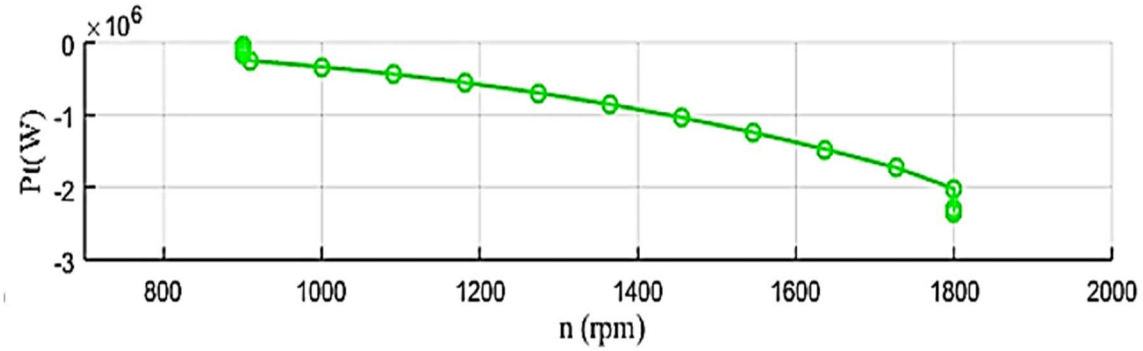

Figure 4.3: The graph of total power (P_t) vs rotor speed (n)

Figure 4.4 shows the rotor and stator active power. The rotor active power P_r varies according to wind speed. It was observed that the DFIG operates in the motor mode when the rotor is driven below the synchronous speed. The negative sign of active power means that the power is absorbed by the induction machine, while when the rotor runs at a speed higher than the synchronous speed of the revolving magnetic field, active power is supplied from the induction generator to the grid.

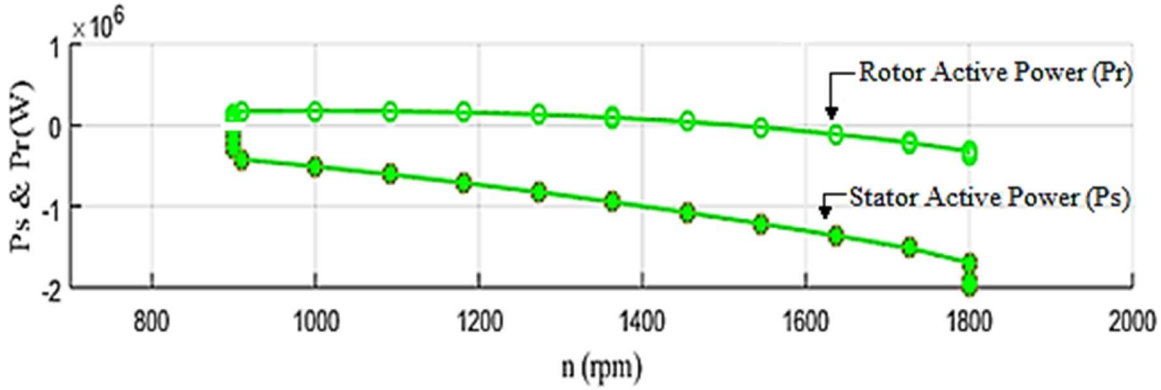

Figure 4.4: The graph of the DFIG stator and rotor active power vs rotor speed

From the graph, at the synchronous speed, the rotor active power remained constant and this corresponds to the rotor losses. The stator active power P_s is always negative in generator mode, with maximum value pf $P_s = -2Mw$ at 1800 rpm. The sign of the rotor active power P_r depends on both the mode of operation of the machine (either motor or generator) and the operating speed (hyper-synchronous or hypo-synchronous) $P_{rmax} = -400w$ at 1800 rpm.

4.2 Simulation Results for Active and Reactive Power

Simulations carried out using the MATLAB script for the active and the reactive power are shown in Figure 4.5 to Figure 4.10. The program was simulated with a reactive power reference $Q_s = 0$ and plotted in red and d-axis rotor current reference $I_{dr} = 0$ as plotted in green as a

separate control strategy. The influence of two different strategies does not make any big differences for variables such as T_{em}, P_t, P_s and P_r. However, some other variables such as I_s plotted in Figure 4.5, I_r plotted in Figure 4.6, Q_s plotted in Figure 4.8 and Q_r plotted in Figure 4.9 were found to have huge differences in amplitudes with respect to the rotor speed.

Figure 4.5 and Figure 4.6 show that with two different control strategies $Q_s = 0$ and $I_{dr} = 0$, stator current I_s has a different value. When $Q_s = 0$ (red plot) as a control strategy is adopted the stator current value is on the lower side as shown in Figure 4.5. On the contrary when $I_{dr} = 0$ (green plot) as a control strategy the rotor current I_r is on the lower side as shown in Figure 4.6.

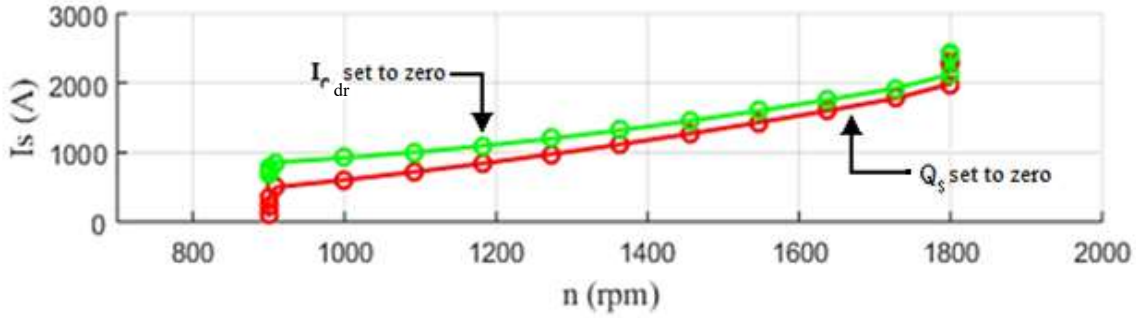

Figure 4.5: The graph of the DFIG I_s (amps) vs n (rpm)

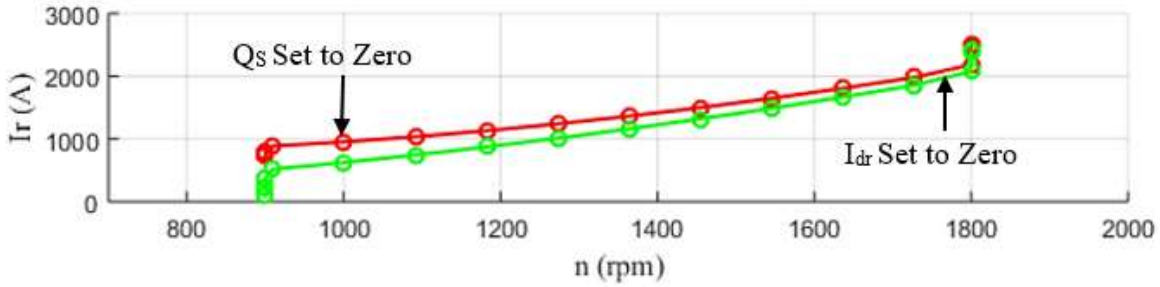

Figure 4.6: The graph of the DFIG I_r (amps) vs n (rpm)

Figure 4.7 shows that for a grid-connected DFIG, there is stator voltage V_s amplitude remained constant with the variable speed, while the rotor voltage V_r amplitude varies with is the variable speed. From the graph, it can be deduced that rotor voltage amplitude V_r is lowest at the synchronous speed of 1500 rpm, and at a minimum and maximum rotor speeds, two peaks rotor voltage amplitudes were observed. In this case, since, the working referencing is the stator side, these peak rotor voltages are not the real rotor voltages. On transforming these rotor voltages to real voltage, these amplitudes will be close to V_s amplitude.

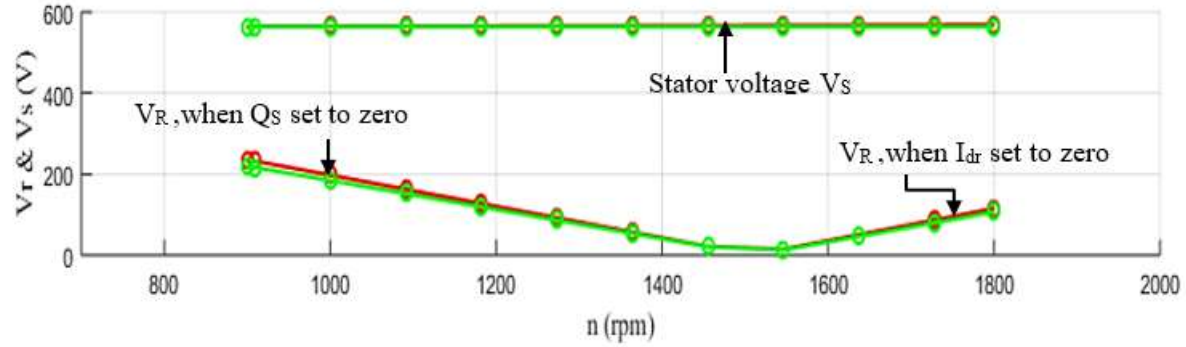

Figure 4.7: The graph of the DFIG V_r & V_s (volts) vs speed n (rpm)

Figure 4.8 shows the rotor and stator reactive power. With $I_{dr} = 0$ as a control strategy, the stator reactive power, Q_s, is higher than compared to when $Q_s = 0$ is a control strategy.

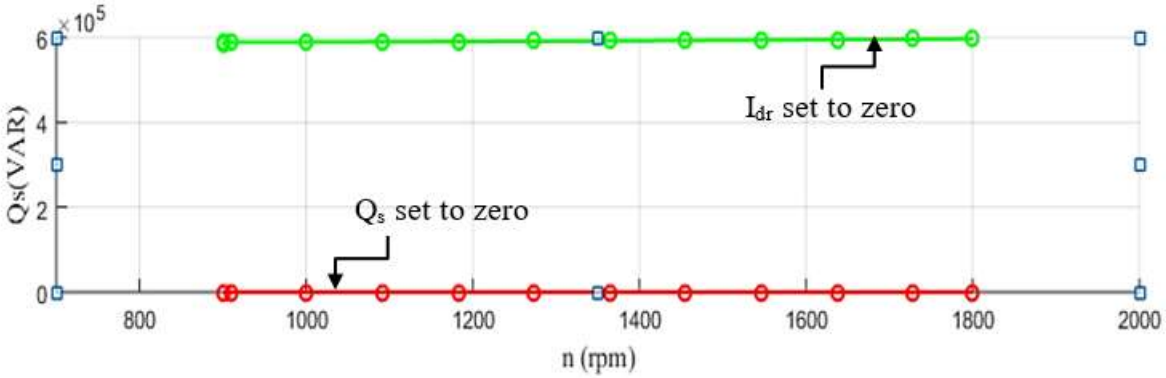

Figure 4.8: The graph of the DFIG Q_s (VAR) vs n (rpm)

Figure 4.9 shows the rotor reactive power $Q_r = 0$ at synchronous speed, with both control strategy $Q_s = 0$ and $I_{dr} = 0$. It also shows the reactive network power varies according to the wind turbine speed.

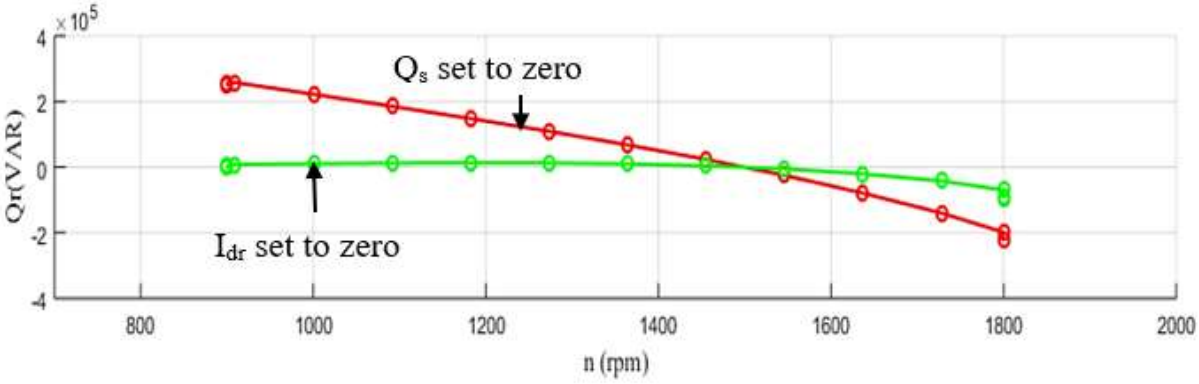

Figure 4.9: The graph of the DFIG Q_r (VAR) vs n (rpm)

Figure 4.10 shows the motor mode has higher efficiency than the machine operated in generator mode since the stator of the machine sinks more reactive power in the generator mode.

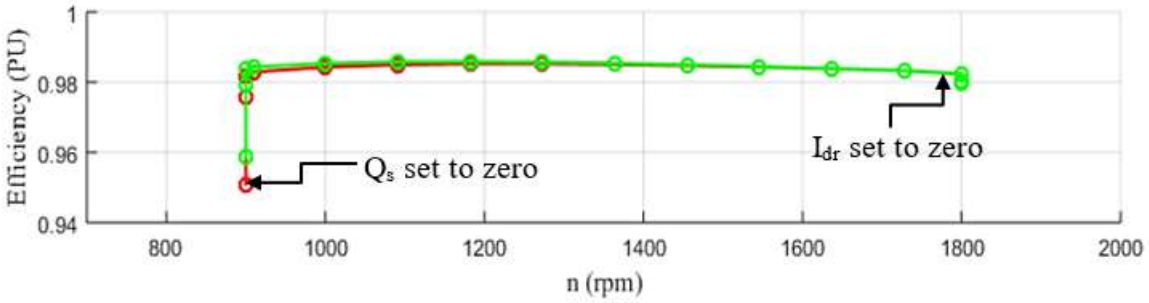

Figure 4.10: The graph of DFIG Efficiency (PU) vs n (rpm)

Earlier, the steady-state analysis was investigated for variable speed, and the next sets of simulation were done for the wind turbine at a defined rotor speed and evaluated against the steady-state operation of the system. From the simulation result, a rotor speed of 1356 rpm (142 rad/sec) corresponds to a torque value of -6050 Nm and a rotor speed of 1691 rpm (177 rad/sec) corresponds to a torque value of -9450 Nm. Considering the generation mode scenarios to evaluate the simulation model. Before commencing the simulation, a rate limiter control component with a (+/- 100 rad/sec) slew rate was added in series with the speed reference input to suppress the step variables/step changes, and also changes were made to the PI regulator gain to make it four times faster than the steady-state condition.

On the commencement of the simulation, during the transient state, the initialization is very high due to the high stator and rotor transient currents, however, in practice, this approach is not recommended when approaching the simulation steady-state condition with respect to speed and torque (reference vs actual) and current loops. The corresponding values of speed, torque, stator, and rotor current, and the rotor voltage are tabled in Table 4.1. For the specified wind turbine speeds, the steady-state results were obtained and compare with simulation model results. The comparison was used to evaluate the simulation model at the desired rotor speed against the steady-state.

Characteristic curves for the speed n, rotor current (I_r), torque (T_{em}), d-axis rotor voltage V_{dr}, and stator current (I_s), are shown in Figure 4.11 to Figure 4.20. Figure 4.11 to Figure 4.15 shows the simulation model graph of speed reference and the speed vs time graph at 142 (rad/sec) speed reference at 1.55 sec modelling time. Figure 4.16 to Figure 4.20 shows the simulation model graph of speed reference and speed vs time graph at 177 (rad/sec) speed reference at 2.1 sec modelling time as steady-state conditions.

Figure 4.12 and Figure 4.17 show the simulation model graphs of rotor currents at $I_{qr} = I_r$ at 1350 amps and 2200 amps respectively. These are equal or close to the steady-state rotor current 1340 amps and 2200 amps as shown in Figure 4.6.

Figure 4.13 and Figure 4.18 show the simulation model graphs of $V_r = \sqrt{(V_{dr})^2 + \left(V_q\right)^2}$ = 60V and 100V respectively which are equal to the steady-state value $V_r = 60V$ and 110v as shown in Figure 4.7.

Figure 4.14 and Figure 4.19 show the simulation model graph of torques -6050 Nm and -9450 Nm as shown in Figure 4.2.

Figure 4.15 and Figure 4.20 show the stator current magnitudes $I_s = 1000$ amps and 1500 amps are close as shown in steady-state Figure 4.5.

Table 4.1: Wind Turbine simulation model at different turbine speed

Sn	Speed		Torque (N-m)		I_r		I_s		V_r	
	Steady-state	Simulation Model	Steady-state	Simulation Model	Steady-state	Simulation Model	Steady-state	Simulation Model	Steady State	Simulation Model
1	1182	1182	-4550	-4550	875	920	1090	1100	110	100
2	1356	1356	-6050	-6000	1160	1200	1325	1350	60	60
3	1691	1691	-9450	-9455	1770	1790	1850	1860	73	75

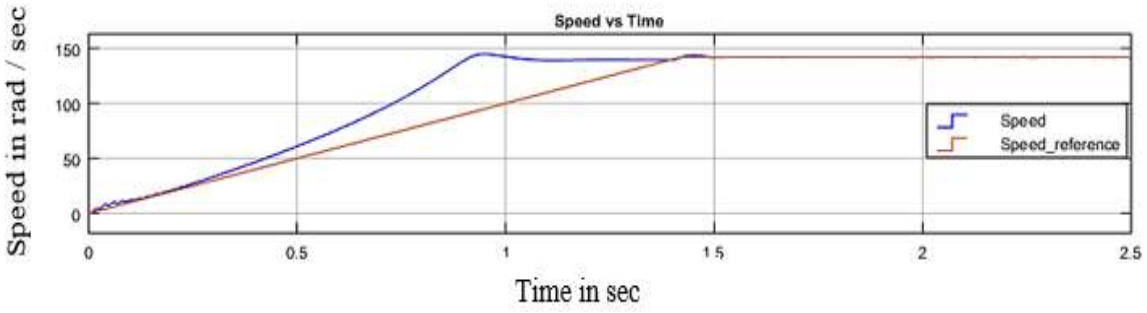

Figure 4.11: The steady state simulation graph at 142 rad/sec speed vs time

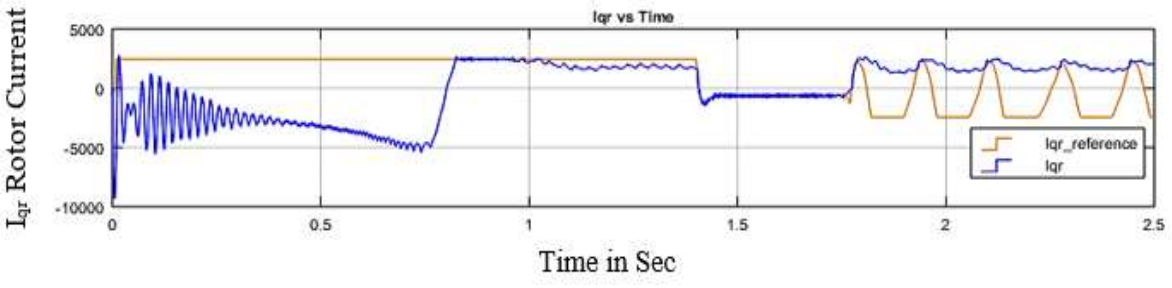

Figure 4.12: The study state simulation graph of I_{qr} vs time

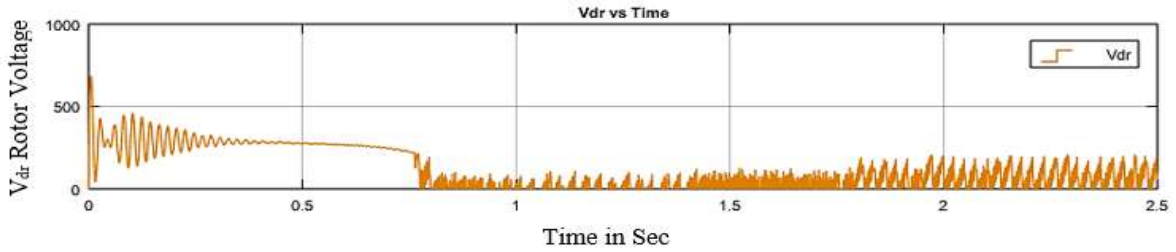

Figure 4.13: The steady state simulation graph of V_{dr} vs time

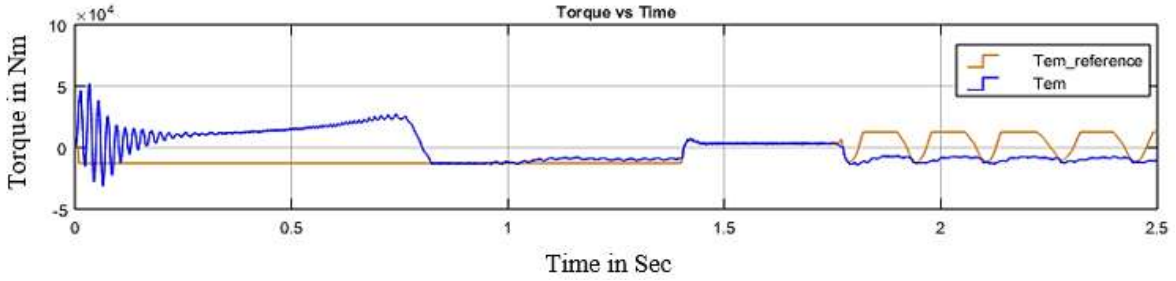

Figure 4.14: The steady state simulation graph of torque vs time

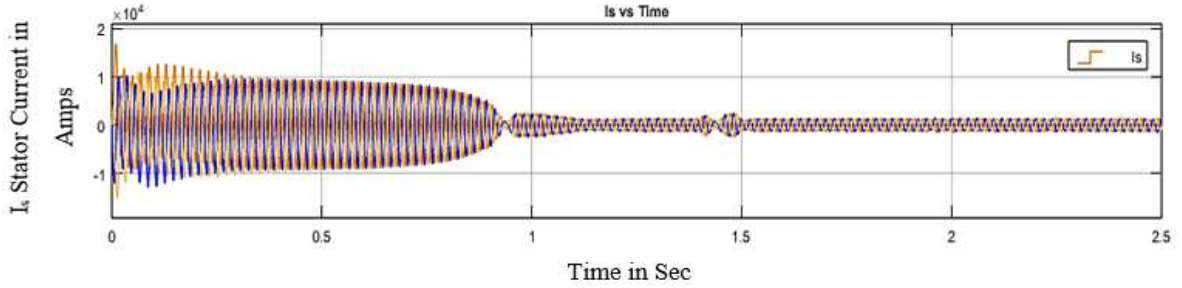

Figure 4.15: The steady state simulation graph of I_s vs time

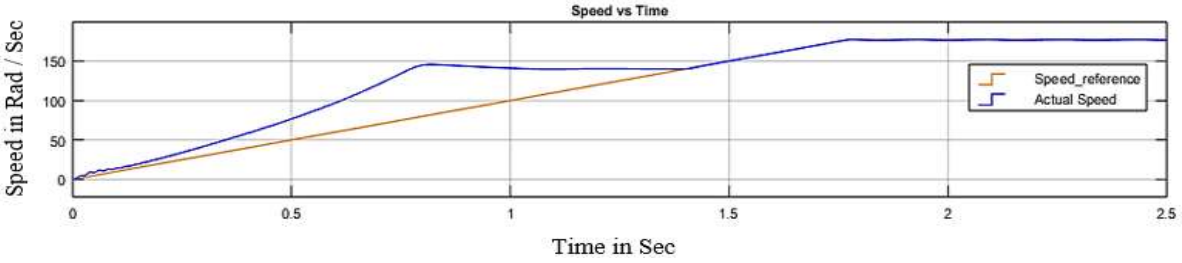

Figure 4.16: The steady state simulation graph at 177 rad/sec speed vs time

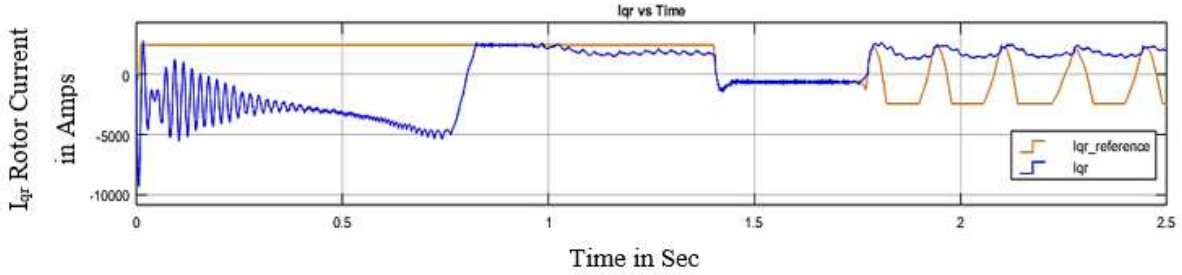

Figure 4.17: The steady state simulation graph of I_{qr} vs time

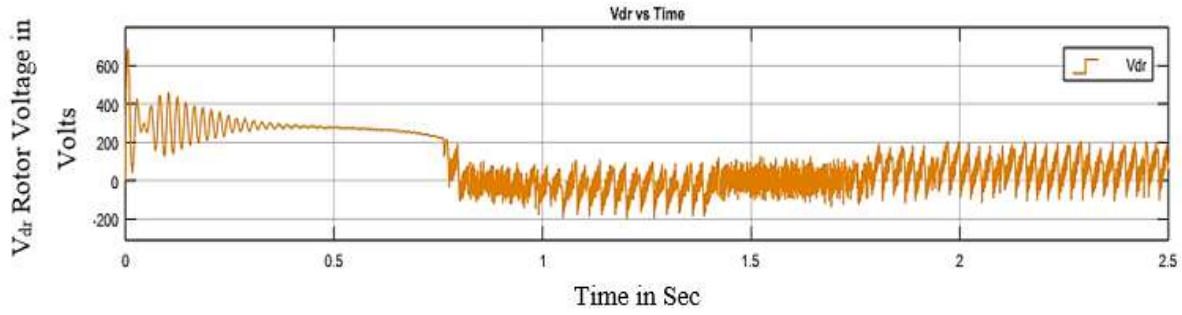

Figure 4.18: The steady state simulation graph of V_{dr} vs time

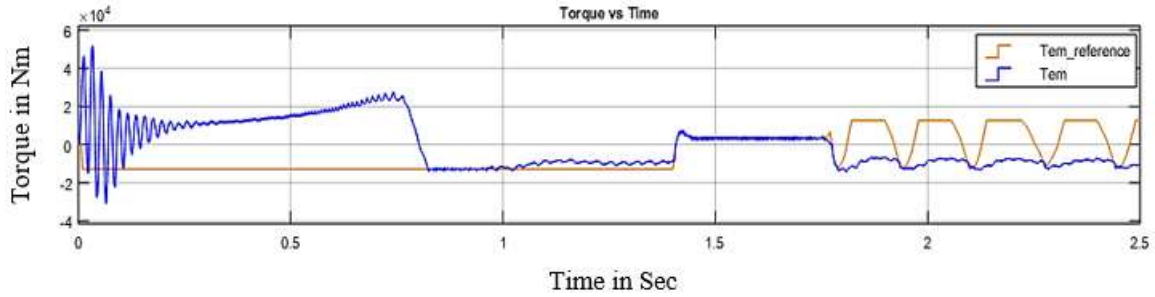

Figure 4.19: The steady state simulation graph of torque vs time

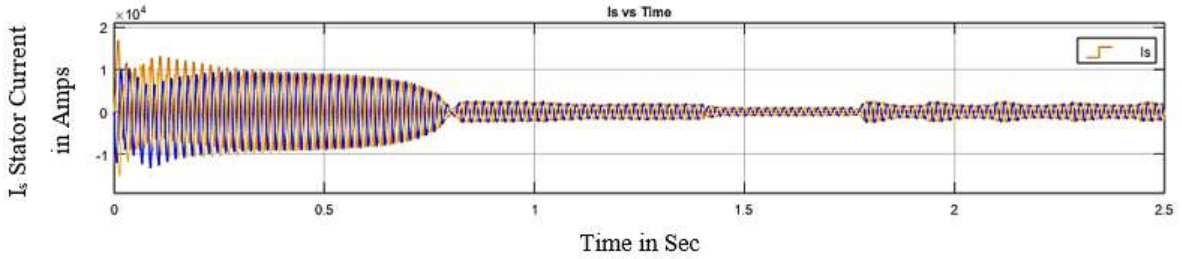

Figure 4.20: The steady state simulation graph of I_s vs time

4.3 Analytical Simulation of DFIG Model

This section presents the simulation of the DFIG connected directly to the network through the stator, where the integration of power is controlled by its rotor through an AC/DC and DC/AC converter. The MATLAB/Simulink model is depicted in Figure 4.21, using the WT MPPT control Simulink block. The utilization of the DFIG for WT with variable rotating speed allow for the possibility to decrease the power of the converters. For a normal operation, the rotor converter VSC controls the rotating speed or the torque of the DFIG, and the grid converter VSC is responsible for the delivery of the produced energy into the grid and the reactive power control. The DFIG and WT parameters used for the wind turbine maximum power point tracking, and block dynamic control was formulated and implemented using a MATLAB script. In this script, a 2 MW stator power of the DFIG model has been loaded.

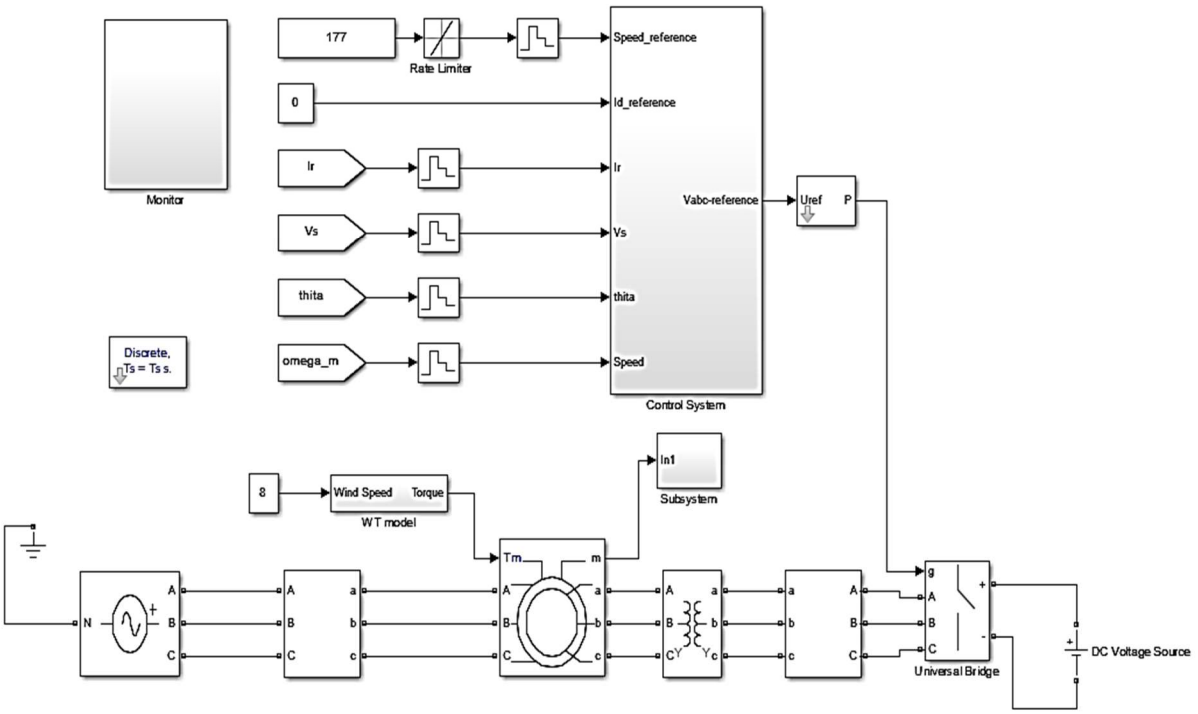

Figure 4.21: Block diagram of the WT maximum power point tracking control model

As shown in Figure 4.21, is the wind turbine model which has already included in the steady-state model as depicted in Figure 4.1. The input to the proposed wind turbine model was the variable wind speeds, for instance, where the wind speed of 8 m/s was chosen as the input to the WT model. Within the WT block, the value of $\lambda_{opt} = \frac{R\Omega_t}{V_v}$, will be calculated by, using the values of turbine rotational speed Ω_t, wind speed V_v, and the turbine blade radius R. In this WT model, as referred to the low-speed shaft and this requires the consideration of gear ratio N. The calculated value of λ_{opt} can be obtained by indexing the torque coefficient C_t as shown in Figure 4.22. On achieving both λ_{opt} and C_t, with the variable wind speeds V_v, the following $T_t = \frac{1}{2}\rho\pi R^3 V_v^2 C_t$ turbine torque formula can be implemented, obtained by dividing the torque by the gear ratio N in order to achieve the turbine torque at the shaft rotating at a high speed. Finally, the value to be multiplied by (-1) to get the generator convention.

On implementing the indirect speed control, the turbine torque T_e^* is obtained by measuring the speed multiplied by the constant k_{opt}, using the damping coefficient of the mechanical system as positive feedback to the closed-loop control system as shown in Figure 3.16. Here the dominant part would be the turbine speed. During the indirect speed control, the system does not require the speed value and PI controllers.

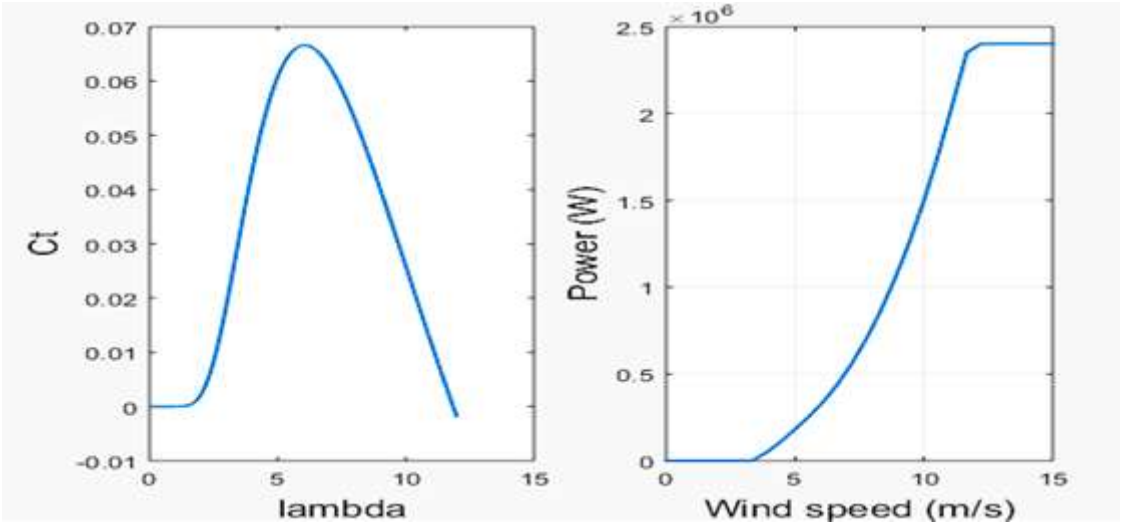

Figure 4.22: The graph of dynamic modelling power coefficient $\boldsymbol{C_t}$ vs tip speed ratio (Lambda) and Wind Turbine power (Watts) vs Wind speed (meter/sec) [63]

Figure 4.23 and Figure 4.24 show the wind turbine MPPT simulation model characteristics at 8 m/sec and 10 m/sec of wind speed. Observed in Figure 4.2, the torque response for the wind speed and i_q current indicate that more oscillations occur at the low torque due to the reduction in mechanical inertia. The more the mechanical inertia, the more the torque oscillations. On achieving the steady-state condition at 2 sec of modelling time, wind turbine speed and correspondence torque values were tabled for angular speed of 140 rad/sec, at a torque of -5500 Nm, and a mechanical wind turbine power output approximately equal to 770 kW was obtained. Further, the wind speed was increased from 8 m/sec to 10 m/sec and the steady-state simulation at 6 sec of modelling time was observed. On achieving the steady-state at 6 sec of modelling time, wind turbine speed and correspondence torque values were tabulated for 170 rad/sec, at -8800 Nm respectively and a mathematical wind turbine power outcome equivalent to 1.49 MW was recorded. These two simulated outcomes are very close to the steady-state characteristics graph numerical values as shown in Figure 4.2 and Figure 4.3.

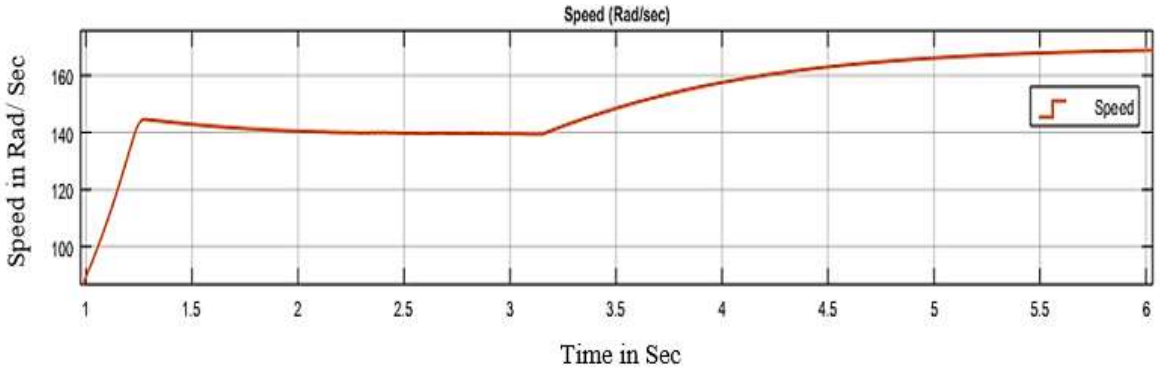

Figure 4.23: The dynamic state WT MPPT graph of speed vs time

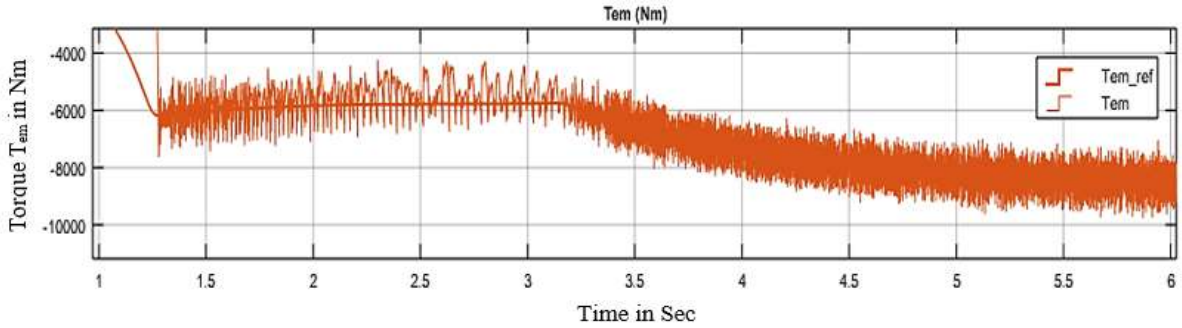

Figure 4.24: The dynamic state WT MPPT graph of torque vs time

4.4 Simulation Model of DFIG Grid-Connected Converter

Figure 4.25 shows the MATLAB/Simulink model coupled with a power electronic converter for connecting the DFIG to the grid. The grid side converter block diagram for the power electronic converter is shown in Figure 4.26, including the DC bus voltage, grid side filters, and resistance, inductance, and *PI* controller gains. The formulation of this model was obtained by incorporating the grid side converter into the already designed WT MPPT steady-state simulation model presented in Figure 4.21.

The simulation started at 7.5 m/sec of wind speed, with the implementation of MPPT algorithm control. The controller strategy itself works with the generator rotor referring to the stator, but this creates output voltage and current as a real reference to the rotor side. All the generator parameters used are referred to as the stator side.

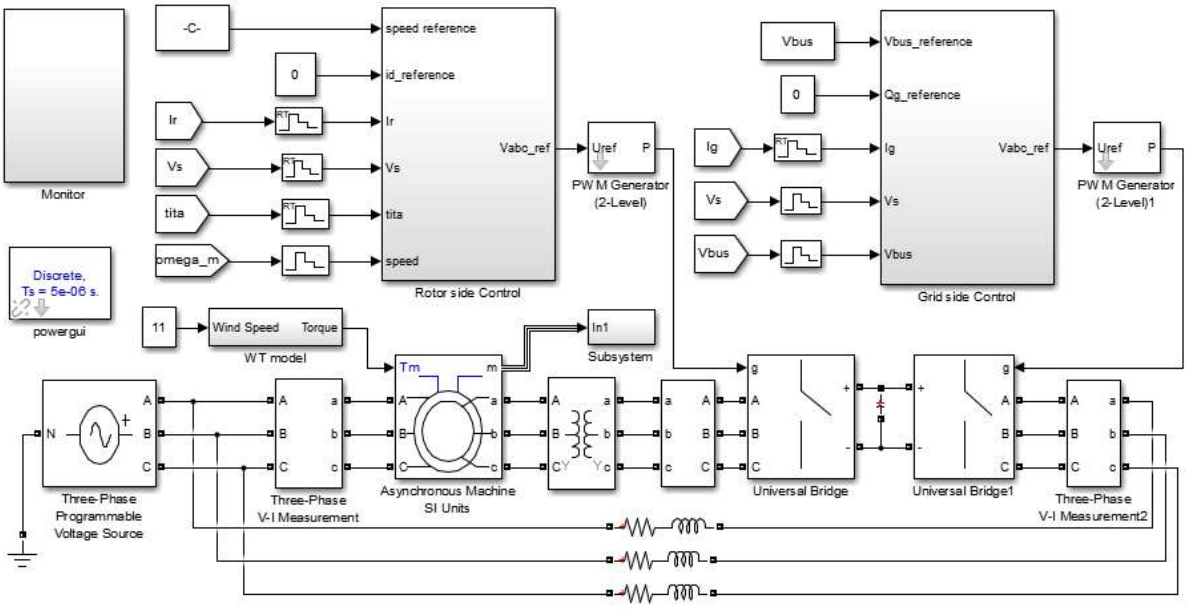

Figure 4.25: MATLAB/Simulink model for the DFIG wind turbine grid-connected converter

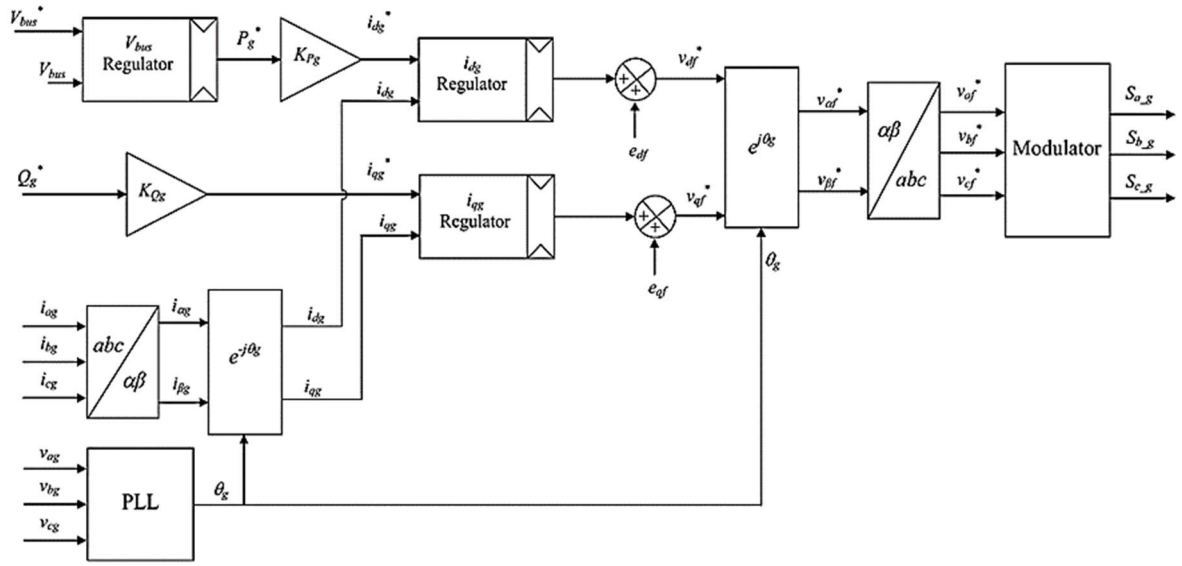

Figure 4.26: Grid voltage oriented vector control (GVOVC) block diagram [52]

During the start-up, the RSC and GSC have a stable operating point, hence the DC bus voltage stabilizes at the maximum set active power corresponds to the i_{dg} current. It indicates the working status of current loops in the GSC. On acquiring the stable grid side performance, it was observed that the RSC current and torque loops controllers were also working and the wind turbine speed accelerated using the MPPT controller to attain its optimum rotational speed corresponding to the input wind speed of 7.5m/sec. On achieving the steady-state conditions at 2.0 sec in the simulation model, the wind speed was increased to 11m/sec until the grid model

achieve steady-state conditions at 5.55 sec with a modelling cycle up to 6.3 sec.

Figure 4.27 and Figure 4.30 show that the DC bus voltage stabilised processes and constant stator voltage, during steady-state condition at 2.0 sec and 5.55 sec simulation period at 7.5m/sec and 11m/sec wind speed respectively.

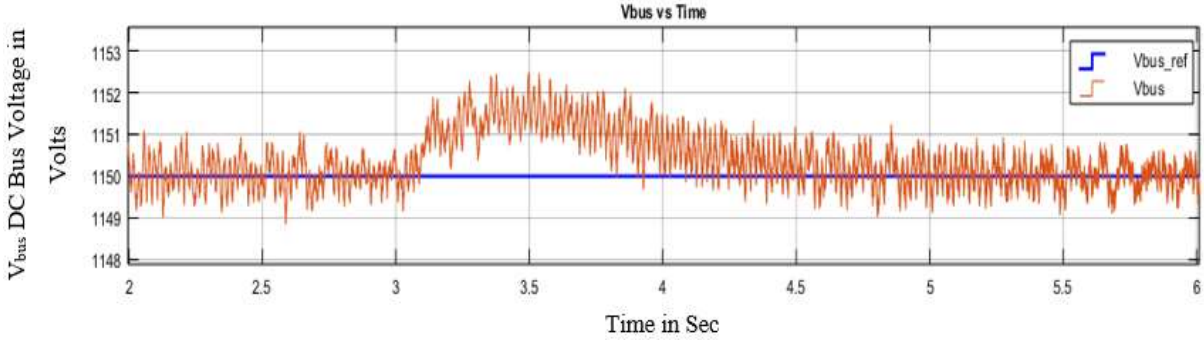

Figure 4.27: The steady-state conditions graph of DC bus voltage vs time

Figure 4.28 and Figure 4.29 represent the d-axis $\boldsymbol{I_g}$ current's stabilization process and $\boldsymbol{V_g}$ voltage reference during steady-state condition at 2.0 sec and 5.55 sec simulation period at 7.5m/sec and 11m/sec wind speed respectively.

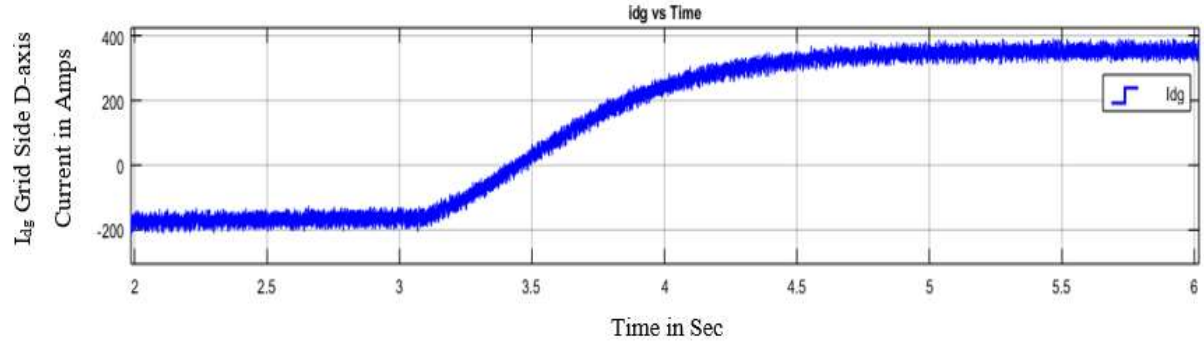

Figure 4.28: The steady-state conditions graph of I_{dg} current vs time

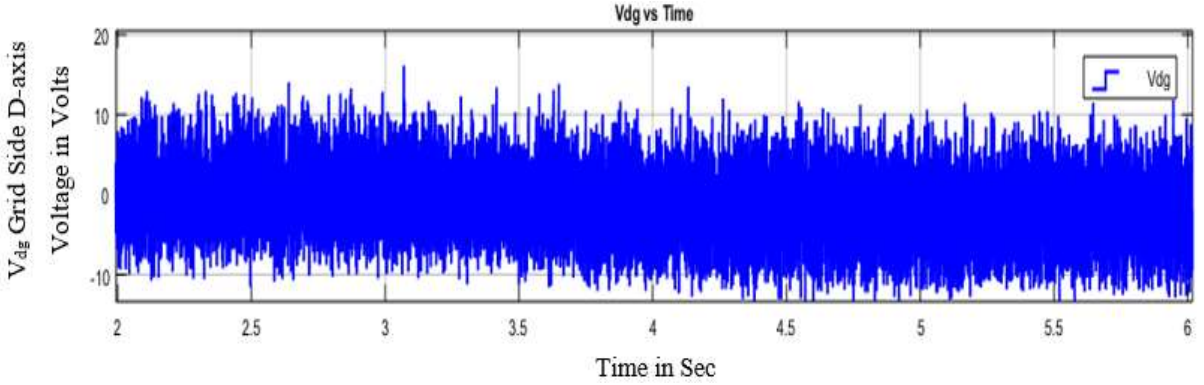

Figure 4.29: The steady-state conditions graph of V_{dg} voltage vs time

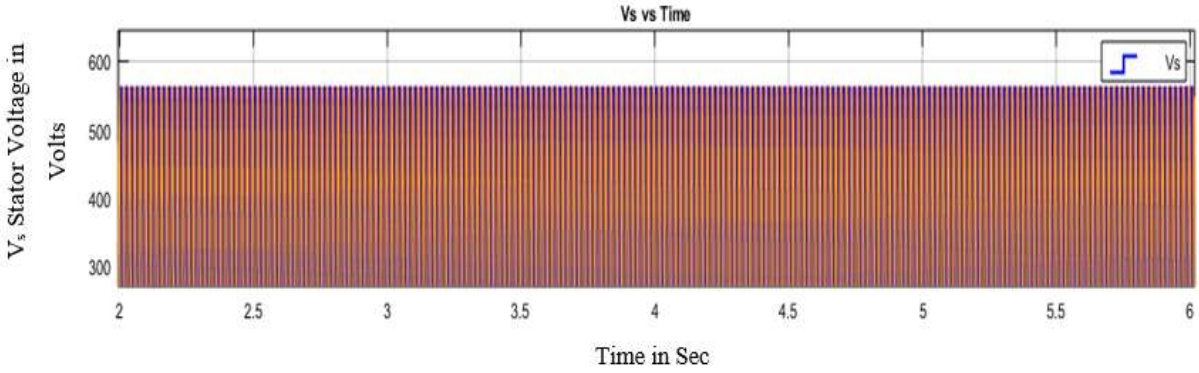

Figure 4.30: The steady-state conditions graph of stator voltage V_s vs time

At 11 m/s input wind speed, the MPPT algorithm operates at less torque and high wind turbine speed. This means the rotor will have more power $\boldsymbol{i_q}$ therefore, it was observed that $\boldsymbol{v_{bus}}$ starting to oscillate. Figure 4.27 to respond to the reference signal, resulting $\boldsymbol{i_{dg}}$ to vary accordingly in Figure 4.28. With the added performance of $\boldsymbol{Q_{g\_ref} = 400VA}$ in the grid side converter, simulation signals shows $\boldsymbol{i_{qg}}$ modified according to the changes in $\boldsymbol{Q_{g\_ref}}$ and at the rotor synchronous speed close to the simulation time of 3.5s the $\boldsymbol{i_g}$ current is minimum as shown in Figure 4.31. The rotor currents are almost constant as shown in Figure 4.35. At hypersynchronous speed, the rotor active power increases, hence, $\boldsymbol{i_g}$ increases Figure 4.31.

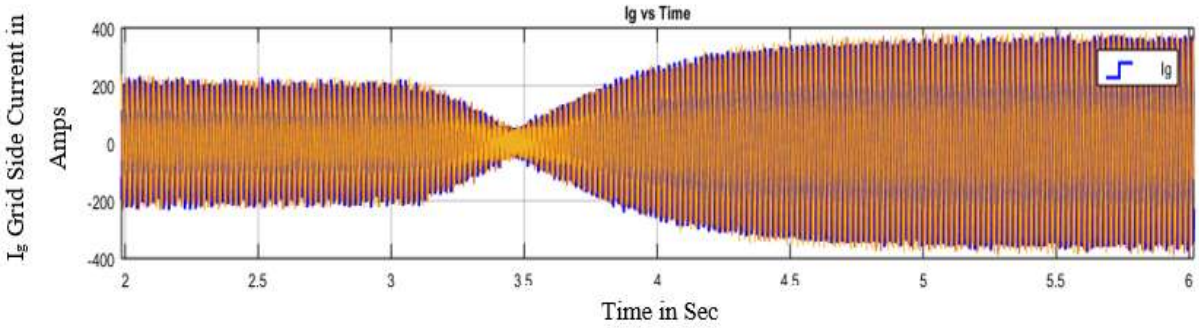

Figure 4.31: The steady-state conditions graph of grid current I_g vs time

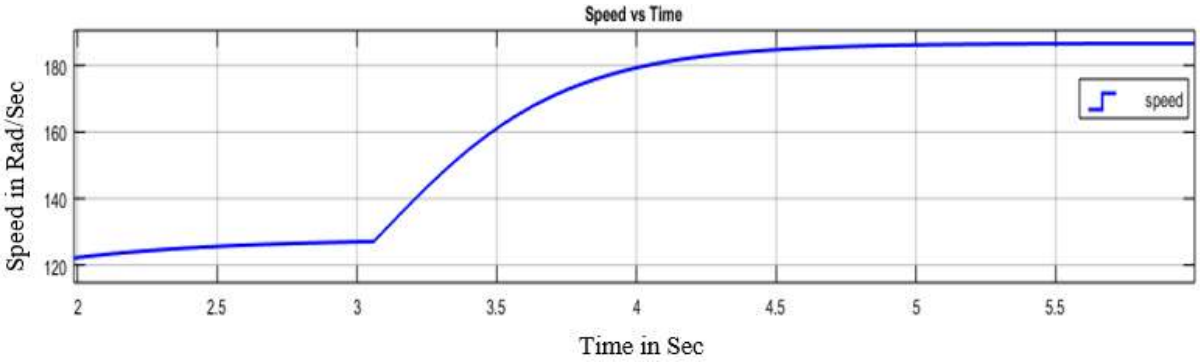

Figure 4.32: The steady-state conditions graph speed vs time

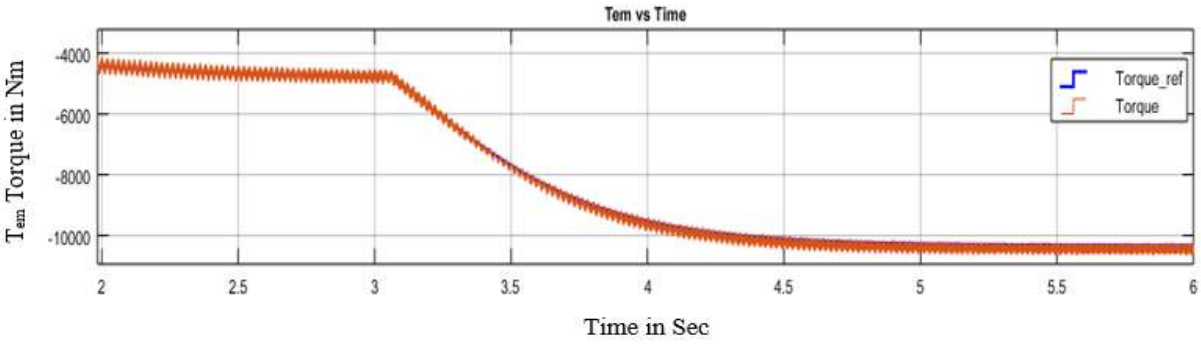

Figure 4.33: The steady-state conditions graph torque vs time

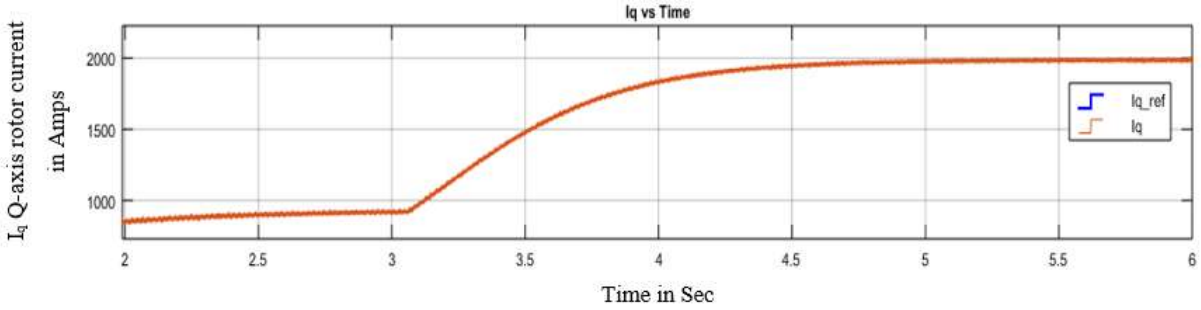

Figure 4.34: The steady state conditions graph I_q vs time

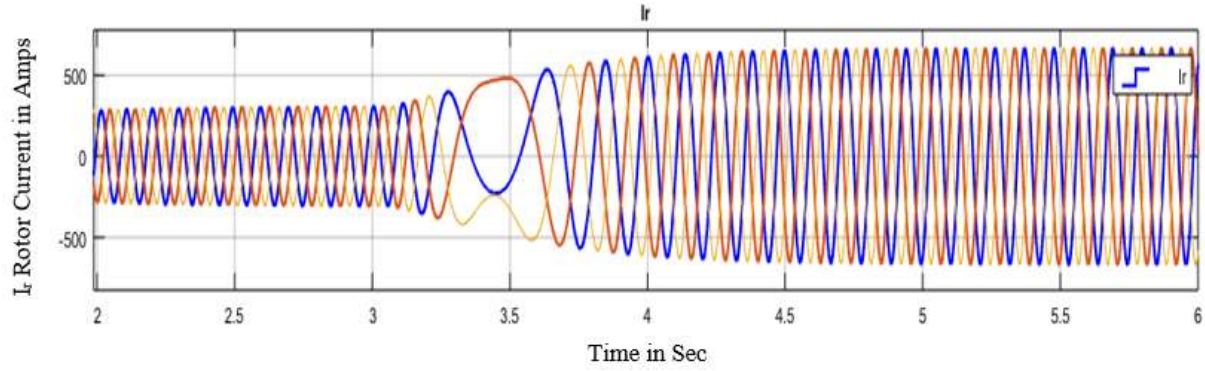

Figure 4.35: The steady state conditions graph rotor current I_r vs time

Chapter 5

Experimentation and Network Analysis

5.1 Introduction

This chapter presents the experimental set-up, experimental results, the design, and control of the DFIG wind turbine. This was followed by the analysis of integration and the control of wind energy into the network as replicated in the laboratory. This experimental study is aimed to achieve the following objectives:

- To further the understanding of the design and operation of the wind power plants.
- To learn about the physical principles and the process of how wind power is transformed into shaft power and finally into electrical power.
- To learn about wind power plants with respect to the design and operation using the doubly-fed asynchronous (induction) generator.
- To investigates the wind turbine generator operation at various wind intensities, as well as control the output voltage and frequency.
- To determine the optimal operating points of the wind turbine power plant under various wind conditions.

The experimental study was carried out at the HVDC, Smart Grid laboratory, situated at the University of KwaZulu-Natal, Westville campus. The experimental studies were done using variable-speed wind turbines. For the experimental set-up, the 0.8 kW doubly-fed asynchronous generator was used with the parameters for this turbine is provided in the next section. This turbine is a laboratory scaled model that can be used to replicate the real-world scenario, thus, has the capability to validate experimentally a real wind turbine [65].

Firstly, the power control of the DFIG was achieve by controlling the magnetising rotor current of the turbine. The effect of change in wind speed and change in supply frequency are also taken into consideration for the performance analysis of the DFIG. The performance of the DFIG speed control operation in a grid-tied wind energy conversion system was also analysed. To generate the maximum power under the variable wind speed, the generated power followed the wind speed profile which is used to verify the robustness of the controller. The results of this experimental study are used to validate the simulations results presented in Chapter 4.

5.2 Experimental Set-up

The variable wind turbine experimental set-up is made up of the Labsoft environment using the LUCAS-NULLE servo-machine that consists of a digital controller, a brake, and the Active-Servo software. The variable speed DFIG controller CO3208-3A test bench with "WindSim" software was used to analyse the performance of the DFIG system under low grid voltage. The figure for the experimental set up is shown in Figure 5.1. These components that comprise the experimental workbench are discussed as follows:

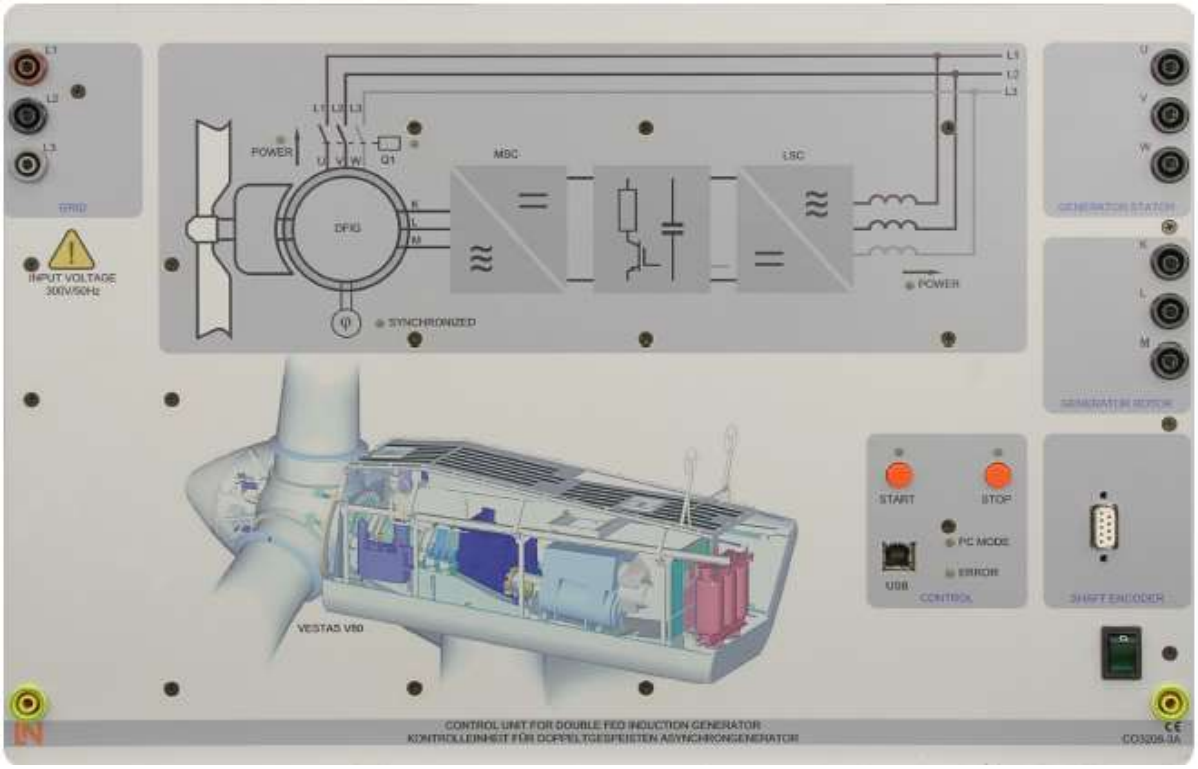

Figure 5.1: The experimental test bench [65]

CO3208-3A –Variable Speed DFIG Controller

The controller employed in this experimentation permits the control and operation of a variable-speed, double-fed induction generator under laboratory conditions. The control unit makes it possible to replicate real scenarios that are of practical significance. The software in the test bench enables the operation and visualisation of measured values. The control unit has the following features: two controlled three-phase inverters, sub-synchronous and super-synchronous operation of the induction generator, integrated power switch for connecting the generator to the grid, independent control of reactive/active power in terms of frequency and voltage, manual and automatic network synchronisation, input for the incremental sensor,

integrated brake chopper for experiments on fault ride-through, connection voltage: 3 x 300 V, 50Hz, maximum output power: 1 kVA.

SE2662-6W -Three-phase motor-generator

Figure 5.2: Three-phase motor-generator (DFIG unit) [65]

The majority of the modern wind turbines uses doubly-fed asynchronous generators to supply power grids with electricity. Figure 5.2 depicts a three-phase, multi-function machine (doubly fed induction generator) which was used for the wind turbine generator. The DFIG unit has the following rated features: voltage: 400/230 V, 50 Hz, current: 2.0 A / 3.5 A, speed: 1400 / 1500 rpm, power: 0.8 kW, cos phi: 0.75, excitation voltage: 130 VAC / 24 VDC, excitation current: 4 AAC / 11 ADC.

CO3208-3B -Three-phase transformer

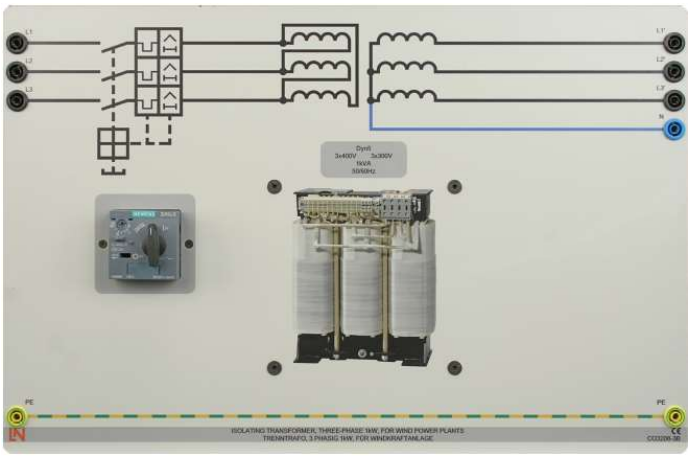

Figure 5.3: Three-phase isolation transformer for the DFIG coupling [65]

Shown in Figure 5.3 is the Three-phase delta to star isolation transformer unit which is used for coupling the doubly-fed wind power plant to the supply network. The transformer unit has the following specifications: primary voltage: 3 x 400 V, secondary voltage: 3 x 300 V, and rated power: 1 kVA.

SE2662-5T –Incremental Encoder

Figure 5.4: Incremental pulse encoder [65]

Figure 5.4 shows the incremental encoder which is used for the wind turbine speed feedback control system operating as a closed-loop control system. It has the following features: 1024 pulses, TTL level, speed: 6000 rpm, and moment of inertia: 35 gcm.

Servo Machine controller SE2663-6U test bench

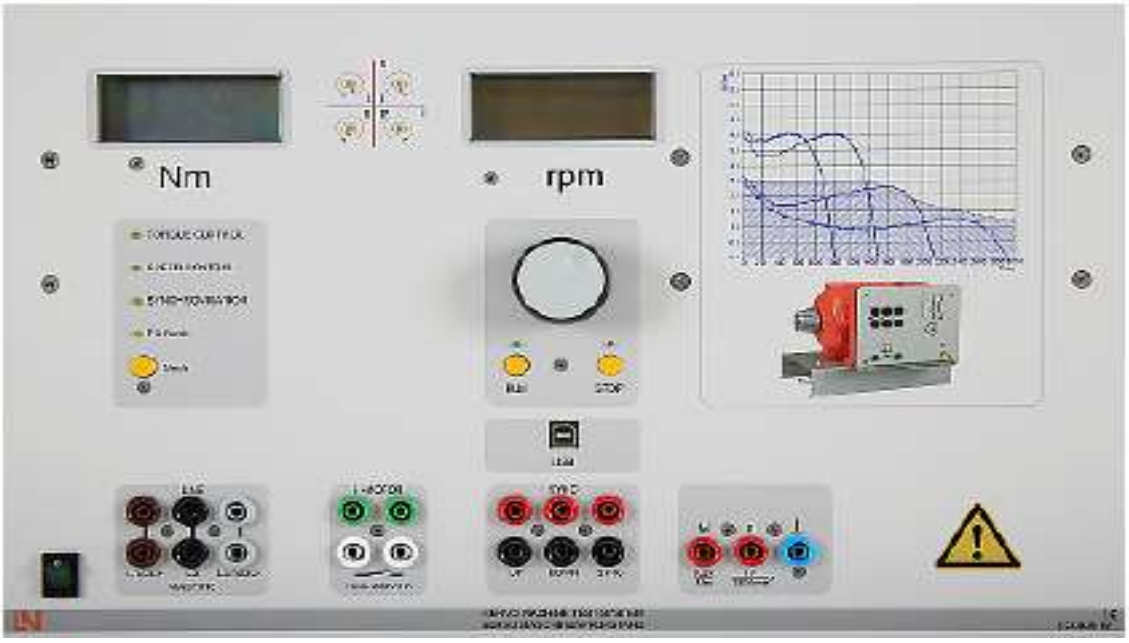

Figure 5.5: Servo machine controller SE2663-6U test bench [65]

Figure 5.5 is the servo-machine SE2663-6U used for testing and examining electrical machines and drives. It consists of a digital controller, a brake, and Active-Servo software. The system is used to manually and automatically carry out synchronisation when connecting DFIG to the grid. The controller has the following features: dynamic and static four-quadrant operation, and 10 selectable operating modes/machine models (torque control, speed control, flywheel, lifting drive, roller/calendar, fan, compressor, winding gear, arbitrarily defined time-dependent, load, manual and automated network synchronization).

Main power supply CO3212

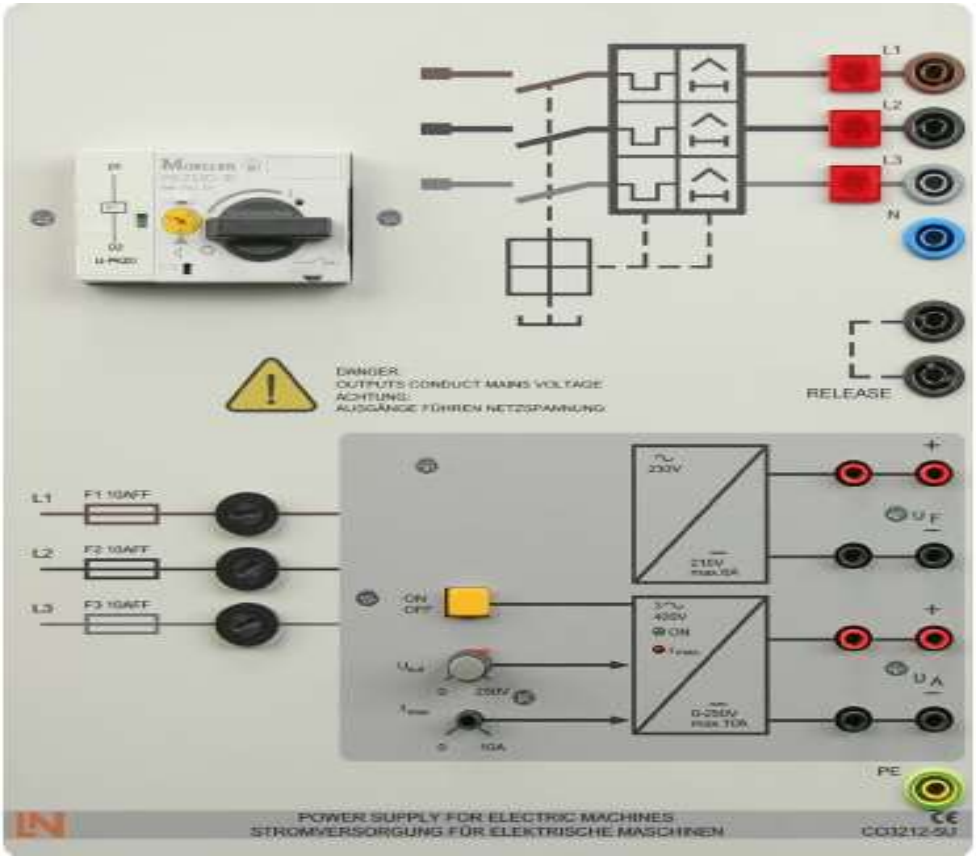

Figure 5.6: Main power supply (laboratory setup) [65]

The mains power supply as shown in Figure 5.6 is used to supply both DC and AC voltages. The power supply unit is specially designed for operation with electrical machines that have the following specification: Three-phase: L1, L2, L3, N accessible via 4 mm safety sockets, DC variable voltage: 0 - 240 V, constant and electronically protected against overload and short-circuit, Output current: 3 - 10 A (adjustable current limitation setting), Second DC voltage 210 V DC, 6A fixed, Protective devices: Motor protection CB switch, adjustable from 6.3...16 A, Under-voltage trip, Emergency OFF switch, Mains connection: CO3212-5U: 3 x 230/400 V, 50 Hz, CO3212-5U7: 3 x 120/208 V, 60 Hz, Dimensions: 297 x 228 x 140 mm (HxWxD), Weight: 3 kg.

5.2.1 Experimental Components Specifications

Several virtual instruments from the Labsoft environment were used for the operation of the experimentation. The experimental arrangement showing the various equipment used is shown in Figure 5.7 and the description of the specification of the main equipment in the Labsoft environment is detailed in Table 5.1.

The experimental set-up consists of a 1 kVA variable power supply, static and dynamic four-quadrant operation servo machine with a digital controller, a brake, the ActiveServo software, and an incremental encoder feedback SE2662-5T used as a wind turbine emulator. Two back-to-back 6 pulse IGBT inverters are used, for the switching frequency. For this study, a 3 kHz was chosen as there is a balance between switching losses and the accuracy of the desired signals achieved. A three-phase delta to star isolation transformer unit CO3208-3B was used for coupling the doubly-fed wind power plant to the supply network, data acquisition system CO5127-1Z, and a real-time digital simulator CO3208-3A, which is a powerful tool for rapid control and has the Intel® Xeon Quad Core 2.4 GHz Processor.

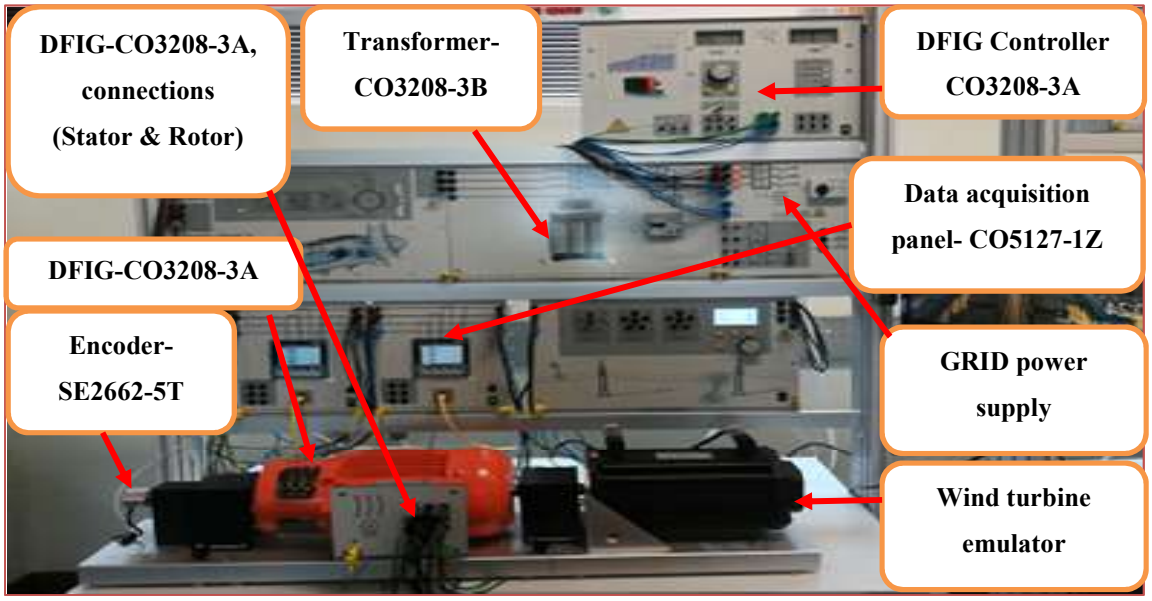

Figure 5.7: Drive train of the experimental rig setup at HVDC center at UKZN

The schematic circuit diagram for the connected experimental set-up to replicate the WECS system is shown in Figure 5.8. The experimental system consists of a 4-pole three-phase wound-rotor induction machine. Each phase of the stator winding is accessible via the connection module to allow wye or delta connection. The rotor is wye connected to four slip rings giving access to all windings, including the neutral.

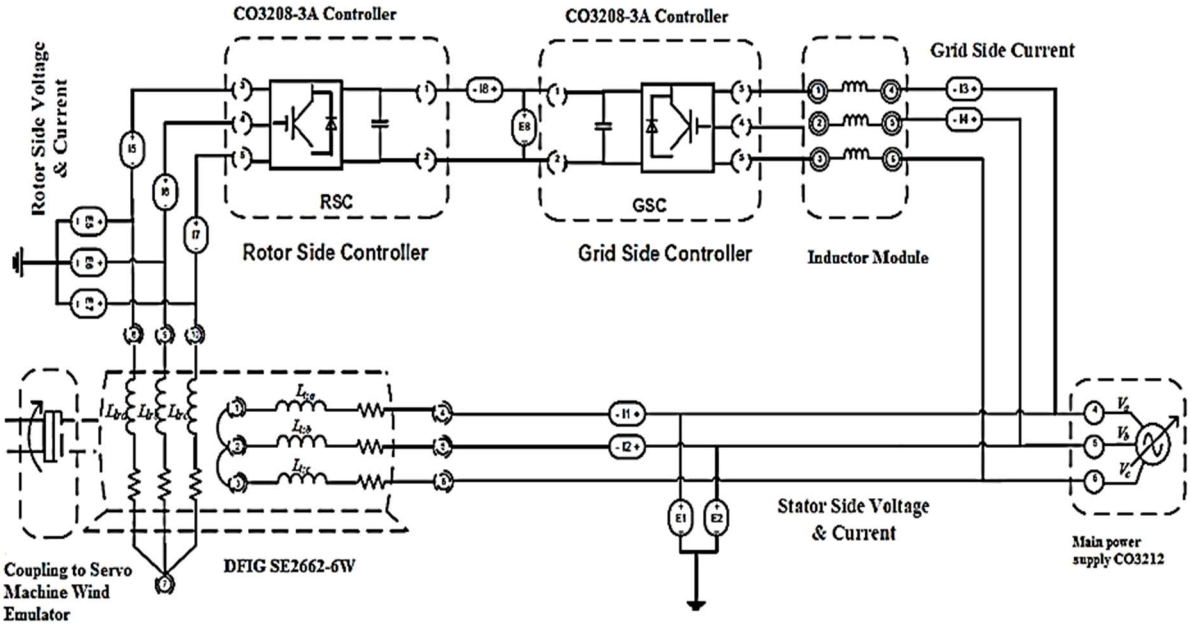

Figure 5.8: Schematic of the connected experimental setup to emulate WECS

5.2.2 The Lab-soft Software Environment

Table 5.1 documents the equipment specifications used in the Labsoft environment with regards to code names, descriptions, and quantity used in the experimentation.

Table 5.1: Equipment's list used in Labsoft environment

Used Virtual Instrument/s	Description	Qty.
CO3208-3A	Controller for a wind power plant's doubly-fed induction generator (1 Unit)	1 (Unit)
SE2662-6W	Three-phase, multi-function machine (doubly-fed generator)	1 (Unit)
CO3208-3B	Three-phase isolating transformer for a wind power plant to the supply network	1 (Unit)
SE2662-5T	Incremental position encoder (1024 pulses)	1 (Unit)
CO3636-6W/CO2663-6U	Servo-machine test stand (1 kW)	1 (Unit)
CO3212-5U	Power supply for electric machine	1 (Unit)
SE2662-6A	Coupling sleeve (1 kW)	2 (Units)
SE2667-6B	Coupling guard (1 kW)	2 (Units)
C)5127-1Z	Analog/digital multimeter, power & power-factor meter	1 (Unit)
SO5148-1L	Set of safety connection cables (4 mm)	1 (Unit)
SO5126-9Y	Safety connection plug (4 mm)	20 (Units)
SO5126-9R	Safety connection plug (19/4 mm) with tap	5 (Units)

Figure 5.9, illustrates the processes involved in the experimentation and how the equipment is arranged to carry out these laboratory experiments. Included in this diagram is the modelling and control aspect developed in MATLAB/Simulink environment. Thus, the mathematical model and the control are created in the MATLAB/Simulink, interfaced with the Labsoft environment. Once the model is running in the real-time simulator, a Simulink-based interface (i.e. console) is created to give the user access in real-time values of the signals and parameters within the model. The graphical user interface (GUI), the operations, and the results from these processes are presented in various sections of this chapter.

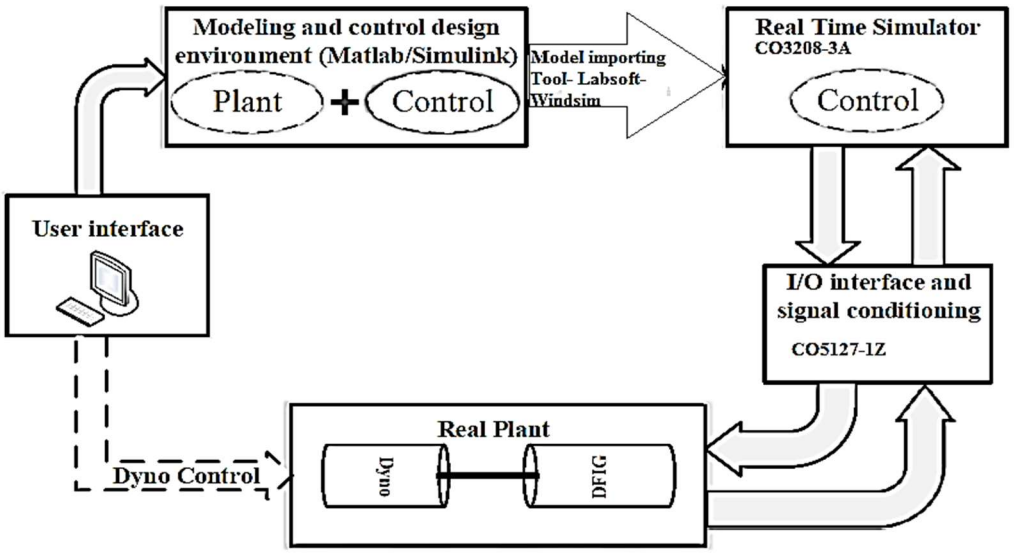

Figure 5.9: Schematic diagram for the monitoring, operation, and control of the experiment on Labsoft

5.3 Operation of GUI for DFIG Control

5.3.1 Influence of mechanical speed on generator voltage at zero rotor frequency

As part of this experiment, the servo machine (wind turbine emulator) is designed to run at variable speed. The experimental workbench parameters used are described in section 5.2. The DFIG in speed control mode and set speed ranges include 1200 rpm, 1300 rpm, 1410 rpm to 1500 rpm at the stator voltage amplitude of 40 % at a rotor frequency of 0 Hz. This indicates that the generator behaves like a synchronous generator and the results for this simulation are presented in Figure 5.10 and Figure 5.11. For these results, Figure 5.10 (a) is at the mechanical speed of 1200 rpm, rotor frequency is 40 Hz and voltage frequency is 40 Hz. Figure 5.10 (b) is at the mechanical speed of 1300 rpm, rotor frequency is 43Hz and voltage frequency is 44 Hz.

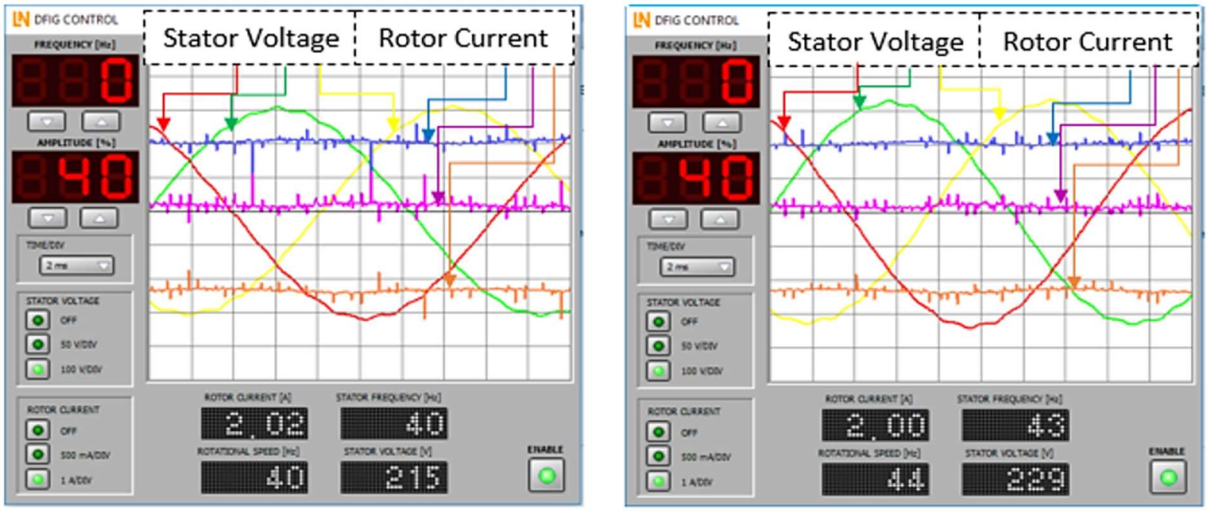

(a) (b)

Figure 5.10: The graph of generator voltage and rotor current at (a) 40Hz and (b) at 44 Hz variable rotor frequency

Figure 5.11 (a) is at the mechanical speed of 1410 rpm, rotor frequency is 47 Hz and voltage frequency is 47 Hz. Figure 5.11 (b) is at the mechanical speed of 1500 rpm, rotor frequency is 50 Hz and voltage frequency is 50 Hz.

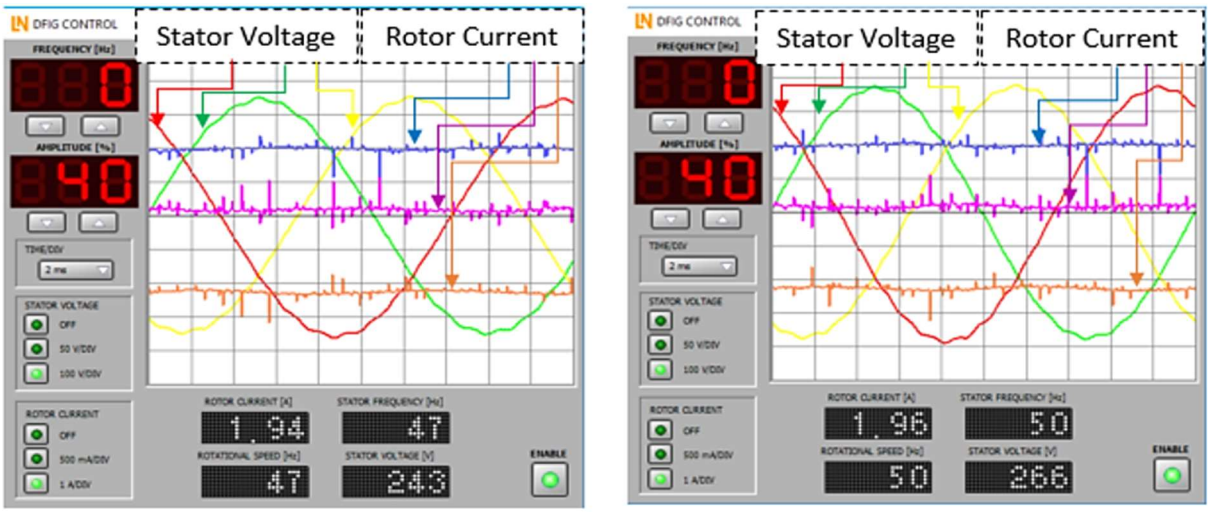

(a) (b)

Figure 5.11: The graph of generator voltage and rotor current at (a) 47Hz and (b) at 50 Hz variable rotor frequency

5.3.2 The Influence of Variable Rotor Frequency on Stator Frequency

In this experiment, with the wind turbine running at variable speed and explains the relationship between generator speed, rotor current frequency, and stator frequency. This experiment was performed to determine the feed frequency required by the rotor to raise the voltage frequency

of the generator's stator to 50 Hz at a speed of 1200 rpm to 1400 rpm. Setting the DFIG in the speed control mode, the stator voltage amplitude is at 40 %, at a rotor frequency of 0 Hz.

For Figure 5.12 (a) at the speed of 1200 rpm, the rotor voltage's frequency was set at 10 Hz while for Figure 5.12 (b) at speed of 1300 rpm, the rotor voltage's frequency was set at 7 Hz. As shown in Figure 5.12 (c) at Speed of 1400 rpm, the rotor voltage's frequency was set at 3 Hz.

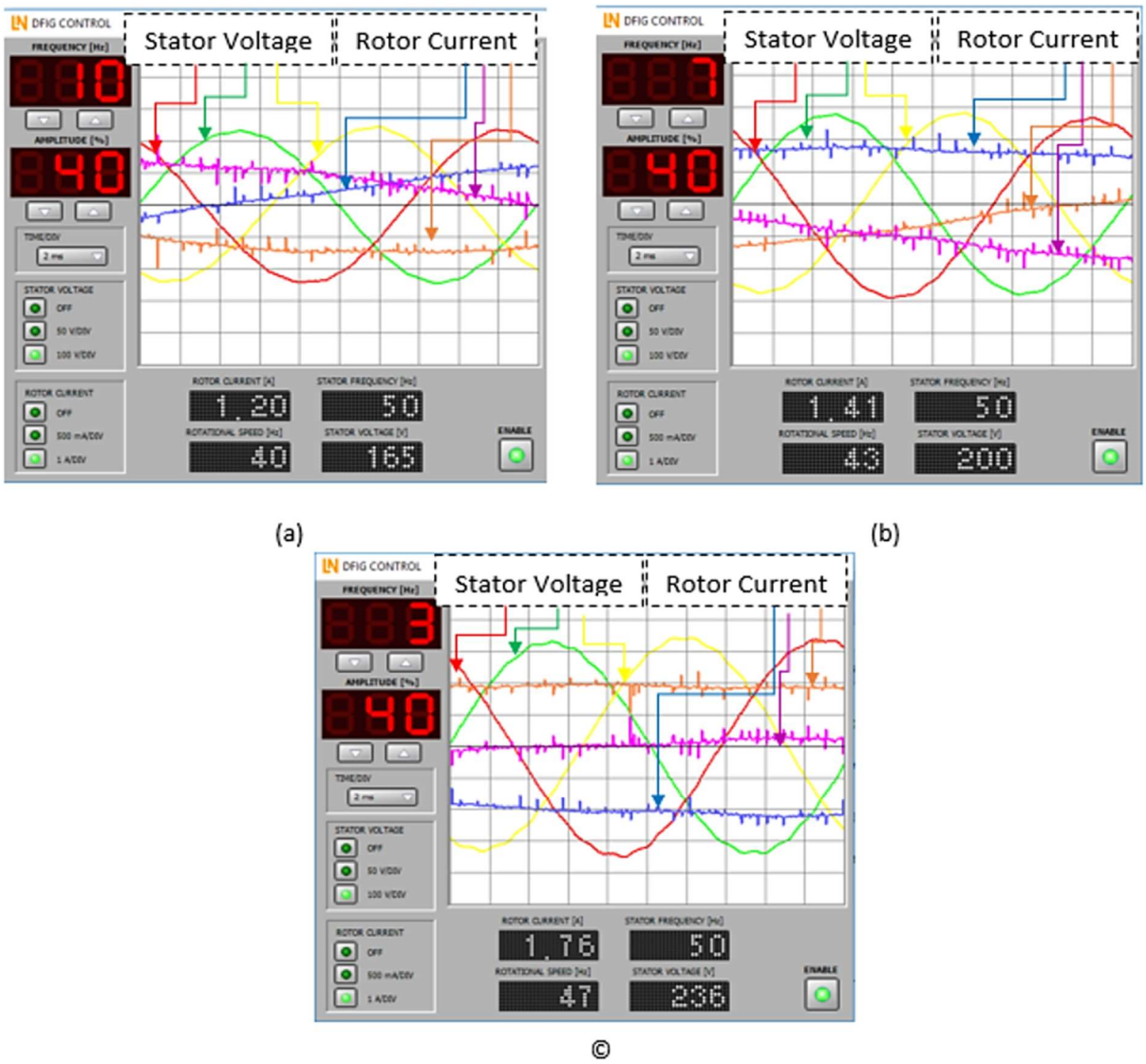

Figure 5.12: (a) The graph of generator voltage and rotor current at variable rotor frequency 40 Hz vs stator voltage frequency 50 Hz (b) The graph of generator voltage and rotor current at variable rotor frequency at 43 Hz vs stator voltage frequency 50 Hz and (c) The graph of generator voltage and rotor current at variable rotor frequency 47 Hz vs stator voltage frequency 50 Hz

Graphical results as shown in Figure 5.12, established that, for the variable mechanical speed, the stator frequency can be held constant by adjusting the rotor frequency, and at the constant rotor speed, the stator frequency can be varied via the rotor frequency.

5.3.3 The Influence of rotor current on stator voltage

The relationship between the rotor current and the stator voltage was analysed using the laboratory experiment. This experiment determined the influence of the rotor current on the stator voltage at different rotor frequencies for 0 Hz and 10 Hz. The experimental workbench parameters were kept as used in previous experiments, the DFIG was set at the speed control mode, and the set speed was 1200 rpm. Here, the rotor frequency was set to 0 Hz, and slowly the rotor current was varied from 0.5 A to 3.0 A. To obtain the corresponding stator voltage, the experiment was repeated for 10 Hz at the varying range of 0.5 A to 3.0 A. Experimental results are outlined in Table 5.2 showing that increasing the rotor frequency at constant amperage also increases the stator voltage and the rotor current. The mechanical rotor speed and rotor current frequency also increase thereby increasing the speed of the rotor's magnetic field and raising the stator voltage.

Table 5.2: Corresponding DFIG stator voltages at various rotor frequencies and variable rotor currents

	IRot [A]	0.5	1.0	1.5	2.0	2.5	3.0
Rotor Freq. 0Hz	UStat [V]	52	116	175	201	240	257
Rotor Freq. 10Hz	UStat [V]	78	150	215	277	305	344

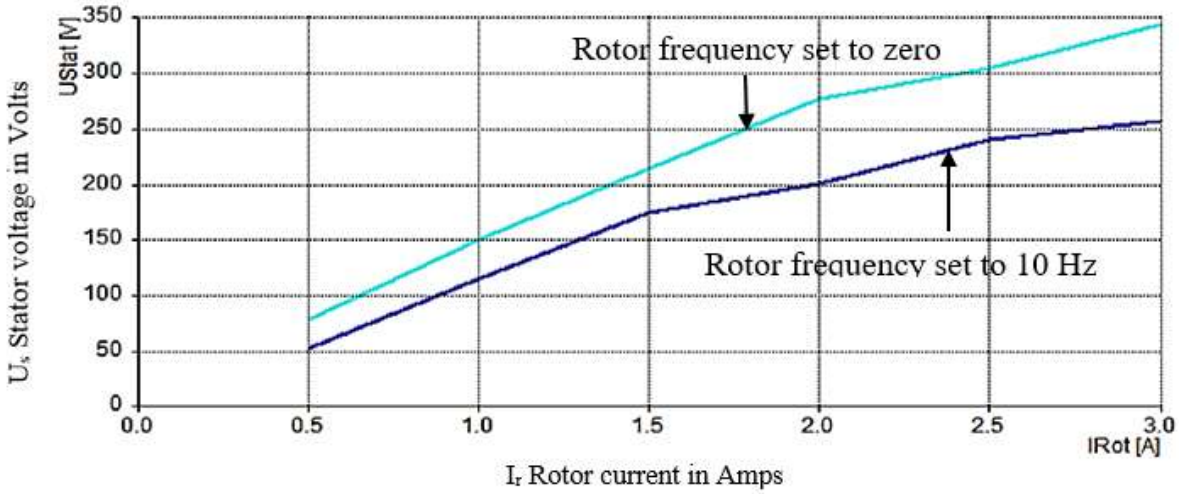

Figure 5.13: The graph of DFIG stator voltage vs rotor current

As shown in Figure 5.13, 0 Hz rotor frequency and 10 Hz rotor frequency. The experiment's results revealed that a change in rotor current from 2 A to 3 A increases the stator voltage to a lesser extent than a change from 1 A to 2 A. This is due to the generator's saturation effects so increasing the speed at a constant rotor current increases the stator voltage.

5.3.4 Grid synchronization for a DFIG

Discussed in this section is the synchronization of the generator with the grid under the influence of rotor current and frequency. For the synchronizing of the generator to the grid, the following conditions must be met;

- Grid frequency must be equal to generator frequency
- The grid voltage must be equal to generator voltage; and
- The grid phase angle is equal to the generator phase angle.

On the machine test stand, the speed control loop mode was selected and set the speed of 1200 rpm. The generator's voltage amplitude and frequency were slowly varied so that all criteria for synchronizing the generator to the grid are met as shown in Figure 5.14. This was achieved by fine-tuned the experiment by using the synchroscope for adjustment of the frequency as shown in Figure 5.15, where the frequencies of the turbine and the grid were synchronized.

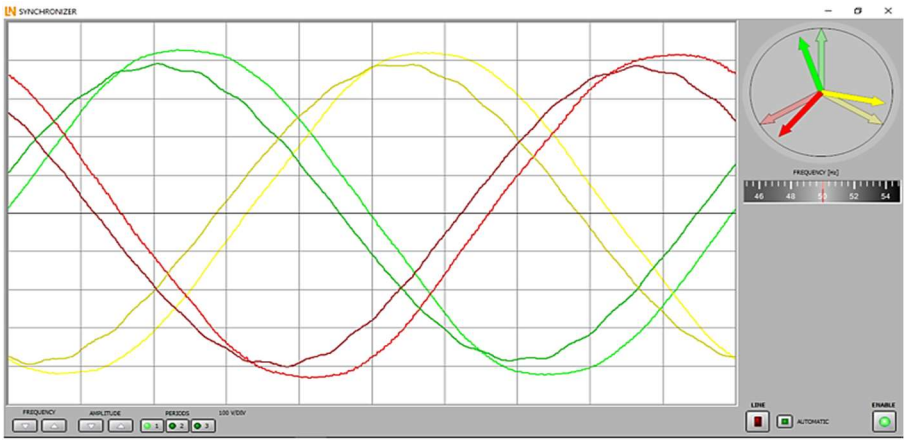

Figure 5.14: Synchroscope status before synchronization of DFIG with the grid

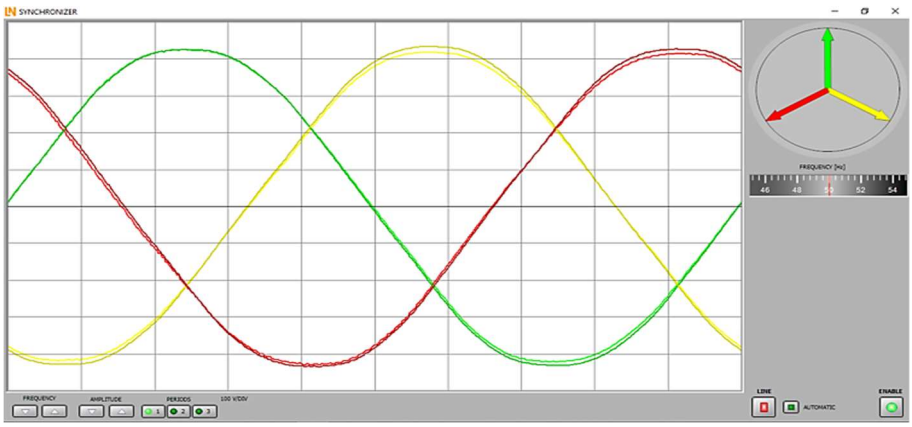

Figure 5.15: Synchroscope status after synchronization of DFIG with the grid

The experiment inferred that, if the generator and grid frequencies are similar, a phase shift occurs between the generator and grid. In this case, the phase angle can be adjusted through

minor changes in the generator frequency. At the same time, it reveals that the rotor current influences the generator voltage's magnitude and influences the synchronization of the DFIG into the grid. Thus, as the speed changes, the generator voltage, frequency, and phase angle are regulated to achieve synchronization with the grid.

5.3.5 Operation of the GUI for Power control

This experiment provides an analysis of how to control the doubly-fed induction generator to supply the grid with energy. Key aspects of the experiment are the active and the reactive power control during the sub-synchronous operation, and the super-synchronous operation.

5.3.5.1 Active power control during sub-synchronous operation:

In this experiment, the power control instrument was selected at the stator power mode. On the machine test stand, the speed control mode was selected the speed set at 1200 rpm, and the generator slowly synchronize with the grid. This experiment was used to investigate the power distribution and the excitation power at various generator output power levels. At the same time, supplying the grid with power was to ascertain the influence of generator speed on the integration of power into the grid. At the MSC, as shown in Figure 5.16, the active set-point value is 0, the active power of LSC value is -78 W and the grid side is -76 W, which indicates that only the active power is received from the grid. The power which is being used for generator excitation, showed that a rise in speed does not significantly influence the power consumption for generator excitation. On the machine test stand, the speed is set at 1300 rpm. The active set-point power for the MSC was varied progressively from 0 to 500W, and the results are presented in Table 5.3.

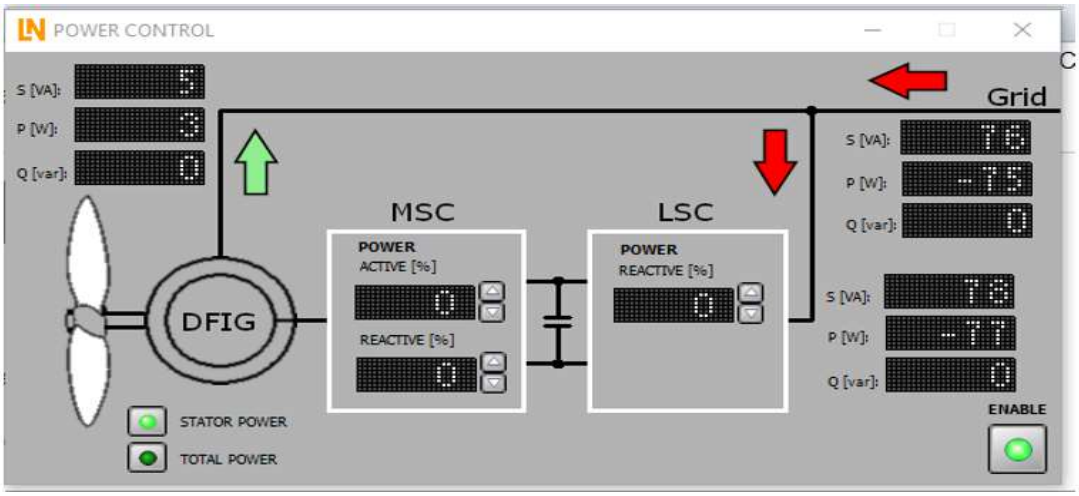

Figure 5.16: Power control instrument- stator power mode at zero (0) active power set point

Table 5.3: Corresponding grid side and load side active powers vs set MSC active power from 0-500W

DFIG	P(Watts)	0	50	100	150	200	300	400	500
Grid	P(Watts)	-77	-35	5	44	82	156	225	302
LSC	P(Watts)	-76	-82	-90	-100	-110	-132	-159	-192

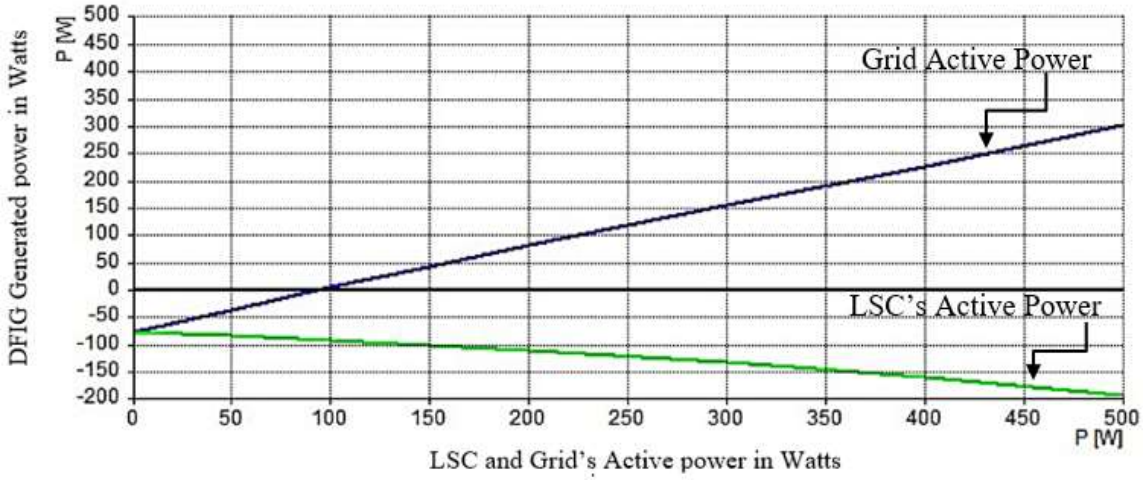

Figure 5.17: The graph of LSC's and Grid's active power vs DFIG power

The experiment results in Figure 5.17 reveal that at a constant generator speed, the LSC's active power consumption rises as the generator power rises. On the other side, at the set DFIG speed to 1200 rpm and with an adjustment to the MSC's set point power the generator active power output was maintained at 400 W. By increasing the generator speed from 1200 rpm in steps of 50 rpm, while keeping the generator power constant, the resultant corresponding values were captured, as documented in Table 5.4.

Table 5.4: DFIG, LSC, and grid's active powers at corresponding progressive variable DFIG speeds from 1200 rpm to 1450 rpm

	N (rpm)	1200	1250	1300	1350	1400	1450
Grid	P(Watts)	203	219	236	250	265	280
LSC	P(Watts)	-197	-181	-165	-149	-133	-117
DFIG	P(Watts)	400	400	400	400	400	400

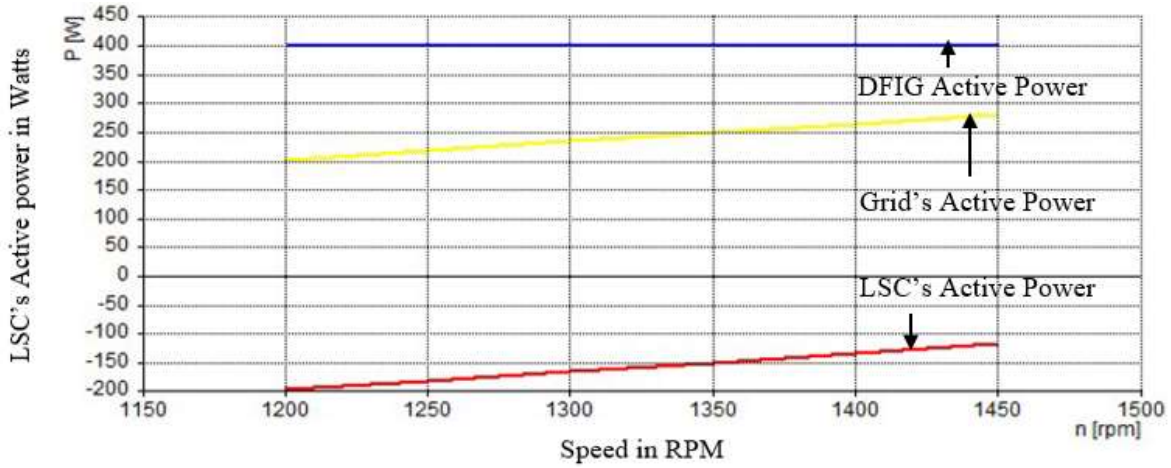

Figure 5.18: The graph of DFIG, grid, LSC's active power vs speed

The experiment results as shown in Figure 5.18 reveal that, if the generator's active power remains constant, the grid's input active power rises and LSC's active power consumption drops responding to progressive changes in the speed. During the sub-synchronous operation of the generator, LSC consumes power from the grid all the time, however, the generator's power can be adjusted independently of the speed.

5.3.5.2 Active power control during super-synchronous operation:

This experiment investigates the doubly-fed induction generators power components work while supplying the grid with power in the super-synchronous mode, with regards to the effect of speed variations. This experiment the synchronizing the generator with the grid, thus, it was used to investigate the power distribution and excitation power at various output.

In this experiment, the power control instrument was selected to be the stator power mode and on the machine test stand, speed control mode was selected and set at the speed of 1200 rpm, slowly synchronising the generator into the grid. In this case, the generator runs without any power being transmitted to the grid via the stator, increasing the generator speed further to 1900 rpm. At the MSC by setting an active set-point value of 0, the active power of LSC is -72W and the grid side is -72 W. On the machine test stand, the active set-point power was varied for the MSC progressively from 0 to 500W, and the results obtained are tabulated in Table 5.5.

Table 5.5: DFIG, LSC, and grid's active powers at super synchronous speed 1900 rpm at varied MSC set points

GRID	P(Watts)	-72	-11	47	150	163	277	400	500
LSC	P(Watts)	-72	-59	-49	-39	-28	-9	7	20
DFIG	P(Watts)	0	50	100	150	200	300	400	500

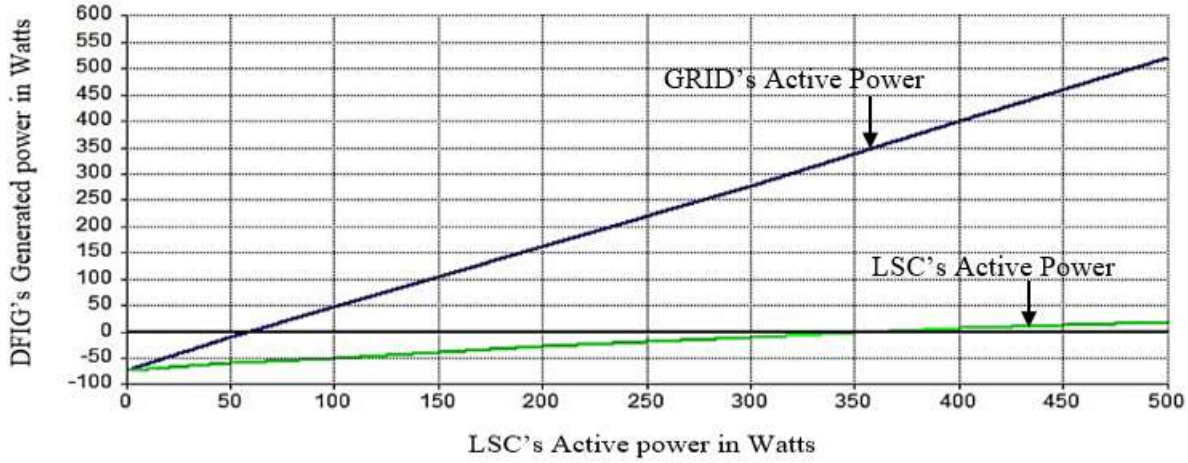

Figure 5.19: The graph of the GRID and LSC's active power vs variable MSC set points

The experimental results as plotted in Figure 5.19 reveal that, as the generator power rises, the LSC's active power consumption drops and even turns negative, in super synchronous speed. When the generator speed was slowly varied to 1650 rpm and the MSC's set point adjusted to zero power, the generator output active power of 500 W was obtained. Thereafter, the generator speed increases in steps of 50 rpm up to 1900 rpm while keeping the generator output power constant at 500 W. Thus, the results for this experiment are documented in Table 5.6.

Table 5.6: Grid and LSC's active power at a variable speed from 1600 rpm to 1900 rpm at constant DFIG power

	N (rpm)	1650	1700	1750	1800	1850	1900
Grid	P(Watts)	440	455	470	485	504	520
LSC	P(Watts)	-63	-46	-30	-14	3	18
DFIG	P(Watts)	500	500	500	500	500	500

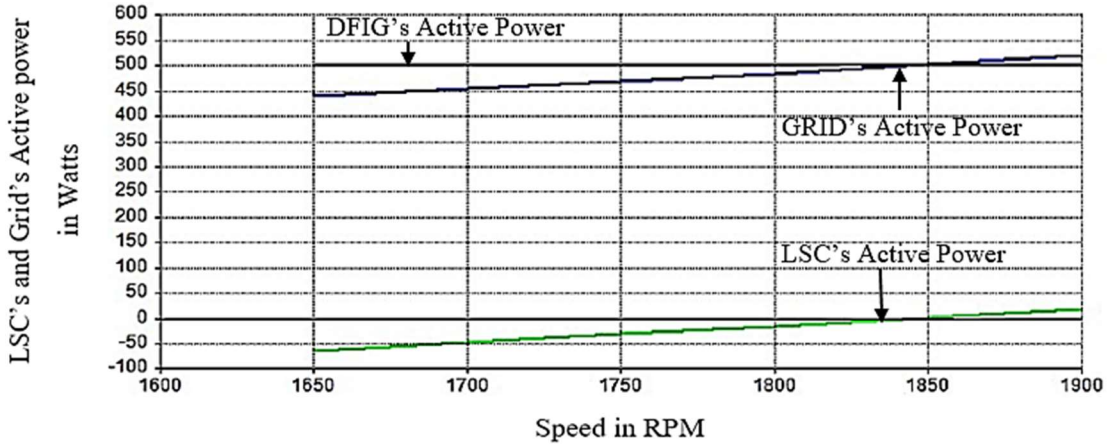

Figure 5.20: The graph of the grid and LSC's active power vs Speed (RPM)

The experiment results as plotted in Figure 5.20 reveal that as the speed rises in the super synchronous stage, the LSC's active power consumption drops, and as a consequence, the grid's

input active power rises.

5.3.5.3 Power distribution

This experiment investigates for the relationship between the stator and rotor power of DFIG with respect to the variations in the DFIG speed. In this experiment, the power control instrument for the stator power mode was selected and on the machine test stand, speed control mode was selected and set to the speed of 1200 rpm. The generator was then slowly synchronized with the grid. In this case, the generator runs without any power being transmitted to the grid via the stator and the MSC set-point power was increased until a stator output power of 400 W was achieved. The sets of speed used are indicated in Table 5.7 with obtained values showing corresponding power levels on the LSC and rotor active power.

Table 5.7: Corresponding rotor active power, slip, and LSC active power at variable DFIG speeds from 1200 rpm to 1800 rpm

	N (RPM)	1200	1300	1400	1500	1600	1700	1800
Slip		0.20	0.15	0.07	0.00	-0.07	-0.15	-0.20
P_{ROT}	P(Watts)	-80	-60	-28	0	28	60	80
LSC	P(Watts)	-197	-167	-137	-102	-75		

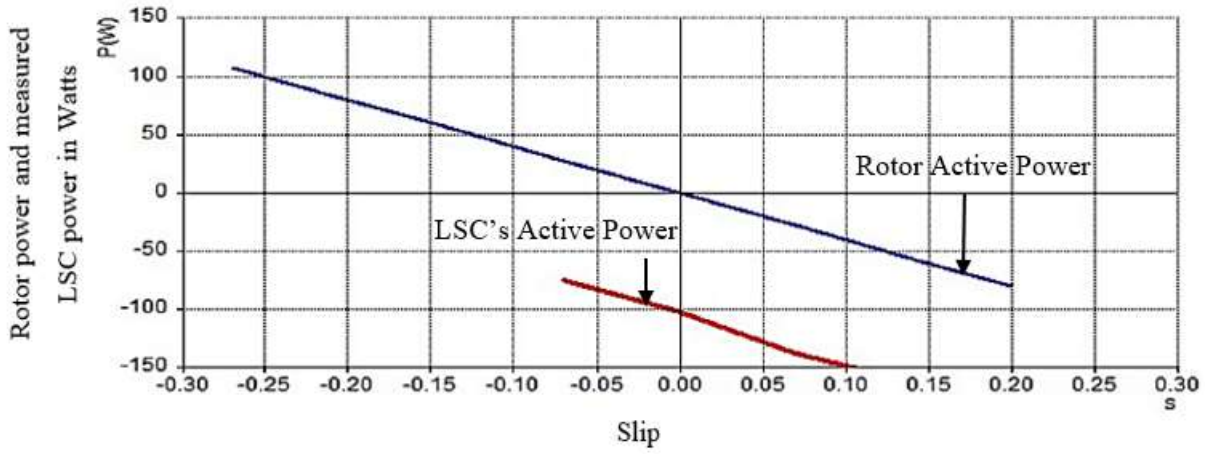

Figure 5.21: The graph of the rotor and LSC's active power vs slip

In plotting the measured values with theoretically calculated values of $P_r = -sP_s$ as shown in Figure 5.21, the measured curve for LSC active power shifted considerably from the theoretical rotor active power curve. This shift is due to the system's power losses. To eliminate the power losses from the measured values, it is assumed that the LSC's power is 0 at synchronous speed, with the power at synchronous speed subtracted from the other measured values. The new values are presented in Table 5.8.

Table 5.8: Eliminating the measured value losses from table 5.7 to determine the corresponding power levels on the LSC

	N (rpm)	1200	1300	1400	1500	1600	1700	1800
Slip		0.20	0.15	0.07	0	-0.07	-0.15	-0.20
P_{ROT}	P(Watts)	-80	-60	-28	0	28	60	80
LSC	P(Watts)	-60	-30	0	-32	-62		

Figure 5.22, shows a comparison between the measured values and theoretical values with the elimination of the power losses from the measured values. It can be inferred from the graph that the losses occur during switching operations from the generator's controller during the excitation of the generator.

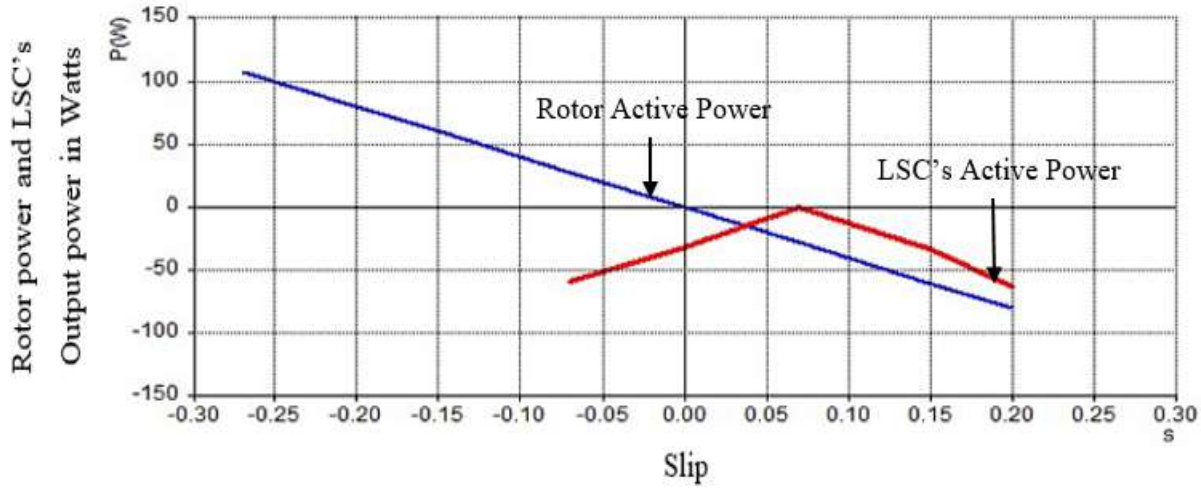

Figure 5.22: The graph of the calculated rotor power and LSC's power vs slip

5.3.5.4 Reactive power control

This experiment provides an analysis of the relationships between a DFIG's reactive power, rotor current, and torque in terms of the overexcited and under excited modes under the influence of various generator's speed. In this experiment, the power control instrument was selected to the stator power mode and on the machine test stand, speed control mode was selected and the speed was set at 1200 rpm, before slowly synchronising the generator with the grid. In this stage, the generator runs without any power being transmitted to the grid via the stator. This varied the MSC set point reactive power as indicated in Table 5.9 and the values obtained corresponding to rotor currents, and torque levels are presented.

Table 5.9: Values of rotor currents at different DFIG speed and reactive power

	QDFIG (VAR)	-300	-200	-100	0	100	200	300
N=1400	IRot(A)	0.7	1.2	1.8	2.5	3.2		
N=1900	IRot(A)	0.7	1.2	1.8	2.5	3		

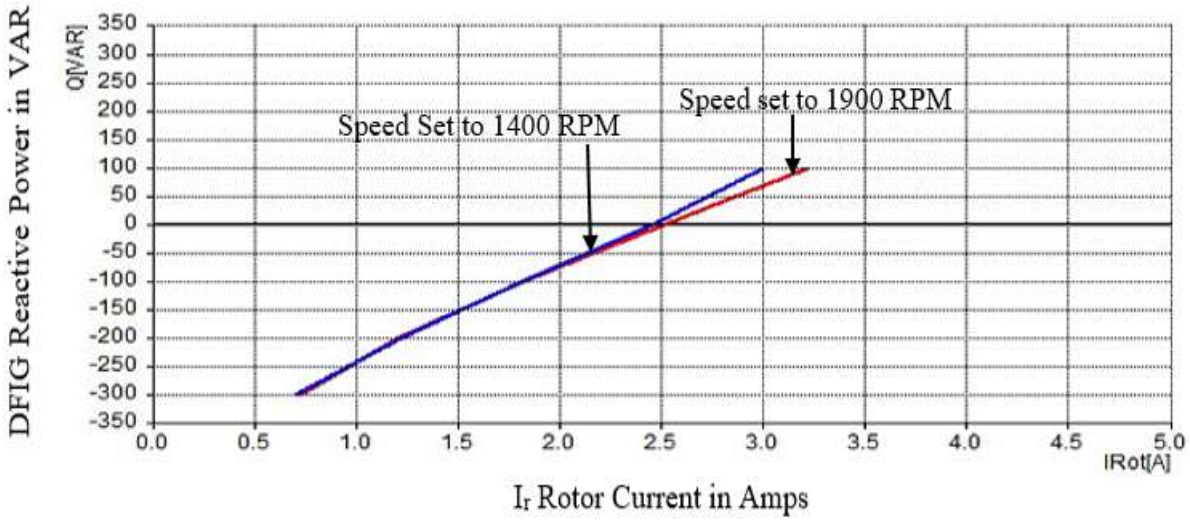

Figure 5.23: The graph of the DFIG reactive power (VAR) vs rotor current (amps)

The experimental results as presented in Figure 5.23 reveal that the DFIG should be operated in the overexcited mode, hence, the rotor current rises and the generator supplies reactive current to the grid. The disadvantage of operating the generator while the outputs is reactive power is that the output of active power is limited to prevent the generator from being overloaded.

The experiment results as documented in Figure 5.24 reveal that the DFIG supplies both at high active and reactive powers with a corresponding higher rotor torque.

Table 5.10: Values of DFIG active and reactive power at different rotor torque

PDFIG [W]	0	0	0	0	100	200	300
M[Nm]				-0.6	-1.4	-2.2	-3
QDFIG (VAR)	-300	-200	-100	0	100	200	300

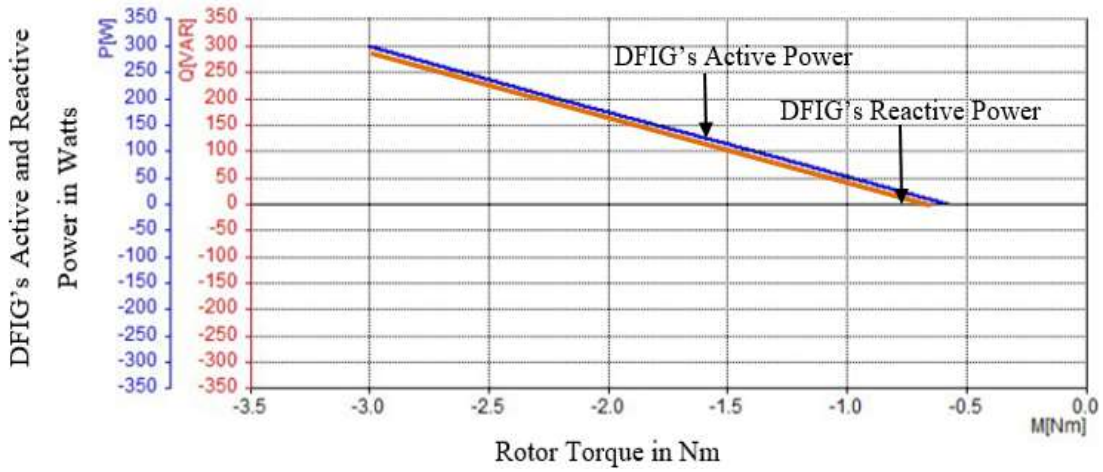

Figure 5.24: The graph of DFIG's electrical power vs mechanical power

5.3.6 Operation of the GUI for the Control center

5.3.6.1 Auto power control

This subsection explains how to operate the generator supplying the grid at varying wind speeds. This helps to determine the generator's behavior with respect to varying speed and also determine the optimal operating points needed for understanding the control characteristics of wind turbines. Hence, ascertaining the operating points for starting a wind turbine are used to understand the transition from the rated operation to a super-synchronous operation. As shown in Figure 5.25, the control center instrument was selected to the stator power mode and on the machine test stand, slowly wind speed was increased in steps, presented in Table 5.11. This ensure that, at each of the various wind speeds, the DFIG raises the power to a level where the grid's input power is maximised with a stable operation.

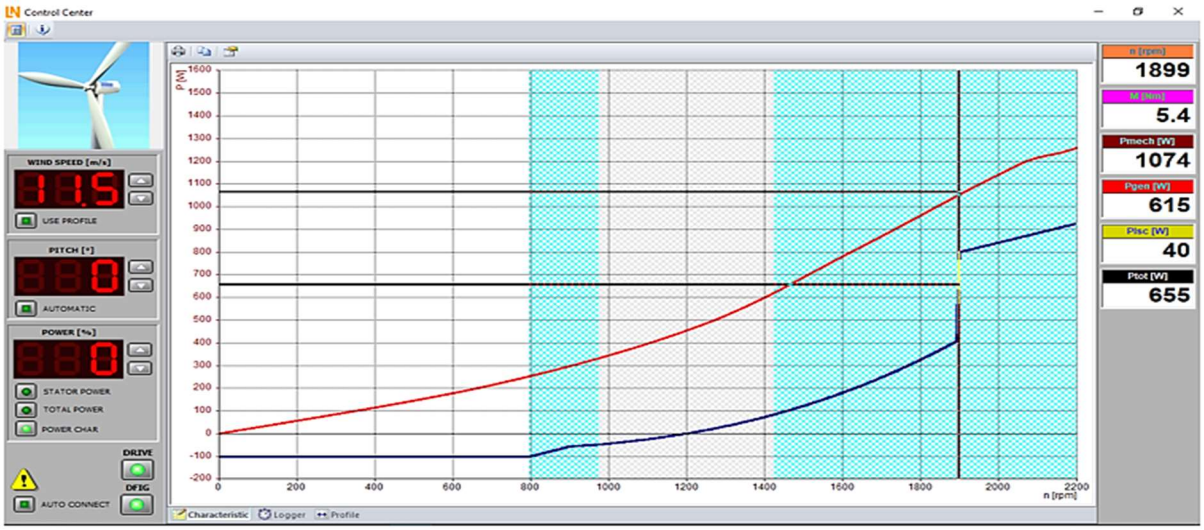

Figure 5.25: Control centre GUI display at 11.5 m/s wind speed and DFIG speed at 1899 rpm

Table 5.11: Total generated power at variable wind speed and corresponding generator speed

V (m/s)	5	6	7	8	9	10	11	11.5
n (RPM)	1020	1210	1390	1580	1775	1890	1899	1899
P tot (W)	-50	2	75	172	300	462	604	662

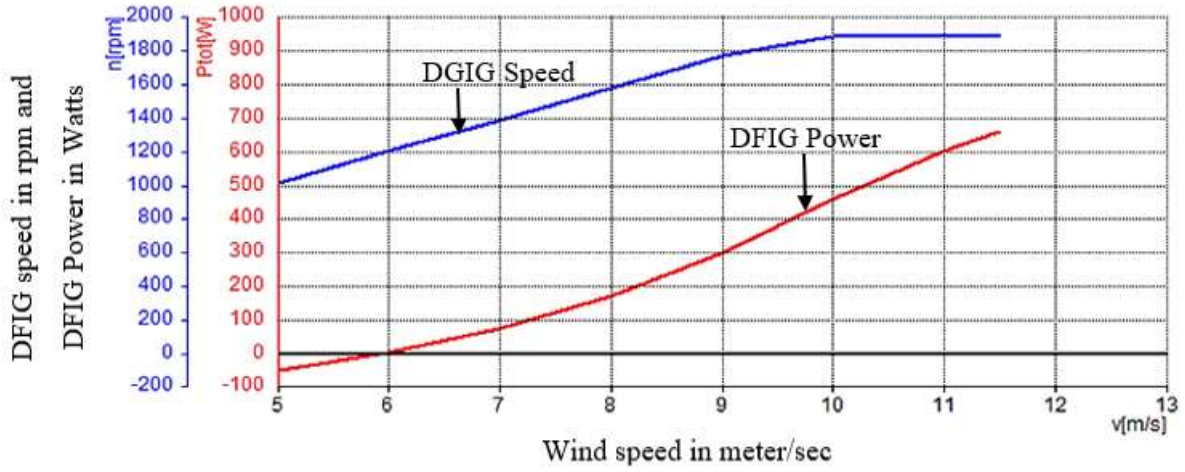

Figure 5.26: The Graph of the DFIG speed and power vs variable wind intensity

Experimental results as shown in Figure 5.26, indicate that the generated feed power responds to the corresponding generator speed at various wind speeds, as indicated by this characteristic curve. The operating point at different wind speeds was chosen so that the wind turbine can maximises the utilisation of the available wind power. This applies to a large portion of the curve. Near the top of the characteristic curve, the wind turbine no longer operates at maximum power. The speed selected for operation under full load is usually lower than the cp characteristic's optimum level. This improves the wind turbine utilization in the partial load range.

The wind speeds for the operating points are specified as starting (when power is fed into the grid) at 6.0 m/s, the transition to super-synchronous operation is at 8.0 m/s, and rated operation (when the rated power of 800 W is fed into the grid) at between 11.5 m/s to 12 m/s.

5.3.6.2 Influence of pitch angle on the power

In this aspect of the experiment, the effects of adjusting the pitch angle on the operation of the generator under full load were assessed. Operating the plant with a pitch controller determined the fed power at various pitch angles and wind speeds, and to ascertain the operating points at various wind speeds during operation of the pitch angle. The control center instrument was selected in the stator power mode in auto pitch control and on the machine test stand, slowly increased the wind speed in the steps indicated in Table 5.12. This ensure that, at each of the

various wind speeds, the DFIG raises the power to a level where the grid's input power is maximized with stable operation.

Table 5.12: Wind speed vs generator speed, pitch angle, and total power table

N[RPM]	1200	1580	1900	1900	1900	1900	1900	1900
V[m/s]	6	8	10	12	14	16	18	20
Pitch[°]	0	0	0	0	0	0	0	0
P tot [W]	0	180	470	700	780	790	795	790

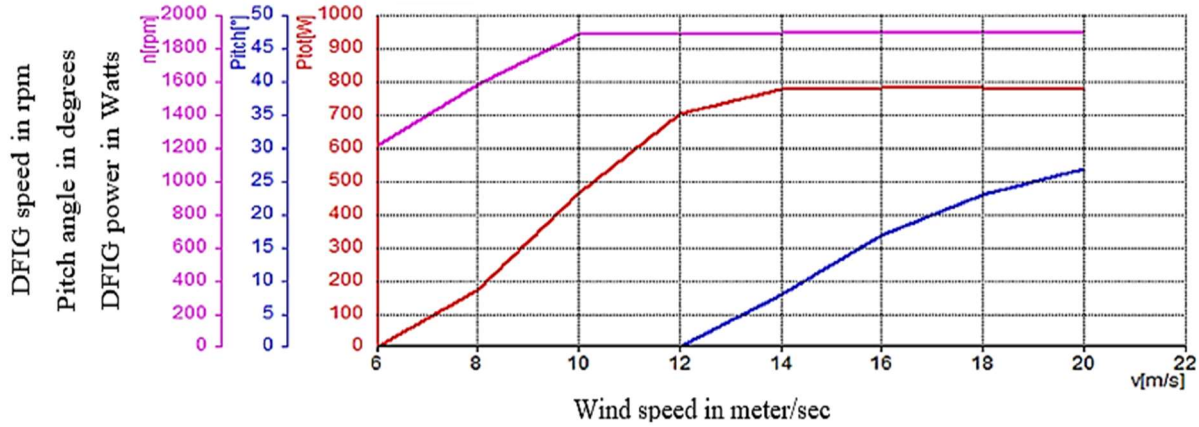

Figure 5.27: The graph of DFIG speed, power and the pitch angle vs wind speed

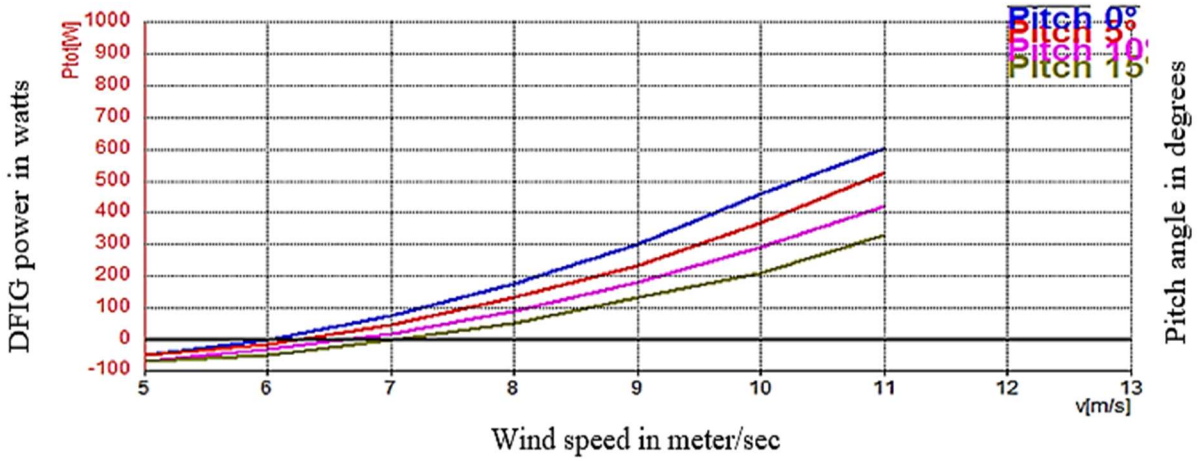

Figure 5.28: The graph of the DFIG power and pitch angle vs wind speed

The manual mode of pitch angle control as shown in Figure 5.28 reveals that increasing the pitch angle decreases the feed power and there is no linear relationship between pitch angle and power reduction. In the partial-load range, pitch control is not of use under normal operation. This is because the maximum possible power is not fed into the grid under normal operation. If any mechanical problems occur with the gearbox or bearings, for instance, pitch control allows the wind turbine to be operated at reduced speed (power) until repairs are completed.

The effect of pitch controller in auto mode as shown in Figure 5.27, reveals that pitch control has no effect in the partial load range, hence the pitch angle remains at zero degrees. Under full load, the pitch controller regulates the speed to maintain the generator power at the rated level.

5.3.6.3 Dynamic response

For the analysis of the wind turbine with regards to the dynamic response, the wind power plant's operation was demonstrated by varying wind speeds to examine the effect of a pitch controller. This concept was used to ascertain a wind turbine's dynamic response in the partial load range and over the entire operating range. The control center instrument was selected to the auto pitch angle control and wind profile was then entered. For this experiment, there was a gust profile of wind with a maximum speed of 12 m/s, presented in Figure 5.29 and the maximum speed of 18 m/s presented in Figure 5.31. For the machine test set-up the wind speed was slowly increased in the steps of 50 rpm and the generator was operated in the speed range of between 1000 rpm to 1400 rpm. Automatically synchronised the generator into the grid, the logger then displayed the plots for the wind speed, total active power, generator speed, and pitch angle, as shown in Figure 5.30. This process was repeated for the maximum speed, as shown in Figure 5.31, and the results presented in Figure 5.32.

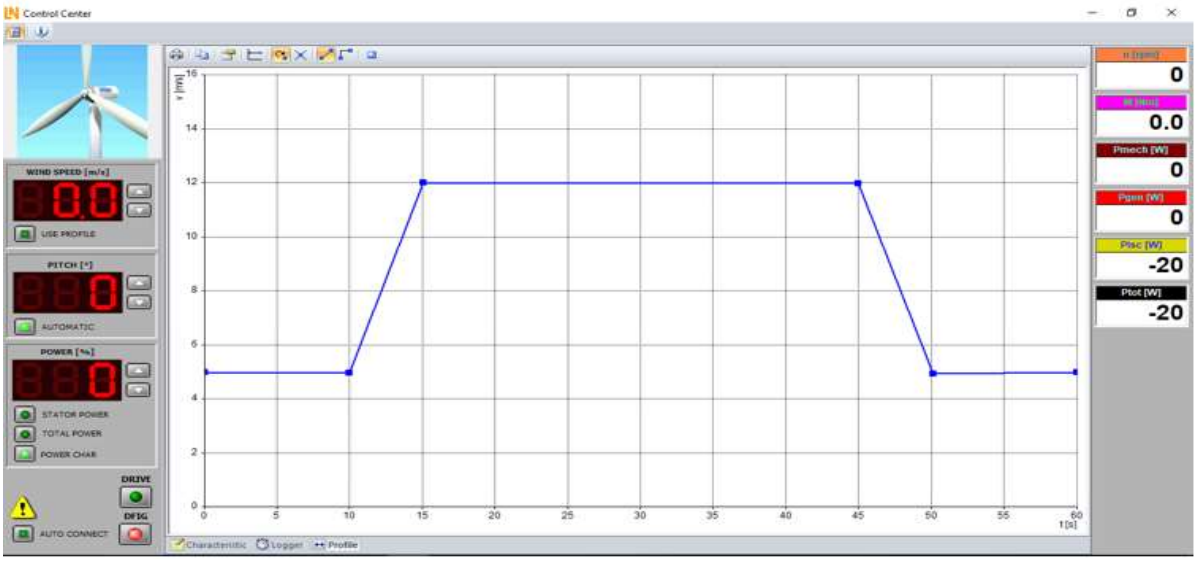

Figure 5.29: Wind turbine control centre gust profile at 12 meters/sec wind speed

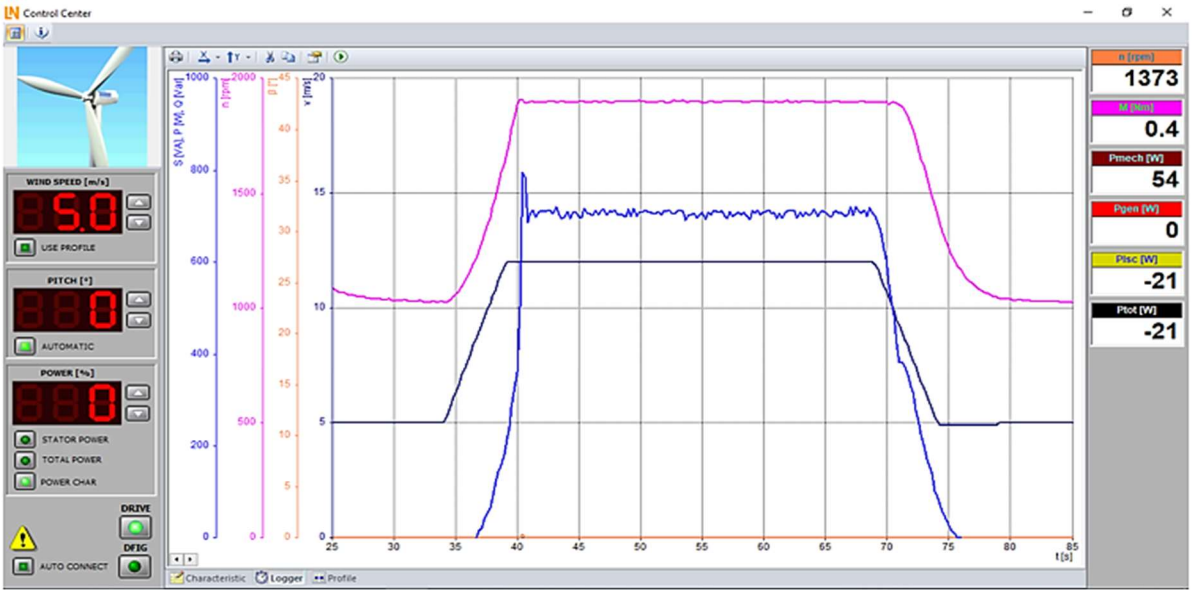

Figure 5.30: The graph of the DFIG's dynamic response at 12 m/s gust wind

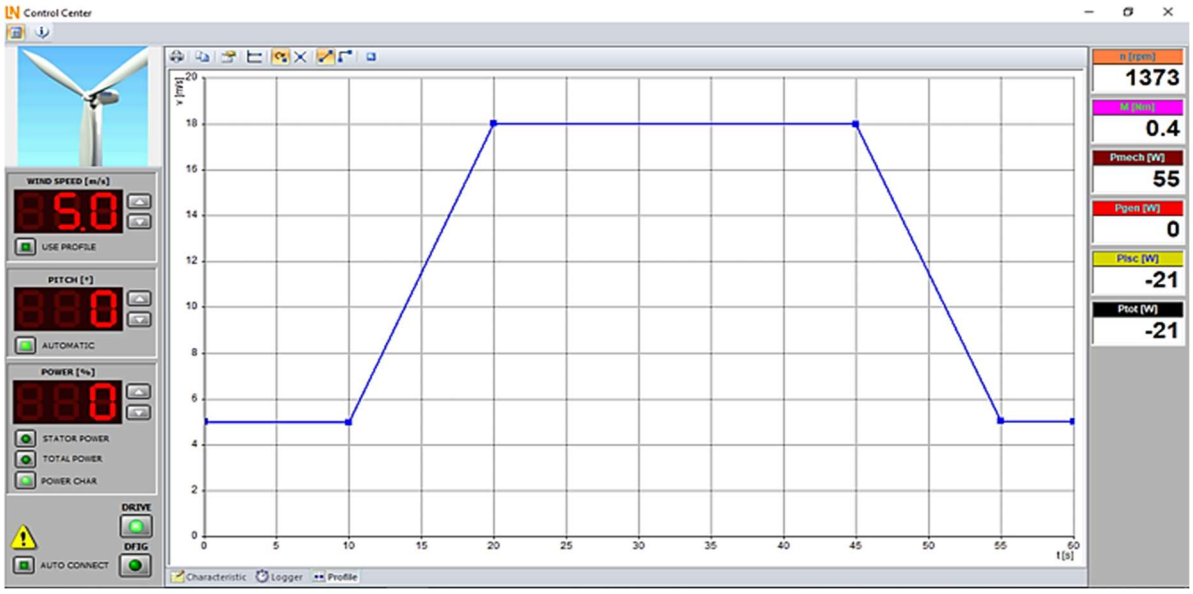

Figure 5.31: Wind turbine control centre gust profile at 18 m/s wind speed

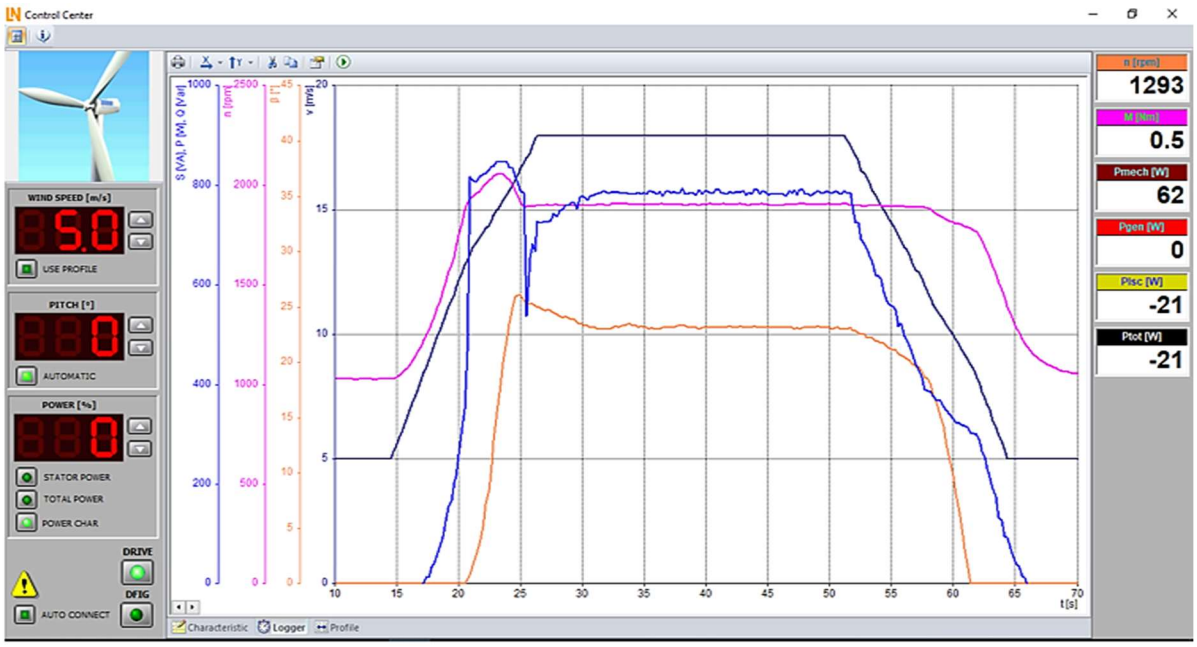

Figure 5.32: The graph of the DFIG's dynamic response at 18 m/s wind gust

These experiments were used to demonstrate that the wind power plant responds to changes in wind speed under partial load. When the rotor blade's pitch is not adjusted under partial load as the wind speed rises, the generator's power output rises accordingly. In these experiments, the generator's rated speed was not exceeded. During a transition from partial to full load, the response to changes happens, as shown in Figure 5.30 and Figure 5.32. Based on these results, the following was inferred:

- The faster the change in wind speed the faster the changes in the generator power.
- There is no need to adjust the rotor blades in the partial load range.
- Under full load, the rotor blades are adjusted to limit generator speed and, consequently, generator power to the rated values as accurately as possible.
- A gust of wind can cause the generator to operate briefly above the rated power level until the pitch controller performs the required readjustment.

Chapter 6

Conclusions and Future Work

6.1 Conclusion

This study was to investigate the impacts of integrating the wind power into the distribution systems. Thus, the fundamentals and principles of WECS were analysed in the work. Two forms of research methodologies were used; the analytical and the experimental study.

The first methodology was the Analytical study.

- The modelling of the whole wind energy conversion system based on the DFIG (Back- to-Back convertor, filters, DFIG, wind turbine, grid) was presented. It was found that DFIG model built in MATLAB/SIMULINK showed satisfactory performances and validated the system model and dealt with various operational conditions. This configuration had several benefits such as higher efficiency, fewer mechanical parts, and ease of control. Also, modelled were the control strategies used to control both active and reactive power operations of the wind turbine and the level of power penetration into the distribution network.
- For the grid connection, the rotor side converter controller was used to control the active and reactive power control, achieved by controlling rotor current and the speed of the DFIG.
- The employed *PI* controller tested for controlling the grid side converter. This helps to maintain the constant frequency of the generated power from the wind turbine by matching the grid frequency and generated voltage with the grid voltage.

The second methodology was the experimental study.

- This study was done in the laboratory conduction capable of replication real world scenarios. The experimental results provide proof for developed control strategies, using a wind turbine simulator with a digital controller and Active Servo software. The control scheme and controller used for the experimental section assured that the wind power supplied into the grid at varying wind speeds behaved like a synchronous generator, at a zero Hz rotor frequency.
- In wind power conversion, the automatic power control system plays a significant role in the efficiency and reliability of the entire system. Currently, the wind energy industry is adapting the trend towards the research and development of grid-connected wind turbines. The major interests of the current wind turbine manufacturers include variable speed (Type-4) technology, a direct-driven double fed induction generator of low voltage operation, and

the development of sophisticated control systems to increase the efficiency of wind energy conversion to meet grid code requirements.

- The experimental results presented in sections 5.4.1 to 5.4.6 serve as a proof of the developed control strategies, using a wind turbine emulator consisting of dynamic and static four-quadrant operation. The rotor side converter controller was used for the implementation and testing of wind energy extraction, reactive power, and grid voltage support controls of the wind turbine, namely the active and reactive power control by controlling rotor current and the speed control of the DFIG.
- Using measured stator voltages, stator currents, rotor currents, and the rotor position through the encoder feedback signal of the employed *PI* controlled algorithm, there was substantial improvement in control robustness, improving its immunity to generated noise in the system, which was a major finding in previous reviews.
- In the auto power control mode, the speed selected for operation under full load is usually lower than the c_P characteristic's optimum level. This improves wind turbine utilization in the partial load range.

The control scheme and controller employed for the experimental section assured the wind generator supplying the grid at varying wind speeds behaves like a synchronous generator, at a zero Hz rotor frequency and LSC's active power consumption drops progressively from sub synchronous to super synchronous speeds. This controller can improve the power factor which attempts to maintain it at unity, so that the use of an additional capacitor bank can be avoided in the power grid, ultimately reducing the cost of power generation.

6.2 Future work

While some discoveries have been accomplished in this thesis, further investigations are required as follows:

1. Higher-order models of the drive train system and the doubly-fed induction generator model with saturation effect should be considered in wind turbine systems.
2. The performances of the DFIG-based wind turbine system should be compared with a wind turbine system equipped with a multi-pole permanent magnet synchronous generator, connected to the grid through a full-scale power converter.
3. Advanced control strategies can be implemented in the DFIG control blocks.
4. The transient behaviours of the DFIG-based wind turbine system under disturbances of grid failures should be studied.

Reference

[1] Corin Millais Wind Energy Association and Sven Teske Greenpeace, *WIND FORCE 12 A BLUEPRINT TO ACHIEVE 12% OF THE WORLD'S ELECTRICITY FROM WIND POWER BY 2020*, Brussels - Belgium, 2004. [E-book] Available: Catalogue e-book. http://www.choose-positive-energy.org/docs/wind-force-12-2002.pdf.

[2] P. Dr. Minqi Li, "World Energy 2017-2050: Annual Report," Department of Economics, University of Utah, Annual Tech. Report. 1–29, June 2017.

[3] World Wide Fund For Nature, WWF Report on Renewable Energy, "World energy consumption," 2017. [Online]. Available: http://www.wwf.org.za/renewable-energy-facts-and-future. [Accessed: Aug. 15 2018].

[4] J. van den B. Mari-Louise van der Walt and M. C. Cameron, "State of Renewable Energy in South Africa," Department of Energy, Pretoria, South Africa, Tech. Report. 1–222, Nov. 2018.

[5] M. Gulati, Gaylor Montmasson-Clair, Karin Kritzinger, Louise Scholtz and Design, "New Roles for South African Municipalities in Renewable Energy - A Review of Business Models," South African-German Energy Partnership, Pretoria, South Africa: Office of Federal Ministry for Economic Affairs and Energy, 2017.

[6] James F. P. Robert E. Gabler, "Atmospheric Pressure, Winds, and Circulation Patterns," *Weather*, Cengage, 2008 [E-Learning platform] Available: https://www.cengage.com/resource_uploads/downloads/0495555061_137182.pdf.

[7] B. Parsons, M. Milligan, B. Zavadil, D. Brooks, B. Kirby, and J. Caldwell, "Grid Impacts of Wind Power : A Summary of Recent Studies in the United States Preprint," presented at the 2003 European Wind Energy Conference and Exhibition Madrid, Spain, 2003.

[8] V. Rana, R. Gupta, and N. Kumar, "Integration of Wind Farm into A Weak Distribution Network," *International Journal of Emerging Technolgy Advance Engineering*, vol. 4, no. 1, pp. 404–409, 2014.

[9] K. Mikkelsen, "Effect of free stream turbulence on wind turbine performance," M.S Thesis, Norwegian University of Science and Technology, Norway, 2013.

[10] T. R. Ayodele and J. T. Agee, "Statistical analysis of wind speed and wind power potential of Port Elizabeth using Weibull parameters," *Journal of Energy South. Africa*, vol. 23, no. 2, May., pp. 30–38, 2012.

[11] A. Hemami, *Wind Turbine Technology*. NY: Cengage learning, 2012.

[12] Bonus Energy Info Newsletter, "The wind turbine components and opeations," *Bonus Energy AS*, 1998. [Online]. Available: https://users.wpi.edu/~cfurlong/me3320/DProject/BonusEnergy-1998.pdf [Accessed: Nov. 12 2017].

[13] P. J. Schubel and R. J. Crossley, "Wind Turbine Blade Design," *Energies*, vol. 5, no. 10, September, 2012. [Online serial]. Available: https://www.researchgate.net/publication/307687949_Wind_Turbine_Blade_Design. [Accessed Dec. 4, 2017].

[14] N. R. Chaudhuri, *Integrating Wind Energy to Weak Power Grids using High Voltage Direct Current Technology.* Switzerland AG: Springer Nature 2019.

[15] Z. Li, R. Han, P. Gao, and C. Wang, "Analysis and implementation of a drag-type vertical-axis wind turbine for small distributed wind energy systems," *Advances in Mechanical Engineering*, vol. II, no. 1, Jan., pp. 1–16, 2019.

[16] M. Ragheb, *"Wind Energy Conversion Theory, BETZ Equation,"* July, 2005. [Online Serial]. Available: http://50.63.38.179/NPRE%20475%20Wind%20Power%20Systems/Wind%20Energy%20Conversion%20Theory%20Betz%20Equation..pdf [Accessed July 15, 2018]

[17] M. Ragheb and A. M. Ragheb, “Wind Turbines Theory - The Betz Equation and Optimal Rotor Tip Speed Ratio,” London, UK, Intechopen, 2011. [E-book] Available: Intechopen e-book. https://www.intechopen.com/books/fundamental-and-advanced-topics-in-wind-power/wind-turbines-theory-the-betz-equation-and-optimal-rotor-tip-speed-ratio.
[18] T. Ackermann, *Wind Power in Power Systems*. Chichester, West Sussex PO19 8SQ, England: John Wiley & Sons, Ltd, 2005.
[19] L. H. Hansen, L. Helle, F. Blaabjerg, E. Ritchie, H. Bindner, and P. Sørensen, *Conceptual survey of Generators and Power Electronics for Wind Turbines.* Roskilde, Denmark : Pitney Bowes Management Services, 2002.
[20] E. H. Camm, M. R. Behnke, O. Bolado, M. Bollen, M. Bradt, C. Brooks, W. Dilling, M. Edds, W. J. Hejdak, D. Houseman, S. Klein, F. Li, J. Li, P. Maibach, T. Nicolai, J. Patino, S. V. Pasupulati, N. Samaan, S. Saylors, T. Siebert, T. Smith, M. Starke, R. Walling, “Characteristics of Wind Turbine Generators for Wind Power Plants,” *IEEE*, vol. 09, no. 6, June, pp. 1–5, 2009.
[21] A. A. Tanvir, “Control System for Doubly Fed Induction Generator Based Wind Energy Conversion System,” M.S thesis, Saint Mary’s University, Halifax, Nova Scotia, 2016.
[22] B. Gregory, D. Broad, and E. Muljadi, “Self-Excited Induction Generator for Variable-Speed Wind Turbine Generation,” In Proc. POWERSYSTEMS WORLD '96 Conference, 1996, pp. 1–12.
[23] College of Engineering - Michigan State University, “Operation of Induction Generators-Application Note,” 2015. [Online]. Available: https://www.egr.msu.edu/classes/ece480/capstone/fall15/group10/subpage/application%20note%20ari.pdf. [Accessed: Oct. 12, 2017].
[24] J. G. Slootweg, H. Polinder, and W. . Kling, “Dynamic Modelling of a Wind Turbine with Doubly Fed Induction Generator,” in Proc IEEE Power Engineering Society Transmission and Distribution Conference' 01, 2001, pp. 644–649.
[25] A. G. Abo-Khalil, *Impacts of Wind Farms on Power System Stability*, London, UK, Intechopen, 2011. [E-book] Available: Intechopen e-book. https://www.researchgate.net/publication/255568870_Impacts_of_Wind_Farms_on_Power_System_Stability.
[26] N. S. Chouhan, “Doubly fed induction generator with integrated energy storage system for smoothening of output power,” M. S. thesis, Missouri University of Science and Tehnology, Rolla, Missouri, 2010.
[27] R. Gohar and F. Servati, “Modelling a DFIG-Based Wind Turbine Focusing on DFIG and Aerodynamic Models,” *European Online Journal of Natural and Social Sciences 2014*, vol. 3, no. 3, Sep., pp. 744–757, 2014.
[28] M. Ahmed, U. Amin, S. Aftab, and Z. Ahmed, “Integration of Renewable Energy Resources in Microgrid,” *Energy and Power Engineering*, vol. 7, no. Jan., pp. 12–29, 2015.
[29] R. Abhinav, and N. M. Pindoriya, “Grid Integration of Wind Turbine and Battery Energy Storage System : Review and Key Challenges,” *IEEE*, vol. 6, June, pp. 1–6, 2016.
[30] S. Sewchurran and Innocent E. Davidson, “Introduction to the South African Renewable Energy Grid Code Version 2 . 9 Requirements (Part III - Discussions and Conclusions),” in IEEE AFRICON: Science, Technology and Innovation for Africa, Capetown, South Africa, 2017.
[31] S. Sewchurran and Innocent E. Davidson, “Introduction to the South African Renewable Energy Grid Code Version 2 . 9 Requirements (Part II – Grid Code Technical Requirements),” IEEE AFRICON: Science, Technology and Innovation for Africa, Capetown, South Africa, 2017.

[32] National Energy Regulator of South Africa, *GRID CONNECTION CODE FOR RENEWABLE POWER PLANTS (RPPs) CONNECTED TO THE ELECTRICITY TRANSMISSION SYSTEM (TS) OR THE DISTRIBUTION SYSTEM (DS) IN SOUTH AFRICA, version3.0,* NERSA Office of the Headquarters Operations, Pretoria, 2015.

[33] H.K.Tyll, "FACTS Technology for Reactive Power Compensation and System Control," *IEEE /PES Transmission & Distribution Conference & Exposition*, vol. 04, no. 9, Sep., pp. 976–980, 2004.

[34] Ritu Parasher, "Load Flow Analysis Of Radial Distribution Network Using Linear Data Structure," M. S. thesis, Rajasthan Technical University, Kota, Yagyavalkya Institute of Technology, Jaipur, 2013.

[35] Roy Billinton and Yi Gao, "Multistate Wind Energy Conversion System Models for Adequacy Assessment of Generating Systems Incorporating Wind Energy," *IEEE TRANSACTIONS ON ENERGY CONVERSION,* vol. 23, no. 1, March, pp. 163–170, 2008.

[36] National Science Foundation, *Effect of Grid-Connected DFIG Wind Turbines on Power System Transient Stability*, Atlanta, GA: Office of the Intelligent Power Infrastructure Consortium (IPIC), 2008.

[37] F. Shewarega, I. Erlich, and J. L. Rueda, "Impact of Large Offshore Wind Farms on Power System Transient Stability," *IEEE PSCE Seattle*, vol. 09, no. 2, pp. 1–8, 2009.

[38] N. Dizdarevic, M. Majstrovic, and G. Andersson, "FACTS-based reactive power compensation of wind energy conversion system," presented at IEEE Bologna PowerTech Conference, Bologna, Italy, 2003.

[39] H. Xu, I. Kockar, and M. Plecas, "Integration of energy storage to improve utilisation of distribution networks with active network management schemes," In Proc. IEEE 24th International Conference & Exhibition on Electricity Distribution (CIRED), Glasgow, UK, 2017.

[40] C. M. K. S, T. Nivethitha, B. Yazhini, and B. Preethi, "Study on Integration of Wind and Solar Energy to Power Grid," *Nivethitha.T et al Int. Journal of Engineering Research and Applications*, vol. 4, no. 5, May, pp. 67–71, 2014.

[41] Benchagra Mohamed, *"Wind Farm Connected to a Distribution Network,"* London, UK, Intechopen, 2016. [E-book] Available: Intechopen e-book. https://www.intechopen.com/books/smart-cities-technologies/wind-farm-connected-to-a-distribution-network.

[42] W. Tong, *"Fundamentals of wind energy,"* WIT Transactions on State of the Art in Science and Engineering, Vol 44, Billerica MA, WIT Press, 2010. [E-book] Available: Wit press Online. https://www.witpress.com/Secure/elibrary/papers/9781845642051/9781845642051001FU1.pdf

[43] P. Sørensen, Nicolaos Antonio Cutululis, Torsten Lund, Anca D. Hansen, Troels Sørensen, Jesper Hjerrild, Martin Heyman Donovan, Leif Christensen, Henny Kraemer Nielsen*et*, "Power Quality Issues on Wind Power Installations in Denmark," *IEEE*, vol. 07, no. 6, June, pp. 1–6, 2007.

[44] P. Manandhar and N. R. Karki, "Impact Analysis of Wind Power System Installation in Kathmandu Valley Network," In Proc. IOE Graduate Conference, 2015, pp. 180–185.

[45] Y. M. Alharbi, A. M. S. Yunus, and A. Abu-Siada, "Application of STATCOM to Improve the High-Voltage-Ride-Through Capability of Wind Turbine Generator," *IEEE*, vol. 11, no. 6, June, pp. 1–5, 2011.

[46] Z. Fengquan, G. Joós, and C. Abbey, "Voltage Stability in Weak Connection Wind Farms," *IEEE*, vol. 10, no. 2, Oct., pp. 1483–1488, 2005.

[47] V. Yuvaraj, Deepa. S. N, R. A. P. Roger, and K. Madhusudan, “Improving Grid Power Quality with FACTS Device on Integration of Wind Energy System,” *IEEE Fifth Asia Modelling. Symposium.*, vol. 11, no. 4, Apr., pp. 157–162, 2011.
[48] A. Junyent-ferre, O. Gomis-Bellmunt, A. Sumper, Montserrat Mata and M. Sala, “Simulation Modelling Practice and Theory Modeling and control of the doubly fed induction generator wind turbine,” *Elsevier*, vol. 18, June, pp. 1365–1381, 2010.
[49] National Renewable Energy Laboratory, *NREL Dynamic Models For Wind Turbines and Wind Power Plants,* Boulevard Golden, Colorado: Office of Energy Efficiency & Renewable Energy, 2011.
[50] S. Arnaltes and Jose. Luis. R-A. and M. E. Montilla-DJesus, “Control of Variable Speed Wind Turbines with Doubly Fed Asynchronous Generators for Stand-Alone Applications,” *Energies*, vol. 26, no. 11, Nov., pp. 1–16, 2018.
[51] Y. Zhang, L. Zhang, and Y. Liu, “Implementation of Maximum Power Point Tracking Based on Variable Speed Forecasting for Wind,” In Proc. Processes' 03, 2019, pp. 1–18.
[52] G. I. and L. M. Gonzalo Abad, Miguel Angel Rodriguez, *Doubly Fed Induction Machine*, Piscataway, NJ: Hoboken, New Jersey,Wiley Publication, 2011.
[53] S. Romphochai and P. Kumkratug, “Energy Conversion System in MATLAB / SIMULINK,” *Advance Electronic Electrical Engineering*, vol. 07, no. 5, May, pp. 42–45, 2013.
[54] L. A. Soriano, W. Yu, and J. D. J. Rubio, “Modelling and Control of Wind Turbine,” *Hindawi Publishing Corporation, Mathematical Problems in Engineering*, vol. 2013, Oct., pp. 1–13, 2013.
[55] Jonathan Fournier, “Modelling, control and experimental validation of a DFIG-based wind turbine test bench,” M. S thesis, University of Politecnica de Catalunya, Barcelona, Spain, 2013.
[56] M. Hallak, M. Hasni, and M. Menaa, “Modelling and Control of a Doubly Fed Induction Generator Base Wind Turbine System,” In Proc. 2018 International conference on Electrical Sciences and Technologies in Maghreb' 10, 2018, pp. 27–32.
[57] M. Badreldien, R. Usama, A. El-wakeel, and A. Y. Abdelaziz, “Modeling , Analysis and Control of Doubly Fed Induction Generators for Wind Turbines,” In Proc. 9th International Conference on Electrical Engineering' ICEENG' 05, 2014, pp. 1–17.
[58] S. Mazari, “Control design and analysis of doubly-fed induction generator in wind power application,” M. S. thesis, The University of Alabama, TUSCALOOSA, ALABAMA 2009.
[59] S. A. Azmi, K. H. Ahmed, S. J. Finney, and B. W. Williams, “Comparative Analysis Between Voltage And Current Source Inverters in Grid-Connected Application,” In Proc. IET Conference on Renewable Power Generation (RPG 2011)' 09, 2011, pp. 1–6.
[60] G. Michalke, A. D. Hansen, and T. Hartkopf, “Control strategy of a variable speed wind turbine with multipole permanent magnet synchronous generator,” In Proc. European Wind Energy Conference and Exhibition' 07, 2007, pp. 1371–1378.
[61] M. Bezza, B. E. L. Moussaoui, and A. Fakkar, “Sensorless MPPT fuzzy controller for DFIG wind turbine,” *ELSEVIER Energy Procedia 18*, vol. 18, May, pp. 339–348, 2012.
[62] M. Sleiman, B. Kedjar, A. Hamadi, K. Al-haddad, and H. Y. Kanaan, “Modelling , Control and Simulation of DFIG for Maximum Power Point Tracking,” In Proc. 9th Asian Control Conference (ASCC)' 10, 2013, pp. 1–6.
[63] A. Gomez-Exposito, A. J. Conejo, and C. Canizares, *Electric Energy Systems Analysis and Operation*. Boca Raton, FL: CRC Press, 2009.
[64] A. S. Al-toma, Maysam Abbod, and G. A. Taylor, “Intelligent Pitch Angle Control Scheme for Variable Speed Wind Generator Systems,” *IEEE*, vol. 17, no. 2, Feb., pp. 1–6, 2017.

[65] M. Burgmer, Christian Feltes, and Ralf Linnertz, *ILA-Course Wind Power Plants with DFIG EWG1.* Siemensstraße, Kerpen: LUCAS-NÜLLE, 2019.